UNIVERSITY OF CALIFORNIA SAN DIEGO

Investigations into Biological Influences on the Carbon Isotopic Composition ($d^{13}C$) of Nascent Sea Spray Aerosol and Ocean-Aerosol Transfer of Organic Material

A dissertation submitted in partial satisfaction of the requirements

for the degree

Doctor of Philosophy

in

Chemistry

by

Daniel Robert Crocker

Committee in Charge:

Professor Mark H. Thiemens, Chair
Professor Lihini Aluwihare
Professor Grant Deane
Professor Vicki Grassian
Professor Michael Tauber
Professor William Trogler

2021

The dissertation of Daniel Robert Crocker is approved, and it is acceptable in quality and form for publication on microfilm and electronically.

University of California San Diego

2021

DEDICATION

This thesis is dedicated to my parents, Claire and Lee Crocker, for everything you have contributed to my personal and scientific growth. As lifelong educators, you stimulated my passion for learning from an early age. I often recall our family discussions at the dinner table regarding history, politics, and education; that dialogue taught me to think critically about our world and society. I did not always listen to you when I was younger, but while serving as an educator and mentor in graduate school I have constantly drawn inspiration from your wisdom and advice. You have also continued to support my lifelong education (literally so far), even when you didn't understand why my graduate studies were taking so long. I am forever grateful for the love and encouragement you have provided me for all these years. Without your unconditional support and guidance, I certainly would not be here writing this Ph. D dissertation.

I am also dedicating this dissertation to my high school chemistry teacher Mrs. McLellan; your enthusiasm for chemistry was infectious and helped ignite my love of chemistry. The study halls I spent in your chemistry lab doing extra experiments were my first foray into real scientific investigation and exploration. Your creativity and encouragement pushed me think outside of the box and has benefited me greatly during my graduate studies.

TABLE OF CONTENTS

LIST OF FIGURES

LIST OF TABLES

ACKNOWLEDGEMENTS

I want to start by thanking my graduate advisor Professor Mark Thiemens for taking a chance on me 7 years ago when I asked to join his laboratory out of the blue. Your passion for science and chemistry is truly motivational and our many discussions throughout the years have advanced my scientific mindset and analytical abilities. I have achieved immense scientific growth during my graduate work in your lab, and I know my time working in your laboratory will continue to benefit me as I move forward to my postdoctoral studies and the rest of my career.

Of course, my graduate studies would not have been nearly as successful or enjoyable without the friendship, guidance, and assistance from my fellow researchers in the Thiemens laboratory. I especially want to thank our lab manager Terri Jackson, without whom our lab would not continue to function. Your mentorship and friendship have made graduate school easier and your meticulous analytical skills have improved me as a researcher. Additionally, thank you to Subrata Chakraborty, Robina Shaheen, and Mang Lin for their advice and guidance during my graduate studies. Having three experienced researchers in the lab provided me with additional mentorship that enhanced my scientific thinking, research and writing. Finally, I would like to thank the undergraduate students who contributed to my graduate research, Ritchie Hernandez, Danny Huang, Ruochen Cao, and Jiayin Dai. It was a pleasure to work with you and watch you grow as scientists. You should know that you also helped me grow as both a scientist and mentor, and I appreciate the substantial contributions you made to my thesis research.

Next, I would like to thank the National Science Foundation Center for Aerosol Impacts on Chemistry of the Environment (NSF-CAICE) for funding the entirety of my graduate research. I especially want to express my gratitude to the Director Kimberly Prather and Co-Director Vicki Grassian for the amazing scientific and professional opportunities they have provided me with in

graduate school. My graduate studies would not have been possible without your financial support and mentorship as well as that of the CAICE community.

Speaking of which, I also want to thank all of my CAICE colleagues who contributed to my scientific and personal growth. Being part of a large community of skilled and motivated scientists has enhanced my graduate experience and the quality of my work as a whole. Far too many people have contributed to my scientific career for me to name each individually, but I especially want to thank all of the scientists and personnel who contributed to the CAICE-funded Sea Spray Chemistry and Particle Evolution (SeaSCAPE) experiment, from which much of my dissertation research was derived.

I owe a big thank you to Bruce Deck and my doctoral committee member Professor Lihini Aluwihare for allowing me use of their laboratories to complete portions of my dissertation research. Bruce, thank you for analyzing my difficult samples in your laboratory, I know it wasn't always enjoyable, but I am very grateful for your assistance. Lihini, in addition to welcoming me into your laboratory, I want to thank you for your excellent scientific mentorship during my graduate studies. I also want to thank Tran Nguyen and Ralph Torres in the Aluwihare lab for assisting me with my research analyses.

I want to extend a very heartfelt thank you to my doctoral committee member Professor Grant Deane. We met each other at a time when I was struggling in graduate school, and you offered to invest your time in my graduate career without any guarantee of a return on your investment. Your mentorship and guidance helped me right the ship and have been invaluable to my development as a scientist. The many skills that I learned from you about scientific research, writing, and mentorship will serve me well as I continue my career in academia. I want you to know that I am extremely grateful for the time and effort you devoted to me. Hopefully through

our interactions and the publications we have worked on together I have been able to pay back some of the investment you put into me.

Prior to my graduate studies at UCSD, many other mentors contributed to advancing my scientific journey. I have already mentioned my high school chemistry teacher Mrs. McLellan who kindled my passion for chemistry. I would like to thank my undergraduate advisor, Professor Steven Suib, who encouraged my scientific independence while working in his lab. You set an excellent example as a scientific advisor, and I have modeled much of my own advisory skills on your teachings. Additionally, I would like to thank my graduate student advisor at UConn, Dr. Lakshitha Pahalagedara, for introducing me to scientific research and answering the many questions I had. I would also like to thank Professor Michael Hren at UConn for introducing my to stable isotopes and suggesting I work in Professor Mark Thiemens' lab at UCSD. I did not realize it at the time, but your advice greatly impacted the trajectory of my scientific career.

My friends, both here and on the East Coast, deserve a lot of credit for my personal development over the years. I especially want to thank my friends from high school and college for supporting me over the years. Thank you to Dr. Nate Johnson, Daniel McGovern, Dr. Alex Doering, Kate Ikhsanova, Nicole Begley, Zachary Knights, Alyssa Grey, Conrad Anderson-Dollhopf, and Conor Quinn. Your friendship has helped me develop into a person I am proud of today. It has been hard living so far away from you for 7 years and I am looking forward to returning home and seeing all of you. I also want to thank the friends I made while in graduate school. Thank you to Dr. Katharine Lunny, Dr. Dan Mermelstein, Dr. Riley Peacock, Dr. Adriana Corrales, Dr. Tim Wiryaman, Kevin Sweeney, and Adam Maloney.

Once again, I thank my parents, Claire and Lee Crocker, for their perpetual support throughout my graduate career. I also thank my sister, Ashley Crocker, who moved out to Southern

California shortly after myself. I think we have grown closer during this time, and it has been a nice comfort to have a family member nearby. Along the same lines, I would like to thank my extended family in Southern California. Thank you to my aunt and uncle, Kathy and Michael Walsh, for inviting me into your house many times while I lived in Southern California, and making it feel like I had a second home here. I also want to thank Matthew Walsh for keeping me in shape with our sword fighting adventures and keep me up to date on my superhero knowledge. Lastly, I would like to thank my Grandma KT. Having turned 100 earlier this year, and being a veteran of World War II, you are an inspiration to us all including myself.

Finally, I would like to thank my partner, Dr. Nicole Peiris, who has been my best friend and primary support system throughout graduate school. Moreover, you have been a scientific and personal role model for me. I am constantly inspired by your intellect and drive to contribute positive change through your scientific work. You have been faced with so many hardships and challenges, but I have never met someone as strong and resilient as you in the face of adversity. Through the many challenges we have endured over the last five years our bond has only continued to strengthen. I love you and I am excited to keep growing with you as we move forward from UCSD to the next stage of our journey together.

Chapter 2, in part, is a reprint of the material as published in ACS Earth and Space Chemistry, 2020. Crocker, D. R.; Hernandez, R.; Huang D. H.; Pendergraft, M. A.; Cao, R.; Dai, J.; Morris, C. K.; Deane, G. B.; Prather, K. A.; Thiemens M. H. The dissertation author was the primary investigator and author of this paper.

Chapter 3, in part, has been submitted for publication of the material as it may appear in Environmental Science and Technology. Crocker, D. R.; Kaluarachchi, C.P.; Cao, R; Dinasquet,

J.; Franklin, E. B.; Morris, C.K.; Nguyen, T.; Torres R.R.; Martz, T. D.; Malfatti, F. M.; Goldstein, A.H.; Tivanski, A. V.; Prather, K. A.; Thiemens M. H. The dissertation author was the primary investigator and author of this paper.

Chapter 4, in part, has been submitted for publication of the material as it may appear in Geophysical Research Letters. Crocker, D. R.; Deane, G. B.; Cao, R; Santander M. V.; Morris, C. K.; Mitts, B.A.; Malfatti, F. M.; Prather, K. A.; Thiemens, M. H. The dissertation author was the primary investigator and author of this paper.

Chapter 5, in part, has been submitted for publication of the material as it may appear in Environmental Science and Technology. Crocker, D. R.; Kaluarachchi, C.P.; Cao, R; Dinasquet, J.; Franklin, E. B.; Morris, C.K.; Nguyen, T.; Torres R.R.; Martz, T. D.; Malfatti, F. M.; Goldstein, A.H.; Tivanski, A. V.; Prather, K. A.; Thiemens M. H. The dissertation author was the primary investigator and author of this paper.

VITA

2014 Bachelor of Science, University of Connecticut, USA

2016 Master of Science, University of California San Diego, USA

2021 Doctor of Philosophy, University of California San Diego, USA

PUBLICATIONS

Crocker, D. R.; Kaluarachchi, C. P.; Cao, R; Dinasquet, J.; Franklin, E. B.; Morris, C.K.; Nguyen, T.; Torres R.R.; Martz, T. D.; Malfatti, F. M.; Goldstein, A.H.; Tivanski, A. V.; Prather, K. A.; Thiemens M. H. Isotopic Investigations into Organic Composition Differences between Submicron and Supermicron Sea Spray Aerosol. *Manuscript in submission.*

Crocker, D. R.; Deane, G. B.; Cao, R; Santander M. V.; Morris, C. K.; Mitts, B.A.; Dinasquet, J.; Malfatti, F. M.; Prather, K. A.; Thiemens, M. H. Biologically Induced Changes in the Partitioning of Submicron Particulates between Bulk Seawater and Sea Surface Microlayer. *Manuscript in submission.*

Kaluarachchi, C.; Or, V. W.; Lan, Y.; Madawala, C. K.; Hasenecz, E. S.; **Crocker, D. R.**; Morris, C. K.; Lee, H. D.; Mayer, K. J.; Sauer, J. S.; Lee, C.; Dorce, G.; Malfatti, F.; Stone, E. A.; Cappa, C. D.; Grassian, V. H.; Prather, K. A.; Tivanski, A. V. *Manuscript in submission.*

Tumminello, P. R.; James, R. C.; Kruse, S.; Garofalo, L; Kawasaki, A.; Cooper, A.; Guadalupe-Diaz, I.; **Crocker, D. R.**; Mayer, K. J.; Sauer, J. S.; Lee, C.; Bertram, T. H.; Cappa, C. D.; Prather, K. A.; Farmer, D.; Slade, J. H. *Manuscript in submission.*

Kilgour, D. B.; Novak, G. A.; Sauer, J. S.; Moore, A. N.; Dinasquet, J.; Amiri, S.; Franklin, E. B.; Mayer, K. J.; Winter, M.; Morris, C. K.; Price, T.; Malfatti, F.; **Crocker, D. R.**; Lee, C; Cappa, C. D.; Goldstein, A. H.; Prather, K. A.; Bertram, T. H.

Sauer, J. S.; Mayer, K. J.; Lee, C.; Alves, M. R.; Amiri, S.; Bahaveolos, C.; Barnes, E. B.; **Crocker, D. R.**; Dinasquet, J.; Garofalo, L. A.; Kaluarachchi, C. P.; Dang, D.; Kilgour, D.; Mael, L.; Mitts, B. A.; Moon, D. R.; Morris, C. K.; Moore, A. N.; Ni, C.-M.; Pendergraft, M. A.; Petras, D.; Simpson, R.; Smith, S.; Tumminello, P. R.; Walker, J. L.; DeMott, P. J.; Farmer, D. K.; Goldstein, A. H.; Grassian, V. H.; Jaffe, J. S.; Malfatti, F.; Martz, T. R.; Slade, J.; Tivanski, A. V.; Bertram, T. H.; Cappa, C. D.; Prather, K. A. The Sea Spray Chemistry and Particle Evolution Study (SeaSCAPE): Overview and Experimental Methods. *Environ. Sci. Process. Impacts,* 2021.

Angle, K. J.; **Crocker, D. R.**; Simpson, R. M.; Mayer, K. J.; Garofalo, L. A.; Moore, A. N.; Mora Garcia, S.L.; Or, V.W.; Srinivasan, S; Farhan, M; Sauer, J. S.; Lee, C.; Pothier M.H.; Farmer, D.

K.; Martz, T. R.; Bertram, T. H.; Cappa, C. D.; Prather, K.A.; Grassian, V. H. Acidity across the interface from the ocean surface to sea spray aerosol. *Proceedings of the National Academy of Sciences,* 2020, *118* (2). doi:10.1073/pnas.2018397118

Crocker, D. R.; Hernandez, R.; Huang D. H.; Pendergraft, M. A.; Cao, R.; Dai, J.; Morris, C. K.; Deane, G. B.; Prather, K. A.; Thiemens M. H. Biological Influence on $\delta^{13}C$ and Organic Composition of Nascent Sea Spray Aerosol. *ACS Earth and Space Chemistry*. 2020, *4* (9), 1686-1689. doi: 10.1021/acsearthspacechem.0c00072

Lin, M., Biglari, S., Zhang, Z., **Crocker, D.**, Tao, J., Su, B., Liu, L., Thiemens, M. H. Vertically uniform formation pathways of tropospheric sulfate aerosols in East China detected from triple stable oxygen and radiogenic sulfur isotopes. *Geophysical Research Letters*, 2017, *44* (10), 5187–5196. doi: 10.1002/2017gl073637

ABSTRACT OF THE DISSERTATION

Investigations into Biological Influences on the Carbon Isotopic Composition ($d^{13}C$) of Nascent Sea Spray Aerosol and Ocean-Aerosol Transfer of Organic Material

by

Daniel Robert Crocker

Doctor of Philosophy in Chemistry

University of California San Diego, 2021

Professor Mark H. Thiemens, Chair

Atmospheric aerosols remain the largest uncertainty in assessments of the anthropogenic influence on Earth's radiative budget. Aerosols affect Earth's radiative budget directly, by reflecting and absorbing incoming solar radiation, and indirectly, by serving as nuclei for water and ice cloud formation. Current estimates of anthropogenic impacts on the direct and indirect aerosol effects are hindered by an inadequate understanding of how naturally produced aerosols contribute to both processes. Sea spray aerosol (SSA), formed by oceanic wave breaking, represents the largest source of natural aerosol to the atmosphere by mass. The climate-relevant properties of SSA, such as hygroscopicity, reflectivity, and ice nucleation ability, are highly dependent on the amount and composition of the organic material transferred from the seawater

into these aerosols. The composition of this organic material is strongly influenced by microbial activity in the seawater, highlighting the importance of employing new techniques to examine the impact of oceanic biological activity on the organic material transferred into SSA. Carbon isotopic analysis has been frequently employed to differentiate between anthropogenic and natural sources of aerosol carbon, but has not previously been applied to study ocean-aerosol transfer of organic material. In my dissertation work, I measured carbon isotopic compositions ($\delta^{13}C$) of seawater and SSA organic material during two laboratory phytoplankton blooms, identifying an increased contribution of "freshly-produced" carbon to SSA, strongly controlled by the microbial loop. I further demonstrate that not accounting for this biological influence on the $\delta^{13}C$ value of nascent SSA can lead to significant underestimates in the contribution of anthropogenic aerosol carbon to the marine environment (Chapter 2). Building from this work, I investigated differences between submicron and supermicron SSA during a wave channel mesocosm experiment. The stark differences between these two SSA fractions, with supermicron SSA heavily influenced by biological activity and submicron SSA primarily influenced by surface-active anthropogenic compounds originating from the coastal seawater, reveals the importance of biology and ocean-aerosol transfer processes on SSA organic composition and $\delta^{13}C$ (Chapter 3). Finally, I explored biologically induced changes in seawater submicron particulates (SMPs) in the bulk seawater and SSML to better understand how seawater biology may influence the transfer of ice nucleating entities into SSA (Chapter 4).

Chapter 1: An Introduction to Aerosols and Carbon Isotopes

1.1 Importance of Atmospheric Aerosols

Aerosols are solid or liquid particles suspended in a volume of gas (e.g. the atmosphere).[1,2] Atmospheric aerosols are derived from a number of anthropogenic (human-caused) and natural processes such as fossil fuel combustion, biomass burning, agricultural practices, vapor condensation, oceanic and lacustrine wave breaking, wind-blown dust, and volcanic emissions.[3–9] A lot of attention has been paid to atmospheric aerosol concentrations due to their potential harmfulness to human health,[10,11] leading to proposals for reducing anthropogenic aerosol emissions.[12,13] However, when contemplating a reduction in aerosol emissions, we must also consider the important impact that aerosols have on weather and climate. Aerosols influence Earth's radiative budget both directly, by reflecting or absorbing incoming radiation, and indirectly, by seeding water and ice cloud formation.[14] Both of these processes are believed to have a net cooling effect on the planet, meaning that reducing aerosol emissions may actually accelerate the warming of our planet.[15,16] To better understand these processes, an abundance of research has been devoted toward studying how aerosols interact with incoming sunlight and clouds,[17,18] but the latter of these still remains the largest uncertainty in estimates of the anthropogenic influence on Earth's radiative budget (error bars in Figure 1.1).[19]

Because aerosols serve as cloud condensation nuclei (CCN), cloud formation and lifetime depend on aerosol number concentration, size, and chemical composition.[20] Chemical composition plays an important role in controlling the CCN activity of an aerosol by affecting its hygroscopicity, or affinity for water uptake.[21] Typically, inorganic aerosols (e.g. sodium chloride or ammonium sulfate) are more hygroscopic and have higher CCN activity, while organic aerosols have lower hygroscopicity and CCN activity.[22] Therefore, a lot of research has been focused on

aerosols that contain both inorganic and organic chemical species to determine how their internal mixtures influence CCN activity and climate.[23–25]

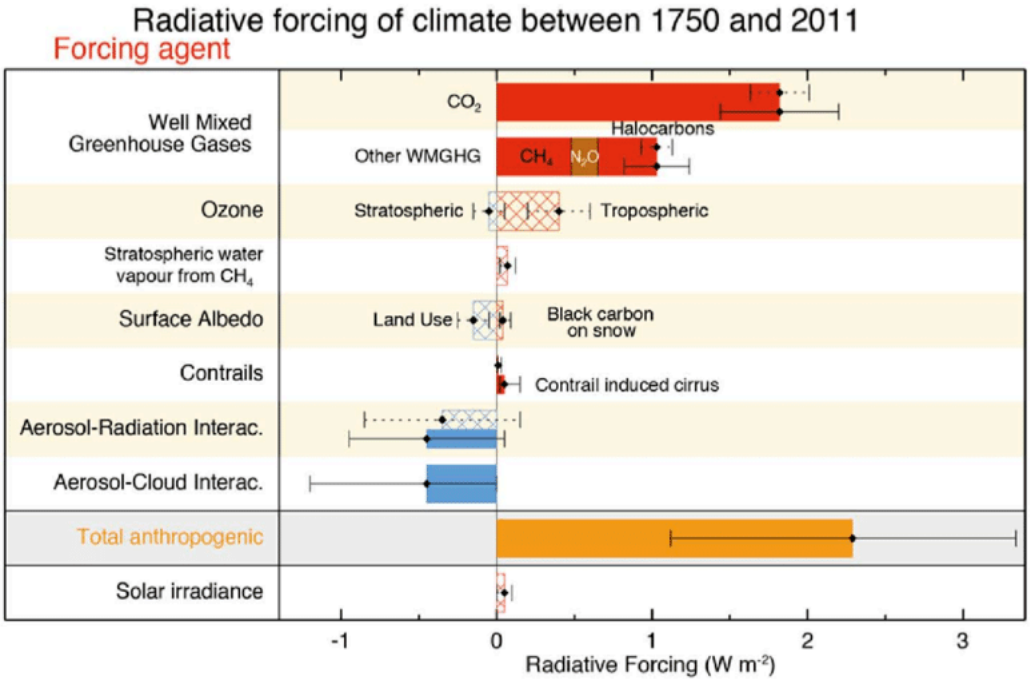

Figure 1.1 The radiative forcing (filled bars) and effective radiative forcing (hatched bars) of climate from 1750 to 2011 for different forcing agents. Collectively, the direct and indirect aerosol effects account for the majority of uncertainty in climate radiative forcing, and the aerosol indirect has the largest uncertainty of any forcing agent. Image reprinted from Myhre et al.[19]

1.2 Sea Spray Aerosol

1.2.1 Sea Spray Aerosol Formation and Composition

Ironically, the largest source of uncertainty in estimating the influence of anthropogenic aerosols on climate actually arises from an inadequate understanding of the impact that naturally produced aerosols have on climate.[26,27] Over 70% of Earth's surface is covered by oceans, so it comes as no surprise that sea spray aerosol (SSA), formed by oceanic wave breaking, represents the largest source of natural aerosol to the atmosphere by mass.[28,29] SSA is a chemically complex mixture of inorganic ions, organic molecules, and biological structures/organisms produced from

the ocean surface by bursting of air bubbles entrained in the seawater by breaking waves.[7,29,30] There are two types of SSA formed by bubble bursting, nominally film drop and jet drop SSA. Film drop SSA are produced by bursting of the bubble film cap at the ocean surface, while jet drop SSA are produced from an unstable seawater jet that forms at the bubble's base during collapse of the bubble cavity.[31] The two different formation mechanisms contribute to the chemical diversity of SSA. Film drop SSA tend to be influenced by the sea surface microlayer (SSML)—the topmost 1-1000 μm of the ocean surface with elevated concentrations of organic molecules and biological components.[32,33] Jet drop SSA are formed from the base of the bubble, and thus often reflect the chemical composition of the underlying seawater.[31] Because of the intricate chemistry and biology in the surface ocean, elucidating the seawater biological and physicochemical processes that drive variability in SSA's chemical composition has been a topic of intense research focus.

1.2.2 Ambient Measurements of SSA

In the last twenty years, a plethora of marine field studies have been devoted to understanding how SSA organic content and composition impact its hygroscopicity and CCN activity.[34–42] Much of this research has focused on elucidating how seawater biological activity influences these climate-relevant SSA properties.[34–38] A number of studies have shown that elevated seawater biological activity correlates with higher SSA organic content,[34,35,38,40] and increased SSA organic content has been further related to changes in SSA hygroscopicity and CCN activity.[36,43–45] Unfortunately, despite the abundance of field research indicating a biological influence on SSA composition, a direct connection between seawater biology and compositional changes that influence its climate-relevant properties has remained elusive.[45–47] This is partly because interpretation of aerosol measurements in the ambient marine environment is complicated

by contributions from secondary marine aerosol (SMA) and terrestrial aerosols transported from the land, in addition to SSA.[44,48] This has prompted researchers to develop innovative laboratory techniques to study SSA in an isolated environment, providing additional insight to help interpret our observations in the marine atmosphere.

1.2.3 Laboratory Generation of Authentic SSA

To properly study SSA in a laboratory setting one must accurately replicate the process of SSA formation while also maintaining the biological and chemical complexity present in the actual ocean. Historically, atomizers and sintered glass filters were commonly used methods for laboratory production of SSA, but more recent studies have scrutinized their applicability because these methods do not produce SSA size distributions analogous to those in the ambient marine environment.[49] In recent years, significant advances in replication of SSA formation and chemistry have been made by the Center for Aerosol Impacts on Chemistry of the Environment (CAICE), an NSF Center for Chemical Innovation. For brevity, I will describe here the two techniques used for the majority of my research presented in this dissertation, an ocean-atmosphere wave channel and a Marine Aerosol Reference Tank (MART).

The ocean-atmosphere wave channel, located at the Scripps Institution of Oceanography Hydraulics Lab, is the most robust method we have for laboratory studies of SSA. The 30-meter-long channel is filled with 11,800 L of natural seawater from the coastal Pacific Ocean, and a paddle is used to create waves that break over a simulated beach forming the SSA.[50,51] This technique has the advantage of using real breaking waves to form the SSA, and the channel is also large enough to attach a suite of different instruments enabling collaborative studies. The MART is a much smaller system (210 L) that uses a plunging waterfall to simulate SSA formation by

breaking waves.[52] One drawback of this system is that the centrifugal pump used to generate the waterfall can damage the biology in the seawater, so aerosol production can only be started after the biological growth has peaked.[53] However, the MART enables directed studies of SSA on a much simpler to operate system and is ideal for smaller studies employing only a few different measurements.

The key aspect that elevates these systems above previously employed aerosol production techniques is their ability to reproduce the same bubble size distribution as actual breaking waves, which generates SSA size distributions analogous to those measured in the marine environment.[51,52] This is essential to accurately study SSA because the chemical composition of SSA is size-dependent. The development of these new aerosol generation techniques has enabled more directed and detailed studies of the biological influence on SSA's composition and climate-relevant properties.

1.2.4 Laboratory Advances in Understanding the Biological Influence on SSA

In order to make our laboratory SSA studies comparable to those in the ambient marine environment, it is essential to mimic the seawater biology and chemistry that gives SSA its chemical complexity. In the ocean, cycling of organic matter is primarily controlled by the microbial loop: phytoplankton convert CO_2 into organic material (primary productivity), and this freshly produced organic material is then incorporated into bacterial biomass. Bacterial utilization also results in much of the organic material being respired back into CO_2, creating a loop that continually forms and degrades organic material.[54,55] Thus, our studies must recreate this microbial loop of phytoplankton and bacteria that control the production, transformation, and respiration of organic matter in the ocean. This is achieved by adding algae growth nutrients to the natural

seawater used in our experiments, inducing a phytoplankton bloom cycle that leads to establishment of the microbial loop.[53]

Using this methodology, CAICE has been able provide more detailed insight into many of the observations made in the ambient environment. Of particular relevance to this dissertation work, the ability to replicate SSA formation and chemistry in a controlled, laboratory setting has led to many advances in our understanding of how the oceanic microbial loop influences the organic composition of SSA. Experiments in the ocean-atmosphere wave channel and MART have demonstrated that seawater bacterial activity, in addition to primary productivity, plays a crucial role in determining the organic composition of SSA.[53,56,57] Moreover, these biologically induced compositional changes have been linked to decreases in SSA's hygroscopicity, affecting its ability to grow into a cloud droplet.[58,59]

Laboratory studies of SSA have also helped elucidate their contribution to ice nucleation, a process that very few aerosols are able to facilitate.[60] Because phytoplankton and their exudates/detritus are known to be ice nucleators,[61,62] it was expected that seawater biological activity might impact the ice nucleating ability of SSA. CAICE research has established a clear link between seawater biological activity and the increased ice nucleating efficiency of SSA, implicating phytoplankton, bacteria, and viruses, as probable biological INEs in SSA.[60,63–65] Furthermore, this research revealed that size-dependent differences in SSA composition result in a higher ice nucleating efficiency for supermicron SSA, a finding that is unaccounted for in most modeling representations of marine INPs.[64]

CAICE has made substantial progress in establishing that marine biology influences SSA's the climate-relevant properties, but a great deal of work still remains to elucidate how biological activity changes the seawater organic composition, and the extent to which these changes are

reflected in the resultant SSA. Therefore, further advancement in our understanding of how seawater biology influences SSA organic composition would benefit from the ability to track the production and transformation of organic material in the seawater as well as its transfer into SSA. To achieve this goal, I have chosen to employ carbon isotopic measurements as a tracer to identify the seawater biological and physicochemical processes that impact the organic composition of SSA.

1.3 Carbon Isotopes and Their Application to Earth System Processes

1.3.1 Introduction to Carbon Isotopes

Atoms are primarily composed of three subatomic particles, protons, neutrons, and electrons. Protons and neutrons are contained in the nucleus while electrons orbit around the outside of the nucleus. Isotopes are atoms that have the same number of protons and electrons but differ in their number of neutrons. The differing number of neutrons means isotopes have different masses, but because the chemical properties of an atom are determined by the number of electrons, isotopes have nearly identical chemical properties (i.e. they are the same element). For example, carbon is the sixth element on the periodic table, so all carbon atoms contain six protons and six electrons. Until the early 20th century it was believed that carbon-12 (^{12}C), containing six protons and six neutrons, was the only isotope of carbon, but in 1930 spectrographic measurements on extraterrestrial molecules pointed to the presence of a second isotope containing six protons and seven neutrons, carbon-13 (^{13}C).[66,67] As it turns out, about 98.9% of all carbon atoms are ^{12}C, while around 1.1% are ^{13}C.[68] However, the actual abundance of ^{12}C and ^{13}C varies slightly between different carbon-containing compounds based on their sources and chemical transformations.[68–70] This work will focus on tracking the biological and chemical processing of organic compounds

based on differences in the abundance of these two stable isotopes using a technique called stable isotope geochemistry.

1.3.2 Stable Isotope Geochemistry

1.3.2.1 History and Important Developments

There is general agreement that the field of stable isotope geochemistry began with three landmark studies published in 1947. During this year, both Urey[71] and Bigeleisen and Mayer[72] used the small difference in free energy between isotopically-substituted molecules to derive thermodynamic calculations for the temperature-dependent equilibrium constants in isotope exchange reactions. At the same time, Nier[73] developed the first isotope mass spectrometer, capable of measuring the small variations in isotopic abundances that occur during physical and chemical processes. By combining these remarkable achievements, scientists were now able to attribute measured changes in the $^{13}C/^{12}C$ ratio to specific physical and chemical processes, and the field of stable isotope geochemistry was born.

1.3.2.2 Isotopic Delta Notation

With the new ability to measure isotopic ratios of carbon-containing species came the need to accurately standardize these measurements among different laboratories using different isotope mass spectrometers. In 1950, McKinney et al.[74] introduced isotopic delta notation ($\delta^{13}C$), a method for standardizing mass spectrometry measurements of isotopic abundances in samples by comparing them to measurements of a reference standard with known isotopic abundances (Equation 1.1). Most published $\delta^{13}C$ values use Pee Dee Belemnite (PDB), a Cretaceous marine

carbonate fossil obtained from the Pee Dee Formation in South Carolina, as the reference standard for carbon isotopes.[75]

$$\delta^{13}C = \left(\frac{\left(\frac{^{13}C}{^{12}C}\right)_{sample}}{\left(\frac{^{13}C}{^{12}C}\right)_{standard}} - 1 \right) \times 1000 \qquad \text{(Equation 1.1)}$$

In practice, an isotope mass spectrometer will measure the $^{13}C/^{12}C$ ratio in both the sample and the reference standard. The measured $^{13}C/^{12}C$ ratio of the sample is then divided by the measured $^{13}C/^{12}C$ ratio in the reference standard before subtracting away 1. The subtraction of 1 means that the $\delta^{13}C$ value will be positive if the sample has a higher $^{13}C/^{12}C$ ratio than the standard, and negative if the $^{13}C/^{12}C$ is lower than the standard. However, it is important to remember that the application of stable isotope geochemistry is usually interested in $\delta^{13}C$ differences between carbon-containing species and how these $\delta^{13}C$ values change during reactions and processes, not the absolute magnitude or sign of $\delta^{13}C$. When the $^{13}C/^{12}C$ ratio changes during a chemical or physical process this is referred to as isotopic fractionation. Because the isotopic fractionation is generally small for most processes, we multiply by 1000 in Equation 1.1 to report $\delta^{13}C$ in permil (‰) notation.

1.3.2.3The Kinetic Isotope Effect

Although ^{12}C and ^{13}C are both carbon atoms with similar chemical properties, their difference in mass leads to slightly different physical properties (e.g. bond strength and vibrational energy).[76] Using the harmonic oscillator approximation, the fundamental vibrational frequency of a bond, ν, is given by Equation 1.2a. Here, k is the force constant, or stiffness of the bond, and μ represents the reduced mass of the two atoms comprising the bond, $\left(\frac{m_1 m_2}{m_1+m_2}\right)$. Substituting a heavier

isotope (e.g. ^{13}C) into the bond in place of a lighter isotope (e.g. ^{12}C) increases the reduced mass, resulting in a lower fundamental vibrational frequency for the bond containing the heavier isotope. The lowest energy of vibration for a bond, the zero-point energy (ZPE), is given by Equation 1.2b, which shows that bonds with lower ν will also have a lower ZPE.

$$\nu = \frac{1}{2\pi}\sqrt{\frac{k}{\mu}} \qquad \text{(Equation 1.2a)}$$

$$ZPE = \frac{h\nu}{2} \qquad \text{(Equation 1.2b)}$$

One consequence of ^{13}C having a lower ZPE, is that a larger activation energy (E_a) is required for a reaction to take place (Figure 1.2). From the Arrhenius equation,[77,78] a larger E_a leads to a smaller reaction rate constant, so the molecule containing ^{13}C will have a slower reaction rate. Because the molecule containing ^{12}C reacts faster, more ^{12}C ends up in the products compared to ^{13}C (i.e. the kinetic effect isotope). The overall result of the kinetic isotope effect is an isotopic fractionation where the products of a reaction are depleted in ^{13}C (lower $\delta^{13}C$) compared to the initial reactant isotopic composition.

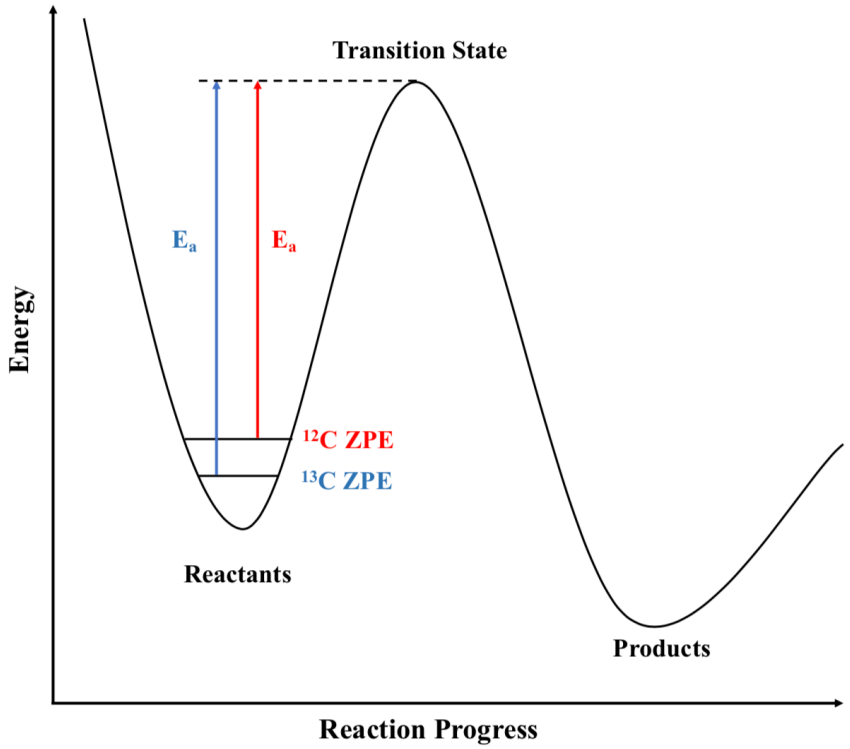

Figure 1.2 A simplified diagram of the difference in ZPE for a bond containing a ^{12}C atom versus a ^{13}C atom. Because ^{12}C sits at a higher energy level, a lower E_a is required to reach the transition state. Thus, more of the molecules containing the ^{12}C atom will overcome the E_a barrier necessary for the reaction, resulting in a lower ratio of $^{13}C/^{12}C$ atoms in the products compared to the reactants. This phenomenon is termed the kinetic isotope effect.

1.3.3 Carbon Isotopes as a Tracer for Seawater Biogeochemical Processes

One of the most common examples of kinetic isotopic fractionation occurs during primary production by plants (photosynthesis). In phytoplankton, there is a large kinetic isotope effect associated with the enzymatic conversion of inorganic CO_2 and HCO_3^- into organic material, by the enzymes RuBisCO and PEP carboxylase, respectively.[79] The isotopic fractionation results from $^{12}CO_2$ ($H^{12}CO_3^-$) having a higher ZPE than $^{13}CO_2$ ($H^{13}CO_3^-$), so it more easily overcomes the activation energy barrier for the enzymatic reactions and becomes incorporated into the product organic material.[80] This usually results in organic material with more negative $\delta^{13}C$ values around -20 ‰,[79,81] compared to the typical $\delta^{13}C$ values for dissolved inorganic carbon (-6.6 ‰ to +3.1

‰).[82] Most of the organic material freshly produced by primary productivity is initially incorporated into larger organic material such as phytoplankton biomass, termed the particulate carbon pool.[83] Eventually, particulate organic material is transformed into smaller, dissolved organic material by exudate release, phytoplankton death/cell lysis, and bacterial utilization,[54,55,84] but these processes proceed with only minor isotopic fractionation leading to a dissolved carbon pool with a similar $\delta^{13}C$ values of -21 to -23 ‰.[85,86] This dissolved carbon pool contains more recalcitrant organic material with longer lifetimes, so it is the most abundant carbon pool in most oceanic regions.

Importantly, researchers have found that the extent to which phytoplankton discriminate in favor of ^{12}C during primary production depends upon the dissolved CO_2 concentration in the seawater.[87,88] There is a general consensus that this relationship arises because when dissolved CO_2 concentrations are low, or phytoplankton abundance is high, the increased competition for CO_2 causes phytoplankton to utilize whatever CO_2 they can obtain, regardless of whether it is $^{12}CO_2$ or $^{13}CO_2$.[89] This is consistent with the lower ^{12}C discrimination observed during large phytoplankton blooms when competition for CO_2 is heightened, resulting in higher (less negative) $\delta^{13}C$ values for freshly produced particulate organic material compared to the older, more processed dissolved organic material.[90] These distinct isotopic values provide a way to distinguish between “freshly produced” and “aged” organic material in the seawater and may also enable us to discern their contributions to organic material in SSA (Figure 1.3).

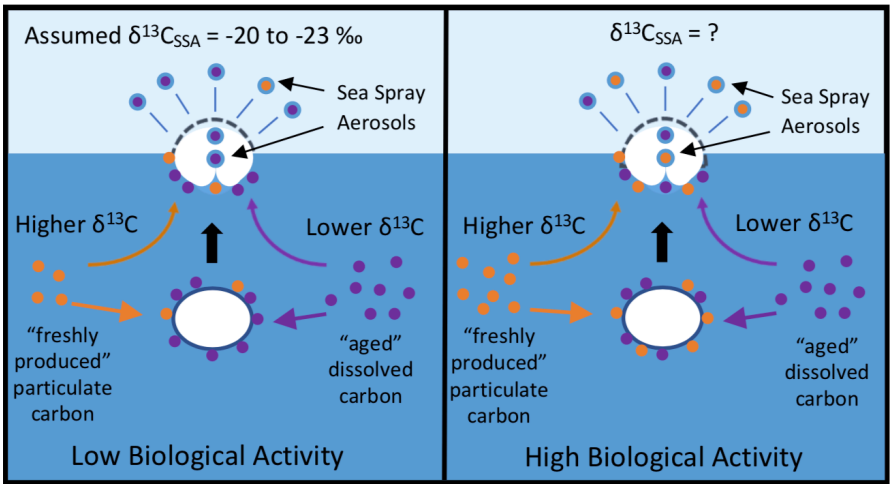

Figure 1.3 In oceanic regimes with low biological activity the "aged" dissolved carbon pool is usually the most abundant (left), so the $\delta^{13}C$ value for SSA is probably similar to the $\delta^{13}C$ for marine dissolved organic carbon. However, under oceanic conditions of high biological activity the freshly produced carbon pool increases from primary productivity (right). This freshly produced carbon pool often has higher (less negative) $\delta^{13}C$ values, which may influence the $\delta^{13}C$ value of SSA produced from biologically active waters.

Based on isotopic measurements of SSA, one study has already proposed that the "freshly produced" particulate carbon pool, and "aged" dissolved carbon pool, both contribute significantly to SSA.[91] This is supported by the higher $\delta^{13}C$ values observed for marine aerosols above oceanic regimes with elevated biological activity,[92,93] however, to date no studies have coupled seawater $\delta^{13}C$ measurements with SSA measurements to track the ocean-aerosol transfer of this organic material. In this dissertation, we combine $\delta^{13}C$ measurements on SSA with $\delta^{13}C$ measurements of seawater particulate and dissolved organic material. These measurements reveal the contribution of both carbon pools to SSA, shedding light on how biological activity impacts the organic material transferred into SSA. In addition to gaining a better understanding of how seawater biology affects SSA organic composition, this research provides insight into its effect on the $\delta^{13}C$ value of SSA ($\delta^{13}C_{SSA}$). Constraining the likely values of $\delta^{13}C_{SSA}$ has important consequences for distinguishing between aerosol sources in the marine environment.

1.3.4 Carbon Isotopes in Aerosol Source Apportionment

Another important consequence of the kinetic isotope effect is that organic material formed by different chemical and biochemical processes will have characteristic $\delta^{13}C$ values. Oftentimes, this leads to carbon reservoirs with distinct $\delta^{13}C$ values that can be used to distinguish between them (e.g. marine-derived and anthropogenically-produced carbon, Figure 1.4). Atmospheric scientists have taken advantage of the source-dependent $\delta^{13}C$ values to estimate the contribution of oceanic (SSA) and continental (anthropogenic) aerosols to the total population of marine aerosols using a method called isotopic source apportionment (Equation 1.3):[93–98]

$$\delta^{13}C_{marine} = (f_{SSA})(\delta^{13}C_{SSA}) + (f_{anth})(\delta^{13}C_{anth}) \quad \text{(Equation 1.3)}$$

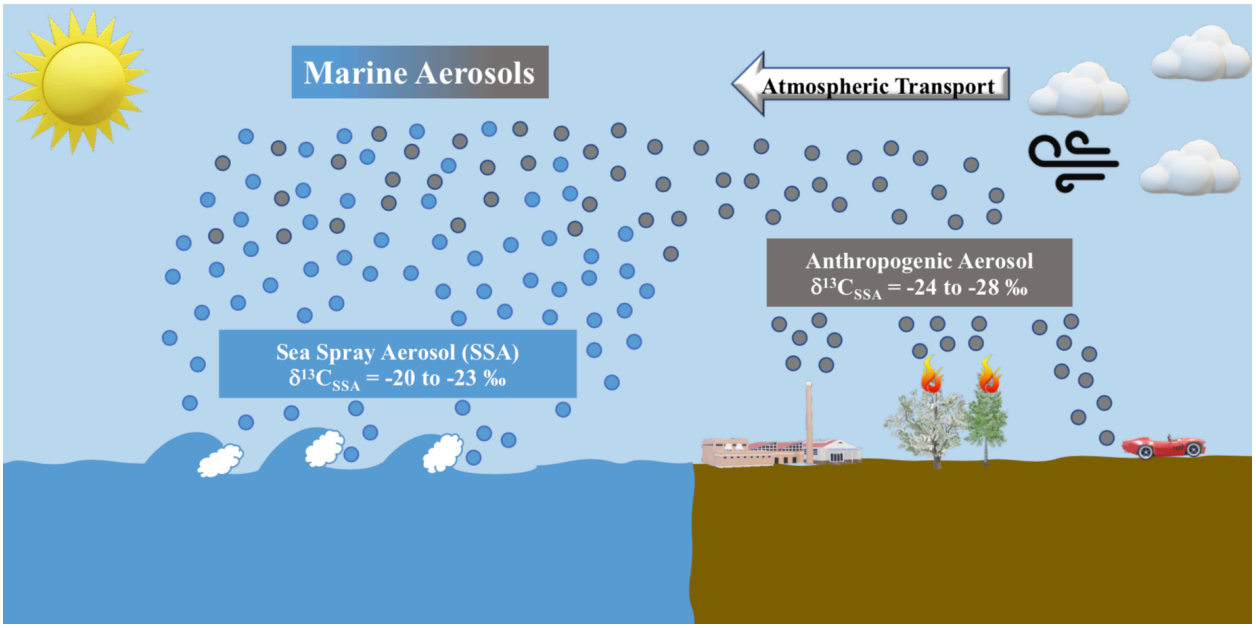

Figure 1.4 The contribution of sea spray and anthropogenic emissions to marine aerosols. Because $\delta^{13}C_{SSA}$ and $\delta^{13}C_{anth}$ have isotopically distinct values, their fractional contribution to the marine atmosphere can be estimated via Equation 1.3.[93–98]

By measuring the $\delta^{13}C$ of the total marine aerosol population ($\delta^{13}C_{marine}$), the fractional contributions of SSA and anthropogenic aerosol carbon (f_{SSA} and f_{anth}) can be estimated as long as

the $\delta^{13}C$ values for the two carbon reservoirs ($\delta^{13}C_{SSA}$ and $\delta^{13}C_{anth}$) are accurately known. When Chesselet et al.[94] first applied Equation 1.3 in 1981, they assumed that $\delta^{13}C_{SSA}$ was equivalent to the $\delta^{13}C$ value of oceanic dissolved organic material (around 21 ‰). Most of the marine aerosol source apportionment studies that followed have applied a similar value for $\delta^{13}C_{SSA}$ based on their work.[95–98] However, the recent observation of increased $\delta^{13}C$ values for marine aerosols during periods of elevated seawater biological activity,[93] suggests there may be more variability in $\delta^{13}C_{SSA}$ values than previously believed (Figure 1.3). A significant portion of this dissertation work is aimed at addressing how seawater biological activity can influence $\delta^{13}C_{SSA}$ and improving constraints on the likely range of nascent $\delta^{13}C_{SSA}$ values. Through this work, I demonstrate how improving our constraints on $\delta^{13}C_{SSA}$ will help to improve estimates of our anthropogenic influence on the marine environment.

1.5 References

(1) Kolb, C. E.; Worsnop, D. R. Chemistry and Composition of Atmospheric Aerosol Particles. *Annu. Rev. Phys. Chem.* **2012**, *63*, 471–491. https://doi.org/10.1146/annurev-physchem-032511-143706.

(2) McMurry, P. H. A Review of Atmospheric Aerosol Measurements. *Atmos. Environ.* **2000**, *34*, 1959–1999. https://doi.org/10.1016/S1474-8177(02)80020-1.

(3) Lighty, J. A. S.; Veranth, J. M.; Sarofim, A. F. Combustion Aerosols: Factors Governing Their Size and Composition and Implications to Human Health. *J. Air Waste Manag. Assoc.* **2000**, *50* (9), 1565–1618. https://doi.org/10.1080/10473289.2000.10464197.

(4) Axson, J. L.; May, N. W.; Colón-Bernal, I. D.; Pratt, K. A.; Ault, A. P. Lake Spray Aerosol: A Chemical Signature from Individual Ambient Particles. *Environ. Sci. Technol.* **2016**, *50* (18), 9835–9845. https://doi.org/10.1021/acs.est.6b01661.

(5) Bauer, S. E.; Tsigaridis, K.; Miller, R. Significant Atmospheric Aerosol Pollution Caused by World Food Cultivation. *Geophys. Res. Lett.* **2016**, *43* (10), 5394–5400. https://doi.org/10.1002/2016GL068354.

(6) Kroll, J. H.; Seinfeld, J. H. Chemistry of Secondary Organic Aerosol: Formation and Evolution of Low-Volatility Organics in the Atmosphere. *Atmos. Environ.* **2008**, *42* (16), 3593–3624. https://doi.org/10.1016/j.atmosenv.2008.01.003.

(7) Quinn, P. K.; Collins, D. B.; Grassian, V. H.; Prather, K. A.; Bates, T. S. Chemistry and Related Properties of Freshly Emitted Sea Spray Aerosol. *Chem. Rev.* **2015**, *115* (10), 4383–4399. https://doi.org/10.1021/cr500713g.

(8) Mills, M. J.; Schmidt, A.; Easter, R.; Solomon, S.; Kinnison, D. E.; Ghan, S. J.; Neely, R. R.; Marsh, D. R.; Conley, A.; Bardeen, C. G.; Gettelman, A. Global Volcanic Aerosol Properties Derived from Emissions, 1990–2014, Using CESM1(WACCM). *J. Geophys. Res.* **2016**, *121* (5), 2332–2348. https://doi.org/10.1002/2015JD024290.

(9) Middleton, N. J. Desert Dust Hazards: A Global Review. *Aeolian Res.* **2017**, *24*, 53–63. https://doi.org/10.1016/j.aeolia.2016.12.001.

(10) Pöschl, U. Atmospheric Aerosols: Composition, Transformation, Climate and Health Effects. *Angew. Chemie - Int. Ed.* **2005**, *44* (46), 7520–7540. https://doi.org/10.1002/anie.200501122.

(11) Maier, K. L.; Alessandrini, F.; Beck-Speier, I.; Hofer, T. P. J.; Diabaté, S.; Bitterle, E.; Stöger, T.; Jakob, T.; Behrendt, H.; Horsch, M.; Beckers, J.; Ziesenis, A.; Hültner, L.; Frankenberger, M.; Krauss-Etschmann, S.; Schulz, H. Health Effects of Ambient Particulate Matter - Biological Mechanisms and Inflammatory Responses to in Vitro and in Vivo Particle Exposures. *Inhal. Toxicol.* **2008**, *20* (3), 319–337. https://doi.org/10.1080/08958370701866313.

(12) Shindell, D.; Kuylenstierna, J. C. I.; Vignati, E.; Van Dingenen, R.; Amann, M.; Klimont, Z.; Anenberg, S. C.; Muller, N.; Janssens-Maenhout, G.; Raes, F.; Schwartz, J.; Faluvegi, G.; Pozzoli, L.; Kupiainen, K.; Höglund-Isaksson, L.; Emberson, L.; Streets, D.; Ramanathan, V.; Hicks, K.; Oanh, N. T. K.; Milly, G.; Williams, M.; Demkine, V.; Fowler, D. Simultaneously Mitigating Near-Term Climate Change and Improving Human Health and Food Security. *Science (80-.).* **2012**, *335* (6065), 183–189. https://doi.org/10.1126/science.1210026.

(13) Seposo, X.; Ueda, K.; Park, S. S.; Sudo, K.; Takemura, T.; Nakajima, T. Effect of Global Atmospheric Aerosol Emission Change on PM2.5-Related Health Impacts. *Glob. Health Action* **2019**, *12* (1), 1–12. https://doi.org/10.1080/16549716.2019.1664130.

(14) Penner, J. E.; Hegg, D.; Leaitch, R. Unraveling the Role of Aerosols in Climate Change. *Environ. Sci. Technol.* **2001**, *35* (15). https://doi.org/10.1021/es0124414.

(15) Hienola, A.; Partanen, A. I.; Pietikainen, J. P.; O'Donnell, D.; Korhonen, H.; Matthews, H. D.; Laaksonen, A. The Impact of Aerosol Emissions on the 1.5 °c Pathways. *Environ. Res. Lett.* **2018**, *13* (4). https://doi.org/10.1088/1748-9326/aab1b2.

(16) Samset, B. H.; Sand, M.; Smith, C. J.; Bauer, S. E.; Forster, P. M.; Fuglestvedt, J. S.; Osprey, S.; Schleussner, C. F. Climate Impacts From a Removal of Anthropogenic Aerosol Emissions. *Geophys. Res. Lett.* **2018**, *45* (2), 1020–1029. https://doi.org/10.1002/2017GL076079.

(17) McNeill, V. F. Atmospheric Aerosols: Clouds, Chemistry, and Climate. *Annu. Rev. Chem. Biomol. Eng.* **2017**, *8*, 427–444. https://doi.org/10.1146/annurev-chembioeng-060816-101538.

(18) Boucher, O.; Randall, D.; Artaxo, P.; Bretherton, C.; Feingold, G.; Forster, P.; Kerminen, V.-M.; Kondo, Y.; Liao, H.; Lohmann, U.; Rasch, P.; Satheesh, S. K.; Sherwood, S.; Bjorn, S.; Zhang, X.-Y. *Clouds and Aerosols*; Stocker, T. F., Qin, D., Plattner, G.-K., Tignor, M., Allen, S. K., Boschung, J., Nauels, A., Xia, Y., Bex, V., Midgley, P. M., Eds.; Cambridge Univeristy Press: Cambridge, 2013. https://doi.org/10.1017/CBO9781107415324.016.

(19) Myhre, G.; Shindell, D.; Breon, F.-M.; Collins, W.; Fuglestvedt, J.; Huang, J.; Koch, D.; Lamarque, J.-F.; Lee, D.; Mendoza, B.; Nakajima, T.; Robock, A.; Stephens, G.; Takemura, T. *Anthropogenic and Natural Radiative Forcing*, Stocker, T.; Cambridge University Press: Cambridge, 2013. https://doi.org/10.1017/CBO9781107415324.018.

(20) Myhre, G.; Myhre, C. L.; Samset, B. H.; Storelvmo, T. Aerosols and Their Relation to Global Climate and Climate Sensitivity. *Nat. Educ. Knowl.* **2013**, *4* (5).

(21) Farmer, D. K.; Cappa, C. D.; Kreidenweis, S. M. Atmospheric Processes and Their Controlling Influence on Cloud Condensation Nuclei Activity. *Chem. Rev.* **2015**, *115* (10), 4199–4217. https://doi.org/10.1021/cr5006292.

(22) Petters, M. D.; Kreidenweis, S. M. A Single Parameter Representation of Hygroscopic Growth and Cloud Condensation Nucleus Activity-Part 3: Including Surfactant Partitioning. *Atmos. Chem. Phys.* **2013**, *13* (2), 1081–1091. https://doi.org/10.5194/acp-13-1081-2013.

(23) Schill, S. R.; Collins, D. B.; Lee, C.; Morris, H. S.; Novak, G. A.; Prather, K. A.; Quinn, P. K.; Sultana, C. M.; Tivanski, A. V.; Zimmermann, K.; Cappa, C. D.; Bertram, T. H. The Impact of Aerosol Particle Mixing State on the Hygroscopicity of Sea Spray Aerosol. *ACS Cent. Sci.* **2015**, *1* (3), 132–141. https://doi.org/10.1021/acscentsci.5b00174.

(24) Jing, B.; Peng, C.; Wang, Y.; Liu, Q.; Tong, S.; Zhang, Y.; Ge, M. Hygroscopic Properties of Potassium Chloride and Its Internal Mixtures with Organic Compounds Relevant to Biomass Burning Aerosol Particles. *Sci. Rep.* **2017**, *7* (January), 1–11. https://doi.org/10.1038/srep43572.

(25) Hodas, N.; Zuend, A.; Mui, W.; Flagan, R. C.; Seinfeld, J. H. Influence of Particle-Phase State on the Hygroscopic Behavior of Mixed Organic-Inorganic Aerosols. *Atmos. Chem. Phys.* **2015**, *15* (9), 5027–5045. https://doi.org/10.5194/acp-15-5027-2015.

(26) Carslaw, K. S.; Lee, L. A.; Reddington, C. L.; Pringle, K. J.; Rap, A.; Forster, P. M.; Mann, G. W.; Spracklen, D. V.; Woodhouse, M. T.; Regayre, L. A.; Pierce, J. R. Large

Contribution of Natural Aerosols to Uncertainty in Indirect Forcing. *Nature* **2013**, *503* (7474), 67–71. https://doi.org/10.1038/nature12674.

(27) Satheesh, S. K.; Krishna Moorthy, K. Radiative Effects of Natural Aerosols: A Review. *Atmos. Environ.* **2005**, *39* (11), 2089–2110. https://doi.org/10.1016/j.atmosenv.2004.12.029.

(28) Gong, S. L.; Barrie, L. A.; Blanchet, J. P.; von Salzen, K.; Lohmann, U.; Lesins, G.; Spacek, L.; Zhang, L. M.; Girard, E.; Lin, H.; Leaitch, R.; Leighton, H.; Chylek, P.; Huang, P. Canadian Aerosol Module: A Size-Segregated Simulation of Atmospheric Aerosol Processes for Climate and Air Quality Models 1. Module Development. *J. Geophys. Res. Atmos.* **2003**, *108* (1). https://doi.org/10.1029/2001jd002002.

(29) De Leeuw, G.; Andreas, E. L.; Anguelova, M. D.; Fairall, C. W.; Lewis, E. R.; O'Dowd, C.; Schulz, M.; Schwartz, S. E. Production Flux of Sea Spray Aerosol. *Rev. Geophys.* **2011**, *49* (2), 1–39. https://doi.org/10.1029/2010RG000349.

(30) Bertram, T. H.; Cochran, R. E.; Grassian, V. H.; Stone, E. A. Sea Spray Aerosol Chemical Composition: Elemental and Molecular Mimics for Laboratory Studies of Heterogeneous and Multiphase Reactions. *Chem. Soc. Rev.* **2018**, *47* (7), 2374–2400. https://doi.org/10.1039/c7cs00008a.

(31) Wang, X.; Deane, G. B.; Moore, K. A.; Ryder, O. S.; Stokes, M. D.; Beall, C. M.; Collins, D. B.; Santander, M. V.; Burrows, S. M.; Sultana, C. M.; Prather, K. A. The Role of Jet and Film Drops in Controlling the Mixing State of Submicron Sea Spray Aerosol Particles. *PNAS* **2017**, *114* (27), 6978–6983. https://doi.org/10.1073/pnas.1702420114.

(32) Cunliffe, M.; Engel, A.; Frka, S.; Gašparović, B. Ž.; Guitart, C.; Murrell, J. C.; Salter, M.; Stolle, C.; Upstill-Goddard, R.; Wurl, O. Sea Surface Microlayers: A Unified Physicochemical and Biological Perspective of the Air-Ocean Interface. *Prog. Oceanogr.* **2013**, *109*, 104–116. https://doi.org/10.1016/j.pocean.2012.08.004.

(33) Wurl, O.; Miller, L.; Röttgers, R.; Vagle, S. The Distribution and Fate of Surface-Active Substances in the Sea-Surface Microlayer and Water Column. *Mar. Chem.* **2009**, *115* (1–2), 1–9. https://doi.org/10.1016/j.marchem.2009.04.007.

(34) O'Dowd, C. D.; Facchini, M. C.; Cavalli, F.; Ceburnis, D.; Mircea, M.; Decesari, S.; Fuzzi, S.; Young, J. Y.; Putaud, J. P. Biogenically Driven Organic Contribution to Marine Aerosol. *Nature* **2004**, *431* (7009), 676–680. https://doi.org/10.1038/nature02959.

(35) Rinaldi, M.; Fuzzi, S.; Decesari, S.; Marullo, S.; Santoleri, R.; Provenzale, A.; Von Hardenberg, J.; Ceburnis, D.; Vaishya, A.; O'Dowd, C. D.; Facchini, M. C. Is Chlorophyll-a the Best Surrogate for Organic Matter Enrichment in Submicron Primary Marine Aerosol? *J. Geophys. Res. Atmos.* **2013**, *118* (10), 4964–4973. https://doi.org/10.1002/jgrd.50417.

(36) Quinn, P. K.; Bates, T. S.; Schulz, K. S.; Coffman, D. J.; Frossard, A. A.; Russell, L. M.;

Keene, W. C.; Kieber, D. J. Contribution of Sea Surface Carbon Pool to Organic Matter Enrichment in Sea Spray Aerosol. *Nat. Geosci.* **2014**, *7* (3), 228–232. https://doi.org/10.1038/ngeo2092.

(37) Bates, T. S.; Quinn, P. K.; Coffman, D. J.; Johnson, J. E.; Upchurch, L.; Saliba, G.; Lewis, S.; Graff, J.; Russell, L. M.; Behrenfeld, M. J. Variability in Marine Plankton Ecosystems Are Not Observed in Freshly Emitted Sea Spray Aerosol Over the North Atlantic Ocean. *Geophys. Res. Lett.* **2020**, *47* (1). https://doi.org/10.1029/2019GL085938.

(38) Miyazaki, Y.; Yamashita, Y.; Kawana, K.; Tachibana, E.; Kagami, S.; Mochida, M.; Suzuki, K.; Nishioka, J. Chemical Transfer of Dissolved Organic Matter from Surface Seawater to Sea Spray Water-Soluble Organic Aerosol in the Marine Atmosphere. *Sci. Rep.* **2018**, *8* (1), 1–10. https://doi.org/10.1038/s41598-018-32864-7.

(39) Ovadnevaite, J.; O'Dowd, C.; Dall'Osto, M.; Ceburnis, D.; Worsnop, D. R.; Berresheim, H. Detecting High Contributions of Primary Organic Matter to Marine Aerosol: A Case Study. *Geophys. Res. Lett.* **2011**, *38* (2), 2–6. https://doi.org/10.1029/2010GL046083.

(40) Sciare, J.; Favez, O.; Sarda-Estève, R.; Oikonomou, K.; Cachier, H.; Kazan, V. Long-Term Observations of Carbonaceous Aerosols in the Austral Ocean Atmosphere: Evidence of a Biogenic Marine Organic Source. *J. Geophys. Res. Atmos.* **2009**, *114* (15), 1–10. https://doi.org/10.1029/2009JD011998.

(41) Zhang, X.; Massoli, P.; Quinn, P. K.; Bates, T. S.; Cappa, C. D. Journal of Geophysical Research : Atmospheres Aerosols in the Marine Boundary Layer. **2014**, No. 1, 8384–8399. https://doi.org/10.1002/2013JD021213.Received.

(42) Cavalli, F.; Facchini, M. C.; Decesari, S.; Mircea, M.; Emblico, L.; Fuzzi, S.; Ceburnis, D.; Yoon, Y. J.; O'Dowd, C. D.; Putaud, J. P.; Dell'Acqua, A. Advances in Characterization of Size-Resolved Organic Matter in Marine Aerosol over the North Atlantic. *J. Geophys. Res. D Atmos.* **2004**, *109* (24), 1–14. https://doi.org/10.1029/2004JD005137.

(43) Vaishya, A.; Ovadnevaite, J.; Bialek, J.; Jennings, S. G.; Ceburnis, D.; O'Dowd, C. D. Bistable Effect of Organic Enrichment on Sea Spray Radiative Properties. *Geophys. Res. Lett.* **2013**, *40* (24), 6395–6398. https://doi.org/10.1002/2013GL058452.

(44) Gantt, B.; Meskhidze, N. The Physical and Chemical Characteristics of Marine Primary Organic Aerosol: A Review. *Atmos. Chem. Phys.* **2013**, *13* (8), 3979–3996. https://doi.org/10.5194/acp-13-3979-2013.

(45) Ovadnevaite, J.; Ceburnis, D.; Martucci, G.; Bialek, J.; Monahan, C.; Rinaldi, M.; Facchini, M. C.; Berresheim, H.; Worsnop, D. R.; O'Dowd, C. Primary Marine Organic Aerosol: A Dichotomy of Low Hygroscopicity and High CCN Activity. *Geophys. Res. Lett.* **2011**, *38* (21), 1–5. https://doi.org/10.1029/2011GL048869.

(46) Rinaldi, M.; Decesari, S.; Finessi, E.; Giulianelli, L.; Carbone, C.; Fuzzi, S.; O'Dowd, C.

D.; Ceburnis, D.; Facchini, M. C. Primary and Secondary Organic Marine Aerosol and Oceanic Biological Activity: Recent Results and New Perspectives for Future Studies. *Adv. Meteorol.* **2010**, *2010*, 1–10. https://doi.org/10.1155/2010/310682.

(47) Creamean, J. M.; Cross, J. N.; Pickart, R.; McRaven, L.; Lin, P.; Pacini, A.; Hanlon, R.; Schmale, D. G.; Ceniceros, J.; Aydell, T.; Colombi, N.; Bolger, E.; DeMott, P. J. Ice Nucleating Particles Carried From Below a Phytoplankton Bloom to the Arctic Atmosphere. *Geophys. Res. Lett.* **2019**, *46* (14), 8572–8581. https://doi.org/10.1029/2019GL083039.

(48) Shank, L. M.; Howell, S.; Clarke, A. D.; Freitag, S.; Brekhovskikh, V.; Kapustin, V.; McNaughton, C.; Campos, T.; Wood, R. Organic Matter and Non-Refractory Aerosol over the Remote Southeast Pacific: Oceanic and Combustion Sources. *Atmos. Chem. Phys.* **2012**, *12* (1), 557–576. https://doi.org/10.5194/acp-12-557-2012.

(49) Fuentes, E.; Coe, H.; Green, D.; De Leeuw, G.; McFiggans, G. Laboratory-Generated Primary Marine Aerosol via Bubble-Bursting and Atomization. *Atmos. Meas. Tech.* **2010**, *3* (1), 141–162. https://doi.org/10.5194/amt-3-141-2010.

(50) Sauer, J. S.; Mayer, K. J.; Lee, C.; Alves, M. R.; Amiri, S.; Bahaveolos, C.; Barnes, E. B.; Crocker, D. R.; Dinasquet, J.; Garofalo, L. A.; Kaluarachchi, C. P.; Dang, D.; Kilgour, D.; Mael, L.; Mitts, B. A.; Moon, D. R.; Morris, C. K.; Moore, A. N.; Ni, C.-M.; Pendergraft, M. A.; Petras, D.; Simpson, R.; Smith, S.; Tumminello, P. R.; Walker, J. L.; DeMott, P. J.; Farmer, D. K.; Goldstein, A. H.; Grassian, V. H.; Jaffe, J. S.; Malfatti, F.; Martz, T. R.; Slade, J.; Tivanski, A. V.; Bertram, T. H.; Cappa, C. D.; Prather, K. A. The Sea Spray Chemistry and Particle Evolution Study (SeaSCAPE): Overview and Experimental Methods. *Environ. Sci. Process. Impacts* **2021**.

(51) Prather, K. A.; Bertram, T. H.; Grassian, V. H.; Deane, G. B.; Stokes, M. D.; DeMott, P. J.; Aluwihare, L. I.; Palenik, B. P.; Azam, F.; Seinfeld, J. H.; Moffet, R. C.; Molina, M. J.; Cappa, C. D.; Geiger, F. M.; Roberts, G. C.; Russell, L. M.; Ault, A. P.; Baltrusaitis, J.; Collins, D. B.; Corrigan, C. E.; Cuadra-Rodriguez, L. A.; Ebben, C. J.; Forestieri, S. D.; Guasco, T. L.; Hersey, S. P.; Kim, M. J.; Lambert, W. F.; Modini, R. L.; Mui, W.; Pedler, B. E.; Ruppel, M. J.; Ryder, O. S.; Schoepp, N. G.; Sullivan, R. C.; Zhao, D. Bringing the Ocean into the Laboratory to Probe the Chemical Complexity of Sea Spray Aerosol. *PNAS* **2013**, *110* (19), 7550–7555. https://doi.org/10.1073/pnas.1300262110.

(52) Stokes, M. D.; Deane, G. B.; Prather, K.; Bertram, T. H.; Ruppel, M. J.; Ryder, O. S.; Brady, J. M.; Zhao, D. A Marine Aerosol Reference Tank System as a Breaking Wave Analogue for the Production of Foam and Sea-Spray Aerosols. *Atmos. Meas. Tech.* **2013**, *6* (4), 1085–1094. https://doi.org/10.5194/amt-6-1085-2013.

(53) Lee, C.; Sultana, C. M.; Collins, D. B.; Santander, M. V.; Axson, J. L.; Malfatti, F.; Cornwell, G. C.; Grandquist, J. R.; Deane, G. B.; Stokes, M. D.; Azam, F.; Grassian, V. H.; Prather, K. A. Advancing Model Systems for Fundamental Laboratory Studies of Sea Spray Aerosol Using the Microbial Loop. *J. Phys. Chem. A* **2015**, *119* (33), 8860–8870. https://doi.org/10.1021/acs.jpca.5b03488.

(54) Azam, F.; Fenchel, T.; Field, J.; Gray, J.; Meyer-Reil, L.; Thingstad, F. The Ecological Role of Water-Column Microbes in the Sea. *Mar. Ecol. Prog. Ser.* **1983**, *10*, 257–263. https://doi.org/10.3354/meps010257.

(55) Pomeroy, L. R.; le Williams, P. J. B.; Azam, F.; Hobbie, J. E. The Microbial Loop. *Oceanography* **2007**, *20* (SPL.ISS. 2), 28–33. https://doi.org/10.5670/oceanog.2007.45.

(56) Wang, X.; Sultana, C. M.; Trueblood, J.; Hill, T. C. J.; Malfatti, F.; Lee, C.; Laskina, O.; Moore, K. A.; Beall, C. M.; McCluskey, C. S.; Cornwell, G. C.; Zhou, Y.; Cox, J. L.; Pendergraft, M. A.; Santander, M. V.; Bertram, T. H.; Cappa, C. D.; Azam, F.; DeMott, P. J.; Grassian, V. H.; Prather, K. A. Microbial Control of Sea Spray Aerosol Composition: A Tale of Two Blooms. *ACS Cent. Sci.* **2015**, *1* (3), 124–131. https://doi.org/10.1021/acscentsci.5b00148.

(57) Cochran, R. E.; Laskina, O.; Jayarathne, T.; Laskin, A.; Laskin, J.; Lin, P.; Sultana, C.; Lee, C.; Moore, K. A.; Cappa, C. D.; Bertram, T. H.; Prather, K. A.; Grassian, V. H.; Stone, E. A. Analysis of Organic Anionic Surfactants in Fine and Coarse Fractions of Freshly Emitted Sea Spray Aerosol. *Environ. Sci. Technol.* **2016**, *50* (5), 2477–2486. https://doi.org/10.1021/acs.est.5b04053.

(58) Forestieri, S. D.; Cornwell, G. C.; Helgestad, T. M.; Moore, K. A.; Lee, C.; Novak, G. A.; Sultana, C. M.; Wang, X.; Bertram, T. H.; Prather, K. A.; Cappa, C. D. Linking Variations in Sea Spray Aerosol Particle Hygroscopicity to Composition during Two Microcosm Experiments. *Atmos. Chem. Phys.* **2016**, *16* (14), 9003–9018. https://doi.org/10.5194/acp-16-9003-2016.

(59) Cochran, R. E.; Laskina, O.; Trueblood, J. V.; Estillore, A. D.; Morris, H. S.; Jayarathne, T.; Sultana, C. M.; Lee, C.; Lin, P.; Laskin, J.; Laskin, A.; Dowling, J. A.; Qin, Z.; Cappa, C. D.; Bertram, T. H.; Tivanski, A. V.; Stone, E. A.; Prather, K. A.; Grassian, V. H. Molecular Diversity of Sea Spray Aerosol Particles: Impact of Ocean Biology on Particle Composition and Hygroscopicity. *Chem* **2017**, *2* (5), 655–667. https://doi.org/10.1016/j.chempr.2017.03.007.

(60) DeMott, P. J.; Hill, T. C. J.; McCluskey, C. S.; Prather, K. A.; Collins, D. B.; Sullivan, R. C.; Ruppel, M. J.; Mason, R. H.; Irish, V. E.; Lee, T.; Hwang, C. Y.; Rhee, T. S.; Snider, J. R.; McMeeking, G. R.; Dhaniyala, S.; Lewis, E. R.; Wentzell, J. J. B.; Abbatt, J.; Lee, C.; Sultana, C. M.; Ault, A. P.; Axson, J. L.; Martinez, M. D.; Venero, I.; Santos-Figueroa, G.; Stokes, M. D.; Deane, G. B.; Mayol-Bracero, O. L.; Grassian, V. H.; Bertram, T. H.; Bertram, A. K.; Moffett, B. F.; Franc, G. D. Sea Spray Aerosol as a Unique Source of Ice Nucleating Particles. *PNAS* **2016**, *113* (21), 5797–5803. https://doi.org/10.1073/pnas.1514034112.

(61) Alpert, P. A.; Aller, J. Y.; Knopf, D. A. Ice Nucleation from Aqueous NaCl Droplets with and without Marine Diatoms. *Atmos. Chem. Phys.* **2011**, *11* (12), 5539–5555. https://doi.org/10.5194/acp-11-5539-2011.

(62) Knopf, D. A.; Alpert, P. A.; Wang, B.; Aller, J. Y. Stimulation of Ice Nucleation by Marine Diatoms. *Nat. Geosci.* **2011**, *4* (2), 88–90. https://doi.org/10.1038/ngeo1037.

(63) McCluskey, C. S.; Hill, E. T. C. J.; Sultana, C. M.; Laskina, O.; Trueblood, J.; Santander, M. V.; Beall, C. M.; Michaud, J. M.; Kreidenweis, S. M.; Prather, K. A.; Grassian, V.; Demott, P. J. A Mesocosm Double Feature: Insights into the Chemical Makeup of Marine Ice Nucleating Particles. *J. Atmos. Sci.* **2018**, *75* (7), 2405–2423. https://doi.org/10.1175/JAS-D-17-0155.1.

(64) Mitts, B. A.; Wang, X.; Lucero, D. D.; Beall, C. M.; Deane, G. B.; DeMott, P. J.; Prather, K. A. Importance of Supermicron Ice Nucleating Particles in Nascent Sea Spray. *Geophys. Res. Lett.* **2021**, *48* (3). https://doi.org/10.1029/2020GL089633.

(65) McCluskey, C. S.; Hill, T. C. J.; Malfatti, F.; Sultana, C. M.; Lee, C.; Santander, M. V.; Beall, C. M.; Moore, K. A.; Cornwell, G. C.; Collins, D. B.; Prather, K. A.; Jayarathne, T.; Stone, E. A.; Azam, F.; Kreidenweis, S. M.; DeMott, P. J. A Dynamic Link between Ice Nucleating Particles Released in Nascent Sea Spray Aerosol and Oceanic Biological Activity during Two Mesocosm Experiments. *J. Atmos. Sci.* **2017**, *74* (1), 151–166. https://doi.org/10.1175/JAS-D-16-0087.1.

(66) King, A.; Birge, R. EVIDENCE FROM BAND SPECTRA OF THE EXISTENCE OF A CARBON ISOTOPE OF MASS 13. *Astrophys. J.* **1930**, *72*, 19–40.

(67) Bobrovnikoff, N. T. Carbon Isotopes in Comets. *Publ. Astron. Soc. Pacific* **1930**, *42* (246), 117–121.

(68) Nier, A. O.; Gulbransen, E. A. Variations in the Relative Abundance of the Carbon Isotopes. *J. Am. Chem. Soc.* **1939**, *61*, 697–698. https://doi.org/10.1190/1.1437185.

(69) Craig, H. The Geochemistry of the Stable Carbon Isotopes. *Geochim. Cosmochim. Acta* **1953**, *3* (2–3), 53–92. https://doi.org/10.1016/0016-7037(53)90001-5.

(70) O'Leary, M. H. Carbon Isotope Fractionation in Plants. *Phytochemistry* **1981**, *20* (4), 553–567. https://doi.org/10.1016/0031-9422(81)85134-5.

(71) Urey, H. C. The Thermodynamic Properties of Isotopic Substances. *J. Chem. Soc.* **1947**, 562–581.

(72) Bigeleisen, J.; Mayer, M. Calculation of Equilibrium Constants for Isotopic Exchange Reactions. *J. Chem. Phys.* **1947**, *15* (5), 261–267.

(73) Nier, A. O. A Mass Spectrometer for Isotope and Gas Analysis. *Rev. Sci. Instrum.* **1947**, *18* (6), 398–411. https://doi.org/10.1063/1.1740961.

(74) McKinney, C. R.; McCrea, J. M.; Epstein, S.; Allen, H. A.; Urey, H. C. Improvements in Mass Spectrometers for the Measurement of Small Differences in Isotope Abundance

Ratios. *Rev. Sci. Instrum.* **1950**, *21* (8), 724–730.

(75) Craig, H. Isotopic Standards for Carbon and Oxygen and Correction Factors for Mass-Spectrometric Analysis of Carbon Dioxide. *Geochim. Cosmochim. Acta* **1957**, *12* (1–2), 133–149. https://doi.org/10.1016/0016-7037(57)90024-8.

(76) Bigeleisen, J. The Relative Reaction Velocities of Isotopic Molecules. *J. Chem. Phys.* **1949**, *17* (8), 675–678. https://doi.org/10.1063/1.1747368.

(77) Arrhenius, S. Über Die Dissociationswärme Und Den Einfluss Der Temperatur Auf Den Dissociationsgrad Der Elektrolyte. *Zeitschrift für Phys. Chemie* **1889**, *4U* (1), 96–116. https://doi.org/10.1515/zpch-1889-0408.

(78) Arrhenius, S. Über Die Reaktionsgeschwindigkeit Bei Der Inversion von Rohrzucker Durch Säuren. *Zeitschrift für Phys. Chemie* **1889**, *4U* (1), 226–248. https://doi.org/10.1515/zpch-1889-0416.

(79) DESCOLAS-GROS, C.; FONTUGNE, M. Stable Carbon Isotope Fractionation by Marine Phytoplankton during Photosynthesis. *Plant. Cell Environ.* **1990**, *13* (3), 207–218. https://doi.org/10.1111/j.1365-3040.1990.tb01305.x.

(80) O'Leary, M. H. Carbon Isotopes in Photosynthesis. *Bioscience* **1988**, *38* (5), 328–336. https://doi.org/10.2307/1310735.

(81) Degens, E. T.; Behrendt, M.; Gotthardt, B.; Reppmann, E. Metabolic Fractionation of Carbon Isotopes in Marine Plankton-II. Data on Samples Collected off the Coasts of Peru and Ecuador. *Deep. Res. Oceanogr. Abstr.* **1968**, *15* (1), 11–20. https://doi.org/10.1016/0011-7471(68)90025-9.

(82) Cheng, L.; Normandeau, C.; Bowden, R.; Doucett, R.; Gallagher, B.; Gillikin, D. P.; Kumamoto, Y.; McKay, J. L.; Middlestead, P.; Ninnemann, U.; Nothaft, D.; Dubinina, E. O.; Quay, P.; Reverdin, G.; Shirai, K.; Mørkved, P. T.; Theiling, B. P.; van Geldern, R.; Wallace, D. W. R. An International Intercomparison of Stable Carbon Isotope Composition Measurements of Dissolved Inorganic Carbon in Seawater. *Limnol. Oceanogr. Methods* **2019**, *17* (3), 200–209. https://doi.org/10.1002/lom3.10300.

(83) Kharbush, J. J.; Close, H. G.; Van Mooy, B. A. S.; Arnosti, C.; Smittenberg, R. H.; Le Moigne, F. A. C.; Mollenhauer, G.; Scholz-Böttcher, B.; Obreht, I.; Koch, B. P.; Becker, K. W.; Iversen, M. H.; Mohr, W. Particulate Organic Carbon Deconstructed: Molecular and Chemical Composition of Particulate Organic Carbon in the Ocean. *Front. Mar. Sci.* **2020**, *7* (June), 1–10. https://doi.org/10.3389/fmars.2020.00518.

(84) Smith, D.; Simon, M.; Alldredge, A.; Azam, F. Intense Hydrolytic Enzyme Activity on Marine Aggregates and Implications for Rapid Particle Dissolution. *Nature* **1992**, *359* (6391), 139–142. https://doi.org/10.1038/246170a0.

(85) Fry, B.; Hopkinson, C. S.; Nolin, A.; Wainright, S. C. 13C/12C Composition of Marine

Dissolved Organic Carbon. *Chem. Geol.* **1998**, *152* (1–2), 113–118. https://doi.org/10.1016/S0009-2541(98)00100-4.

(86) Eadie, B. J.; Jeffrey, L. M.; Sackett, W. M. Some Observations on the Stable Carbon Isotope Composition of Dissolved and Particulate Organic Carbon in the Marine Environment. *Geochim. Cosmochim. Acta* **1978**, *42* (8), 1265–1269. https://doi.org/10.1016/0016-7037(78)90120-5.

(87) Hinga, K. R.; Arthur, M. A.; Pilson, M. E. Q.; Whitaker, D. Carbon Isotope Fractionation by Marine Phytoplankton in Culture: The Effects of CO2 Concentration, PH, Temperature, and Species. *Global Biogeochem. Cycles* **1994**, *8* (1), 91–102. https://doi.org/10.1029/93GB03393.

(88) Rau, G. H.; Takahashi, T.; Des Marais, D. J.; Repeta, D. J.; Martin, J. H. The Relationship between Δ13C of Organic Matter and [CO2(Aq)] in Ocean Surface Water: Data from a JGOFS Site in the Northeast Atlantic Ocean and a Model. *Geochim. Cosmochim. Acta* **1992**, *56* (3), 1413–1419. https://doi.org/10.1016/0016-7037(92)90073-R.

(89) Kukert, H.; Riebesell, U. Phytoplankton Carbon Isotope Fractionation during a Diatom Spring Bloom in a Norwegian Fjord. *Mar. Ecol. Prog. Ser.* **1998**, *173*, 127–137. https://doi.org/10.3354/meps173127.

(90) Esposito, M.; Achterberg, E. P.; Bach, L. T.; Connelly, D. P.; Riebesell, U.; Taucher, J. Application of Stable Carbon Isotopes in a Subtropical North Atlantic MesocosmStudy: A New Approach to Assess CO2 Effects on the Marine Carbon Cycle. *Front. Mar. Sci.* **2019**, *6* (October), 1–17. https://doi.org/10.3389/fmars.2019.00616.

(91) Ceburnis, D.; Masalaite, A.; Ovadnevaite, J.; Garbaras, A.; Remeikis, V.; Maenhaut, W.; Claeys, M.; Sciare, J.; Baisnée, D.; O'Dowd, C. D. Stable Isotopes Measurements Reveal Dual Carbon Pools Contributing to Organic Matter Enrichment in Marine Aerosol. *Sci. Rep.* **2016**, *6* (July), 1–6. https://doi.org/10.1038/srep36675.

(92) Miyazaki, Y.; Kawamura, K.; Jung, J.; Furutani, H.; Uematsu, M. Latitudinal Distributions of Organic Nitrogen and Organic Carbon in Marine Aerosols over the Western North Pacific. *Atmos. Chem. Phys.* **2011**, *11* (7), 3037–3049. https://doi.org/10.5194/acp-11-3037-2011.

(93) Ceburnis, D.; Garbaras, A.; Szidat, S.; Rinaldi, M.; Fahrni, S.; Perron, N.; Wacker, L.; Leinert, S.; Remeikis, V.; Facchini, M. C.; Prevot, A. S. H.; Jennings, S. G.; Ramonet, M.; O'Dowd, C. D. Quantification of the Carbonaceous Matter Origin in Submicron Marine Aerosol by 13C and 14C Isotope Analysis. *Atmos. Chem. Phys.* **2011**, *11* (16), 8593–8606. https://doi.org/10.5194/acp-11-8593-2011.

(94) Chesselet, R.; Fontugne, M.; Buat-Menard, P.; Esat, U.; Lambert, C. E. The Origin of Particulate Organic Carbon in the Marine Atmosphere as Indicated by Its Stable Carbon Isotopic Composition. **1981**, *8* (4), 345–348.

(95) Cachier, H.; Buat-Menard, P.; Fontugne, M.; Chesselet, R. Long-range Transport of Continentally-derived Particulate Carbon in the Marine Atmosphere: Evidence from Stable Carbon Isotope Studies. *Tellus B* **1986**, *38 B* (3–4), 161–177. https://doi.org/10.1111/j.1600-0889.1986.tb00184.x.

(96) Turekian, V. C.; Macko, S. A.; Keene, W. C. Concentrations, Isotopic Compositions, and Sources of Size-Resolved, Particulate Organic Carbon and Oxalate in near-Surface Marine Air at Bermuda during Spring. *J. Geophys. Res. Atmos.* **2003**, *108* (5). https://doi.org/10.1029/2002jd002053.

(97) Miyazaki, Y.; Kawamura, K.; Sawano, M. Size Distributions of Organic Nitrogen and Carbon in Remote Marine Aerosols: Evidence of Marine Biological Origin Based on Their Isotopic Ratios. *Geophys. Res. Lett.* **2010**, *37* (6). https://doi.org/10.1029/2010GL042483.

(98) Kundu, S.; Kawamura, K. Seasonal Variations of Stable Carbon Isotopic Composition of Bulk Aerosol Carbon from Gosan Site, Jeju Island in the East China Sea. *Atmos. Environ.* **2014**, *94*, 316–322. https://doi.org/10.1016/j.atmosenv.2014.05.045.

Chapter 2: Biological Influences on $\delta^{13}C$ and Organic Composition of Nascent Sea Spray Aerosol

2.1 Abstract

Elucidating the influence of oceanic biological activity on the organic composition of sea spray aerosol (SSA) is crucial to understanding marine cloud properties relevant to climate. Numerous marine field studies designed to address this topic have yielded conflicting results mainly due to an inability to distinguish primary SSA composition from terrestrial and marine secondary organic aerosols. In this study, two laboratory-induced phytoplankton blooms were conducted in an isolated system without background aerosol contributions. Values for $\delta^{13}C$ were measured for SSA ($\delta^{13}C_{SSA}$) along with seawater particulate and dissolved organic carbon ($\delta^{13}C_{POC}$ and $\delta^{13}C_{DOC}$) to track changes in carbon transfer and composition between seawater and SSA. Contrary to common assumptions, $\delta^{13}C_{SSA}$ values were not equivalent to $\delta^{13}C_{DOC}$. The consistently less negative $\delta^{13}C_{SSA}$ values indicate nascent $\delta^{13}C_{SSA}$ reflects specific changes in relative contributions to SSA from the available seawater carbon pools, as a function of biological activity. A dual-source isotopic mixing model revealed the difference between $\delta^{13}C_{SSA}$ and $\delta^{13}C_{DOC}$ was explained by increased relative contributions of freshly produced OC to SSA, with the largest contribution of freshly produced OC occurring 2-3 days after the maximum chlorophyll-a concentrations. This finding is consistent with previous mesocosm studies showing organic enrichment in SSA requires processing by heterotrophic bacteria after periods of high primary productivity. This work examining the biological influences on SSA organic composition and nascent $\delta^{13}C_{SSA}$ values provides new insights into ocean-aerosol carbon transfer dynamics, which can be used in future field studies to improve estimates of anthropogenic influences on the marine environment.

2.2 Introduction

Sea spray aerosol (SSA), formed by bubbles bursting at the ocean surface, are one of the most abundant aerosol types globally.[1,2] SSA covers a broad size range from 0.01 to >10 μm in diameter,[3] and consists of complex mixtures of inorganic ions, organic molecules, and marine microorganisms (e.g. phytoplankton, bacteria, viruses) found in the ocean.[4–6] Earth's radiative budget is impacted by SSA through direct scattering of sunlight and by seeding clouds, and the extent to which SSA affects the Earth's radiative budget depends on particle size, number concentration, and chemical composition.[7–9] Higher SSA organic carbon (OC_{SSA}) content has been shown to decrease hygroscopic growth factors, and reduce the light scattering ability of SSA.[10] Additionally, the ice nucleation ability of SSA is strongly controlled by specific organic and biological species,[11,12] highlighting the importance of organic composition in predicting SSA's impact on clouds and climate.

The basic principles controlling SSA formation and organic enrichment have been extensively studied with air entrainment from breaking waves forming bubbles, which then rise scavenging organic material during their ascent to the air-sea interface.[13–15] SSA is primarily formed by two separate mechanisms when bubbles burst at the ocean surface: 1) bursting of the bubble film, the top part that protrudes from the ocean surface, and 2) collapse of the bubble cavity producing SSA from the base of the bubble.[16] Because SSA formation takes place at the air-sea interface, the sea surface microlayer (SSML)—the top 1-1000 μm of the ocean enriched with organic compounds—plays an integral role in ocean-aerosol transfer of organic species.[17,18] During a bubble's ascent, organic material accumulates on the entire bubble surface and organic species in the SSML are concentrated on the bubble film leading to an enrichment of organic matter in SSA once the bubble bursts at the air-sea interface.

Despite the abundance of research addressing transfer processes of organic species into SSA, the relationship between seawater biological activity (i.e. phytoplankton blooms) and SSA organic composition remains a highly debated topic among researchers.[15,19–24] As the main primary producers in the ocean, phytoplankton convert inorganic CO_2 to organic biomass. Initially, most of this freshly produced organic biomass is particulate organic carbon (POC), operationally defined as organic material >0.7 μm in diameter.[25] During bloom growth, POC initially consists of whole, living phytoplankton, with the emergence of bacteria and organic aggregates also contributing to POC biomass after the initial growth phase.[25–27] As a bloom progresses, phytoplankton exudates, death, and bacterial processing result in degradation of freshly produced organic material to smaller sizes <0.7 μm, termed the dissolved organic carbon (DOC) pool.[20,27] Degradation of this organic material continues long after phytoplankton bloom senescence, resulting in an abundance of older, "aged" DOC in oceanic regimes with low biological activity.

Because "aged" OC is far more abundant than freshly produced OC in most oceanic regimes, some researchers have concluded "aged" OC is the only important carbon pool that contributes to OC_{SSA}.[15,19,20] Contrary to this, many field measurements indicate OC_{SSA} concentrations correlate with primary productivity, and track chlorophyll-a (chl-a), implying a substantial contribution of freshly produced OC to SSA in oceanic regimes of high biological activity.[21–24] To resolve these discrepancies between field studies it is prudent to elucidate the contribution of freshly produced OC to OC_{SSA}; however, in the marine environment this is complicated by numerous factors including formation of secondary marine aerosol (SMA), interference from terrestrial aerosol sources, chemical transformations during atmospheric transport, and bacterial-enzymatic degradation of labile, freshly produced OC.[28–32] The first two factors contribute interfering marine aerosol carbon with an organic composition different from

SSA, while the latter two can obscure chemical distinctions between newer, freshly produced and older, "aged" OC in SSA. A recent mesocosm study focusing on the effects of seawater biology on SSA organic composition found that enrichment of aliphatic organics in SSA was different for two consecutive phytoplankton blooms, and controlled by the bacterial-enzymatic activity in the seawater as well as microbial degradation of freshly produced OC.[30] The contradictory conclusions drawn from this abundance of research highlight the necessity for laboratory studies of isolated, nascent SSA to provide insight into ocean-aerosol organic transfer during periods of high biological activity, and identify the seawater carbon sources contributing to OC_{SSA}.

Stable carbon isotopic analysis is an excellent technique for identifying and quantifying sources of carbon species. To date, the primary application of stable carbon isotopic measurements ($\delta^{13}C$) to marine aerosols has been for source apportionment to determine the fractional contributions of OC_{SSA} (f_{SSA}) versus anthropogenic aerosol carbon (f_{anth}) to the marine environment. These source apportionment calculations are made using a dual-source isotopic mixing model with the assumption that the two sources contributing to aerosol carbon in the marine environment are SSA and anthropogenic aerosol (Equation 1.3).[33–39] This equation requires precise knowledge of the SSA carbon isotopic composition ($\delta^{13}C_{SSA}$), but determination of this value in the marine environment is complicated by photochemical aging of primary SSA, formation of marine SMA, and contributions from terrestrial aerosols. Historically, because "aged" OC is the most abundant surface ocean OC reservoir, most studies assume $\delta^{13}C_{SSA}$ is the same as $\delta^{13}C$ for seawater DOC, around -20 to -23 ‰.[37–39] This assumption has come under scrutiny recently, with measurements of primary marine aerosols in the North Atlantic indicating a trend of less negative $\delta^{13}C$ values during periods of high biological activity.[34] The researchers attributed this to incorporation of freshly produced organic material into SSA. A subsequent isotopic study

on marine aerosols led to the proposal that two distinct carbon pools, nominally freshly produced and "aged" OC, contribute to OC_{SSA}.[40] That study, however, did not include seawater $\delta^{13}C_{POC}$ and $\delta^{13}C_{DOC}$ measurements that may have allowed quantification of their relative contributions.

Building upon previous research, this study aims to quantify the contribution of freshly produced OC to OC_{SSA} by combining $\delta^{13}C_{SSA}$ measurements with seawater $\delta^{13}C_{POC}$ and $\delta^{13}C_{DOC}$ measurements. Oftentimes during phytoplankton blooms significant $\delta^{13}C$ increases of 3-5 ‰ occur in freshly produced OC leading to a $\delta^{13}C$ for freshly produced OC that is isotopically distinct from $\delta^{13}C$ values for "aged" OC.[41,42] This is usually due to lower ^{12}C isotopic discrimination by phytoplankton during CO_2 fixation as competition increases for available CO_2.[41–43] It was stated above that generally in seawater freshly produced OC is predominantly POC, while the majority of "aged" OC is DOC. When this is the case, the $\delta^{13}C$ values for freshly produced and "aged" OC can be approximated with measurements of seawater $\delta^{13}C_{POC}$ and $\delta^{13}C_{DOC}$. Therefore, Equation 2.1a, a dual-source isotopic mixing model analogous to Equation 1.3, allows for calculation of the fractional contribution for freshly produced OC to OC_{SSA} (Equation 2.1b):

$$\delta^{13}C_{SSA} = (f_{FreshOC})(\delta^{13}C_{POC}) + (f_{AgedOC})(\delta^{13}C_{DOC}) \quad \text{(Equation 2.1a)}$$

$$\frac{\delta^{13}C_{SSA}-\delta^{13}C_{DOC}}{\delta^{13}C_{POC}-\delta^{13}C_{DOC}} = \text{Fraction}_{FreshOC} \quad \text{(Equation 2.1b)}$$

In this study, two separate phytoplankton blooms were induced an isolated system by nutrient addition to natural, Pacific Ocean seawater. Carbon concentrations and $\delta^{13}C$ values for POC, DOC, SSML, and SSA were measured to elucidate the contributions freshly produced and "aged" organic material SSA. For these experiments, freshly produced OC refers to organic material produced during the phytoplankton bloom experiments, and "aged" OC refers to organic material present in the initial seawater or contributed by the nutrient addition. Our findings provide

insight into how seawater biological activity impacts SSA organic composition and $\delta^{13}C_{SSA}$, and demonstrate that accounting for the biological influence on $\delta^{13}C_{SSA}$ can improve source apportionment of marine aerosols.

2.3 Experimental Methods

2.3.1 Marine Aerosol Reference Tank (MART) Bloom Experiments.

Two separate phytoplankton bloom experiments, henceforth referred to as MART1 and MART2, were carried out in the same MART system for 2-3 weeks each.[44] In each experiment, the 210 L tank was filled with 120 L of natural, filtered (50 μm Nitex mesh to remove zooplankton) seawater collected from Ellen Browning Scripps Memorial Pier (32.8634° N, 117.2546° W) on April 23rd, 2018 and May 31st, 2018 for MART1 and MART2, respectively. After seawater was added, a water chiller was attached to maintain a constant water temperature of 18˚C throughout the experiment, the first chl-a measurement was made, and the seawater was left overnight to equilibrate. The next morning initial samples of DOC, POC, and SSML were collected, followed by the addition of Guillard's f/20 diatom growth medium with sodium metasilicate[45] and the activation of solar simulator lamps to continuously supply ~70 μE m^{-2} s^{-1} of photosynthetically active radiation to the MART for biological growth.[46] Phytoplankton speciation was not determined for these experiments, and microbial communities in the initial seawater were not altered in any way before addition of growth medium. Keeping the initial seawater unaltered, other than the adding growth nutrients, allows the MART experiments to reproduce the chemical complexity of the open ocean.

To aerate the seawater, particle-free room air was pumped into the MART through Tygon tubing until chl-a, measured once daily via a calibrated, handheld fluorometer (Aquafluor, Turner

Designs), reached ~12 μg L^{-1}. The 12 μg L^{-1} threshold has been employed in previous MART experiments to ensure a significant amount of phytoplankton growth before turning on the pump used for water recirculation in the MART, which can lyse fragile cells inhibiting phytoplankton growth.[46] The morning after chl-a reached ~12 μg L^{-1}, the Tygon tubing was moved from the seawater to the MART headspace to flow in particle-free air at 6 L min^{-1}. Once particle concentrations in the MART fell below 1 cm^{-3}, aerosol production via the plunging waterfall technique[44] was commenced with a 4-second on-off waterfall cycle. The plunging waterfall generates SSA with particle size distributions representative of oceanic wave breaking,[3,44] and a centrifugal pump attached to the MART recirculates water from the bottom of the tank to replenish the waterfall. Extensive methodology and specific chemical and biological details for this type of experiment are described elsewhere.[46]

2.3.2 Sample Collection for SSA, POC, DOC, SSML, and Bacteria.

Sea spray aerosol was collected by pulling air from the MART headspace onto 47 mm pre-combusted (500 ˚C, >4 hours) quartz fiber filters at 5 L min^{-1}. A diffusion dryer filled with silica gel was placed before the filters to dry the aerosols before collection. SSA samples consisted of total suspended particles (TSP) collected for >40 hours to ensure adequate sample loadings for isotopic measurements. Field blanks were collected at the end of the experiments in addition to three-day collection filters without aerosol generation (see Section 2.6.1). All SSA samples and blanks were stored at -12˚C in plastic petri dishes wrapped with Teflon tape. The DOC, POC, SSML carbon (OC_{SSML}), and bacteria were collected at the beginning and end of each SSA sampling period. The glass plate method was employed to collect SSML, with care taken to ensure

that a 30 cm length of the glass plate was lowered and raised through the seawater at a consistent rate of 5-6 cm/s for every collection.[47,48] This process was repeated to collect 40 mL of combined seawater and organics in the SSML into a combusted glass vial, corresponding to an SSML thickness of 100 μm across the entire tank surface. The SSML samples were not filtered, so OC_{SSML} contains a combination of both POC and DOC. Bulk seawater was collected from a spigot on the MART located 23 cm below the water surface. The bulk seawater was filtered through a combusted 0.7 μm Whatman glass fiber filter (GF/F) to separate POC from DOC, and two 40 mL DOC aliquots were collected into combusted glass vials. The POC filters were collected into plastic petri dishes and stored at -12˚C, while SSML and DOC vials were immediately acidified to pH 2, wrapped with Teflon tape and stored at room temperature. Heterotrophic bacteria in the bulk seawater were enumerated using a BioRad ZE5 flow cytometer after staining with SYBR Green-I (Thermo Fisher, cat #S7563).

2.3.3 $\delta^{13}C$ Analysis for SSA.

Isotopic analyses are reported in conventional delta notation standardized to Pee Dee Belemnite by Equation 1.1.[49,50] Right after collection, SSA samples and field blanks were cut in half; half was immediately analyzed for $\delta^{13}C$ analysis, and the other half was stored frozen. Following established methods in the Thiemens Stable Isotope Lab at UCSD, the filter half for $\delta^{13}C$ analysis was placed in a 20 cm long quartz tube containing 250 mg CuO and attached to a vacuum line. After evacuation, a valve was closed to seal the tube, and an 850˚C combustion furnace was placed on the quartz tube for 3 hours to convert all carbon to CO_2. The CO_2 was then cryogenically separated, total carbon yield (μmoles CO_2) was measured by capacitance

manometry, and later converted to OC_{SSA} concentration using the total volume of air collected. Subsequently, the CO_2 was collected into a sample tube and $\delta^{13}C$ analysis was conducted on a MAT 253 Isotope-Ratio mass spectrometer. SSA samples were not corrected for carbonates so OC_{SSA} refers to organic carbon and carbonates combined, however research shows that carbonates have a minimal effect on $\delta^{13}C$ of marine aerosols.[33] Measured SSA concentrations and $\delta^{13}C$ were corrected for filter blanks as described in Section 2.6.1.

2.3.4 $\delta^{13}C$ Analysis for POC, DOC, and SSML.

The OC concentrations and $\delta^{13}C$ values for POC samples were measured at the Scripps Institution of Oceanography Stable Isotope Laboratory using a Thermo Finnigan DeltaPlus Isotope-Ratio mass spectrometer interfaced with a Costech 4010 elemental combustion analyzer. Error analyses were made by measuring GF/F blanks to correct for amounts and isotopes (Section 2.6.1). SSA isotopic analysis was not carried out on this instrument as OC amounts were below the limit of quantitation. Acidified, liquid DOC and SSML samples were sent to G.G. Hatch Stable Isotope Laboratory in Ottawa, Canada for $\delta^{13}C$ analysis on an OI Analytical Aurora Model 1030W total organic carbon (TOC) Analyzer interfaced to a Finnigan DeltaPlus XP Isotope-Ratio mass spectrometer with a 1σ analytical precision of ± 0.2 ‰.[51]

2.3.5 Aerosol Size and Mass Measurements.

A Scanning Mobility Particle Sizer (SMPS) and Aerodynamic Particle Sizer (APS) were used to measure SSA size distributions on four days during MART2. The SMPS measured particles with dry mobility diameters from 0.015-0.572 μm, which are equivalent to physical diameters if particle sphericity is assumed. The APS measured aerodynamic diameters from

0.669-19.69 µm, which were corrected to a physical diameter range of 0.498-14.67 µm by assuming spherical particles with an effective density of 1.8 g cm^{-3}.[44,52,53] The SMPS and APS data were merged around a 0.6 µm physical diameter, and SMPS data with larger diameters were excluded. The 0.6 µm diameter is at the high and low end of the respective instruments' detection limit, accounting for SSA size distribution discrepancies in the 0.5-0.7 µm diameter range. The aerosol sizing data displayed in Figure 2.1 demonstrate the reproducibility of the SSA size distribution, despite some variance in total SSA number concentration. MART1 and MART2 were conducted in the same tank, with the same aerosol formation properties, thus the measured aerosol sizes are also applicable to MART1.

SMPS and APS size distribution data was used to calculate total particle mass concentration using the same effective density of 1.8 g cm^{-3}. Because particle flux from the MART varied, total particle mass concentrations for all four days were averaged to approximate the mean particle mass concentration throughout the experiment. The SSA mass concentrations displayed in Figure 2.1 show that slight differences in supermicron size distributions, the main contributors to SSA mass, led to some variance in the total SSA mass which ranged from 195-366 µg m^{-3} (mean = 271 ± 73 µg m^{-3}). These mass differences are more likely attributable to variability in SSA mass flux during the hour-long duration of sizing measurements, not daily changes in total SSA mass concentration.

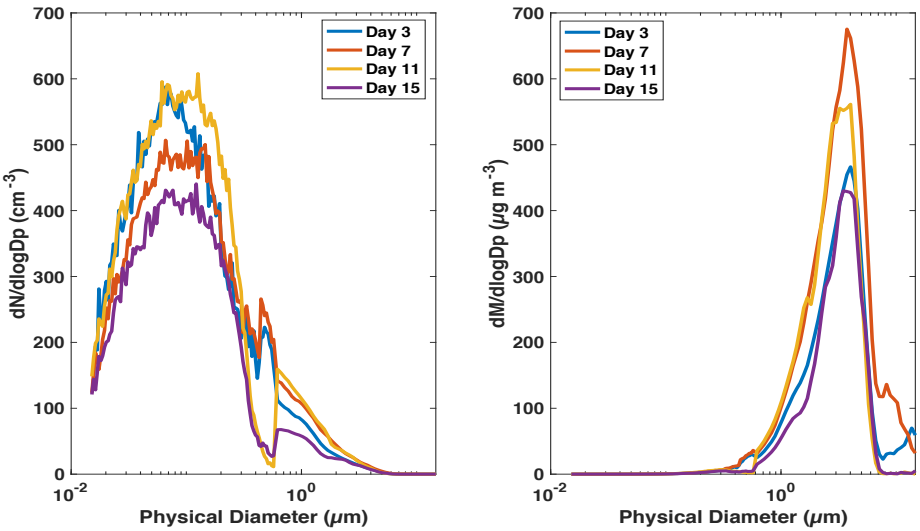

Figure 2.1 The SSA number size distribution (left) and SSA mass distribution (right) for measurements made on four separate days during MART2. The sizing data was averaged to obtain a mean aerosol mass concentration as described above.

2.3.6 Lipid Biomarker Analysis for SSA.

The lipid preparation and analysis were carried out at the UCSD Lipidomics Core. For lipid extraction from SSA samples, the aerosol filters were soaked for 30 minutes in a 13 x 100 mm test tube containing 2 mL of methanol before addition of 2 mL methylene chloride and 250 µL of 0.1 MHCl in H_2O. The tubes were vortexed and chilled on ice for 30 minutes before transferring all the liquid to another 13 x 100 mm tube and carrying out a Bligh-Dyer extraction.[54] Saponification was carried out by adding 0.5 N KOH in methanol to the tube and incubating for 1 hour at 37 ˚C, followed by neutralization to pH 3.0. To extract the "free" fatty acids, 1 mL of isooctane was added to the tubes, and the top layer was transferred to a mass-spec vial after centrifugation. The samples were vortexed and incubated for 20 mins with 50 µL of 1% pentafluorobenzyl bromide and 50 µL of 1% diisopropyl ethylamine for fatty acid derivatization. After evaporation to dryness 50 µL of isooctane was added and samples were run on an Agilent 5975 GC-MS.[55]

2.4 Results and Discussion

2.4.1 POC-DOC-OC_{SSA} Dynamics during Phytoplankton Blooms.

Phytoplankton bloom progression for both experiments was monitored by measuring the chl-a, heterotrophic bacteria, POC, DOC, and OC_{SSML} concentrations (Figure 2.2 and Table 2.1). Initially, chl-a was 2.1 μg L^{-1} in MART1 and 1.5 μg L^{-1} in MART2, increasing after nutrient addition to similar maxima of 27 and 28 μg L^{-1}, respectively. These blooms are larger than those in open marine waters, which typically have peak chl-a values between 1 and 10 μg L^{-1}, but are consistent with previous MART experiments using the same nutrient addition.[46,56,57] After commencing SSA production, the chl-a concentrations for both experiments decreased below 2 μg L^{-1} within two days, remaining below this level for the rest of the experiment. The sharp chl-a decline is partially caused by the aforementioned damage to fragile phytoplankton cells from the centrifugal pump used for SSA generation, and previous MART studies exhibit this same decline with chl-a values dropping to pre-bloom levels in 2-3 days. As a result, most experimental measurements were conducted after the chl-a maximum. In the open ocean, breaking waves produce SSA during all bloom phases. However, the highest OC enrichment in SSA often occurs after the chl-a peak, suggesting the bloom decay phase may be the most important for transfer of freshly produced OC into SSA.[58,59]

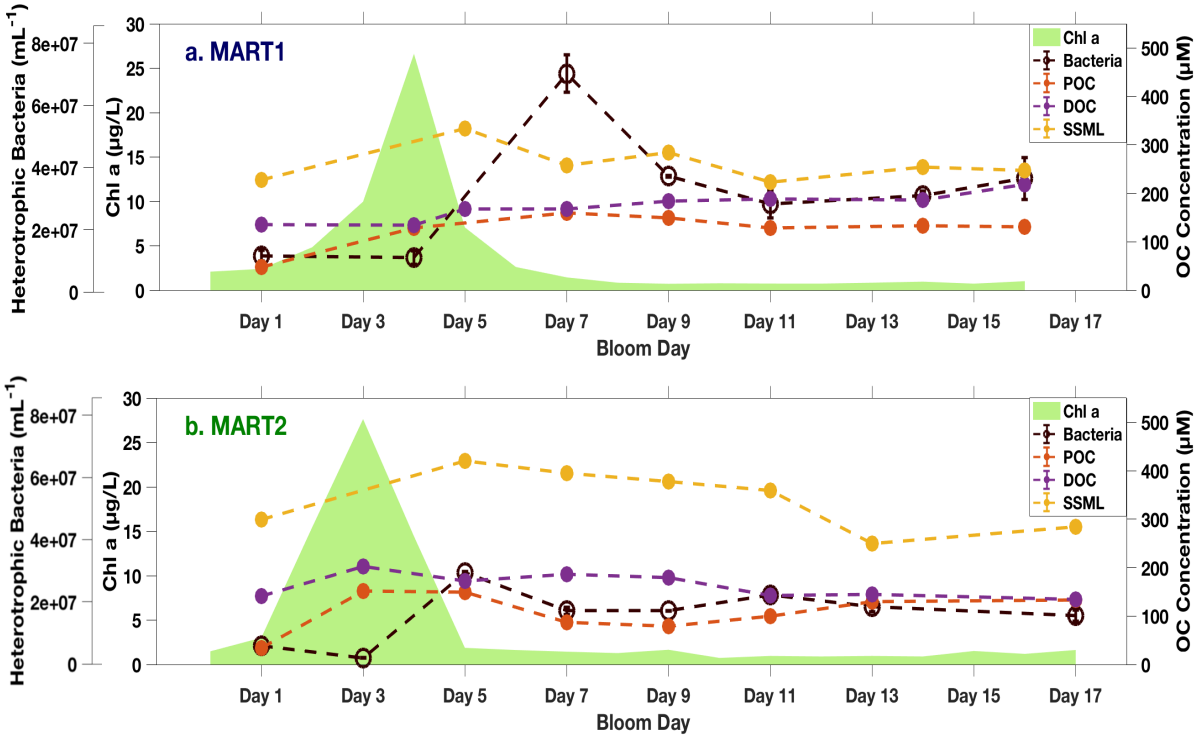

Figure 2.2 A time series displaying the chl-a, heterotrophic bacteria, POC, DOC, and OC_{SSML} concentrations for a) MART1 and b) MART2. The dashed lines denote that measurements were made at individual time points. The initial DOC measurements for a) MART1 and b) MART2 (Day 1) were made before nutrient addition, which contributes 12 µM DOC. Vertical error bars are included for all species, but uncertainty was smaller than the data points for POC, DOC, and OC_{SSML} concentrations.

The initial MART1 and MART2 POC concentrations of 46 µM and 34 µM increased several-fold during the experiments to similar maxima of 160 µM and 151 µM, respectively. The large POC concentration increase can be attributed to increased phytoplankton growth, and indicates the majority of the POC in both experiments is freshly produced OC. A decrease in POC concentration would be expected to accompany the phytoplankton death, as indicated by the chl-a decline, but the POC concentration was almost the same two days after the chl-a peak in MART2 and had even increased slightly three days after the chl-a peak in MART1. Figure 2.2 shows the trends in POC concentrations after the chl-a maximum in MART1 and MART2 are closely linked to changes in the heterotrophic bacteria concentrations. In both experiments, as chl-a began

declining heterotrophic bacteria concentrations rose sharply, reaching their maxima three and two days after the chl-a peak for MART1 and MART2. The bacteria concentrations showed similar increases of 5-6 fold in both experiments compared to the initial seawater concentrations. The initial seawater bacteria concentrations were higher for MART1 than MART2, which likely explains why bacteria concentrations reached a higher peak in MART1 than MART2. Nevertheless, the maximum concentrations in both experiments were on the order of 10^7 cells mL^{-1}, which is similar to previous MART bloom experiments as well as phytoplankton blooms in the open ocean.[32,46,60,61] When phytoplankton blooms decay, heterotrophic bacteria concentrations often increase when bacteria assimilate freshly produced OC including phytoplankton exudates and detritus.[30,46] The close trend suggests that after the chl-a peak heterotrophic bacteria contribute significantly to POC biomass, implying a considerable portion of the freshly produced OC has undergone bacterial processing.

The initial DOC concentrations were 136 μM for MART1 and 141 μM for MART2, which reached similar maximum values of 218 μM and 202 μM during both experiments. Accounting for the 12 μM increase from nutrient addition, the DOC concentrations increased by 70 and 49 μM for MART1 and MART2, respectively, compared to the pre-bloom concentrations. These smaller concentration changes indicate the DOC is mostly comprised of "aged" organic material present in the initial seawater before bloom growth began. Importantly, when compared to the POC concentration increases of 114 μM and 117 μM, it is clear the majority of freshly produced OC was in the form of POC for both experiments.

Table 2.1 Concentration and isotope values for MART1 and MART2 experiments.[a]

Bloom Day	Chl-a ($\mu g\ L^{-1}$)	Bacteria Counts ($10^7\ mL^{-1}$)	POC Conc. (μM)	DOC Conc. (μM)	OC_{SSML} Conc. (μM)	OC_{SSA} Conc.[b] ($\mu g\ m^{-3}$)	$\delta^{13}C$ POC (‰)	$\delta^{13}C$ DOC (‰)	$\delta^{13}C$ SSML (‰)	$\delta^{13}C$ SSA[b] (‰)
					MART1					
Day 1	2.09	1.11	46	136	228	—	-19.9	-22.1	-22.2	—
Day 4	26.6	1.05	129	135	—	—	-18.2	-21.3	-21.7	—
Day 5	7.07	—	—	168	333	5.16	—	-23.0	-20.6	-21.4
Day 7	1.45	6.97	160	168	257	5.23	-17.2	-23.0	-21.7	-20.8
Day 9	0.73	3.67	150	184	284	omit	-16.9	-22.7	-21.1	omit[d]
Day 11	0.75	2.78	128	189	223	3.45	-17.9	-22.2	-22.3	-21.4
Day 14	0.97	3.04	134	187	254	3.91	-18.3	-22.3	-22.3	-21.4
Day 16	1.02	3.60	131	218	248	5.83	-18.4	-23.1	-22.1	-22.0
					MART2					
Day 1	2.24	0.61	34	141	299	—	-18.5	-23.3	-22.7	—
Day 3	27.6	0.21	151	202	—	—	-16.8	-22.7	-21.4	—
Day 5	1.87	2.96	150	172	421	5.06	-15.5	-22.9	-20.8	-19.6
Day 7	1.44	1.73	87	187	394	3.64	-15.0	-23.0	-24.7	-18.3
Day 9	1.66	1.73	79	179	378	3.86	-14.6	-22.9	-23.8	-19.4
Day 11	0.96	2.24	100	142	359	4.28	-15.7	-20.1	-21.1	-19.4
Day 13	0.96	1.86	130	145	249	4.47	-16.5	-22.3	-21.6	-19.8
Day 17	1.63	1.57	133	135	284	5.52	-18.6	-20.5	-20.6	-21.2

[a] Uncertainties for measurements are shown in Figures 2.2 and 2.3.
[b]For the SSA samples the Day refers to when the sampling duration ended.
[c] Dashes denote that variable was not measured for that day.
[d] MART1 Day 9 SSA sample was omitted due to an anomalous concentration and $\delta^{13}C$ value indicative of contamination.

The OC_{SSML} concentrations showed similar trends for both experiments, with the largest OC_{SSML} concentrations, 333 μM for MART1 and 421 μM for MART2, occurring immediately

after the chl-a peak. The OC_{SSML} concentration was higher in MART2 than MART1 following the chl-a peak, but both decreased to stabilize around 250 μM as the experiments progressed. For both experiments, no measurements of OC_{SSML} were reported for days when room air was being bubbled into the seawater, which included the day of maximum chl-a concentrations. Although bubbling air into the seawater in the isolated MART is necessary to facilitate phytoplankton growth, this process does not occur in oceanic environments, and the air bubbles likely transported organic material to the seawater surface leading to an over-enrichment of organics in the SSML. For this reason, with the exception of Day 1 before bubbling was initiated, OC_{SSML} measurements were only reported after the bubbling was stopped and SSA production had commenced.

The OC_{SSA} concentrations for MART1 and MART2 ranged from 3.45-5.83 μgC m^{-3} (mean 4.93 μgC m^{-3}) and 3.86-5.52 μgC m^{-3} (mean 4.47 μgC m^{-3}), respectively (Figure 2.3). The higher OC_{SSA} concentrations compared to open ocean measurements reflects higher SSA particle concentrations from the MART, but carbon comprised only 1-2% of TSP SSA mass (Figure 2.3), comparable to marine observations.[23,62] Similar values for OC_{SSA} concentrations in both experiments is consistent with the similar seawater OC concentrations and reproducibility of the SSA generation method.

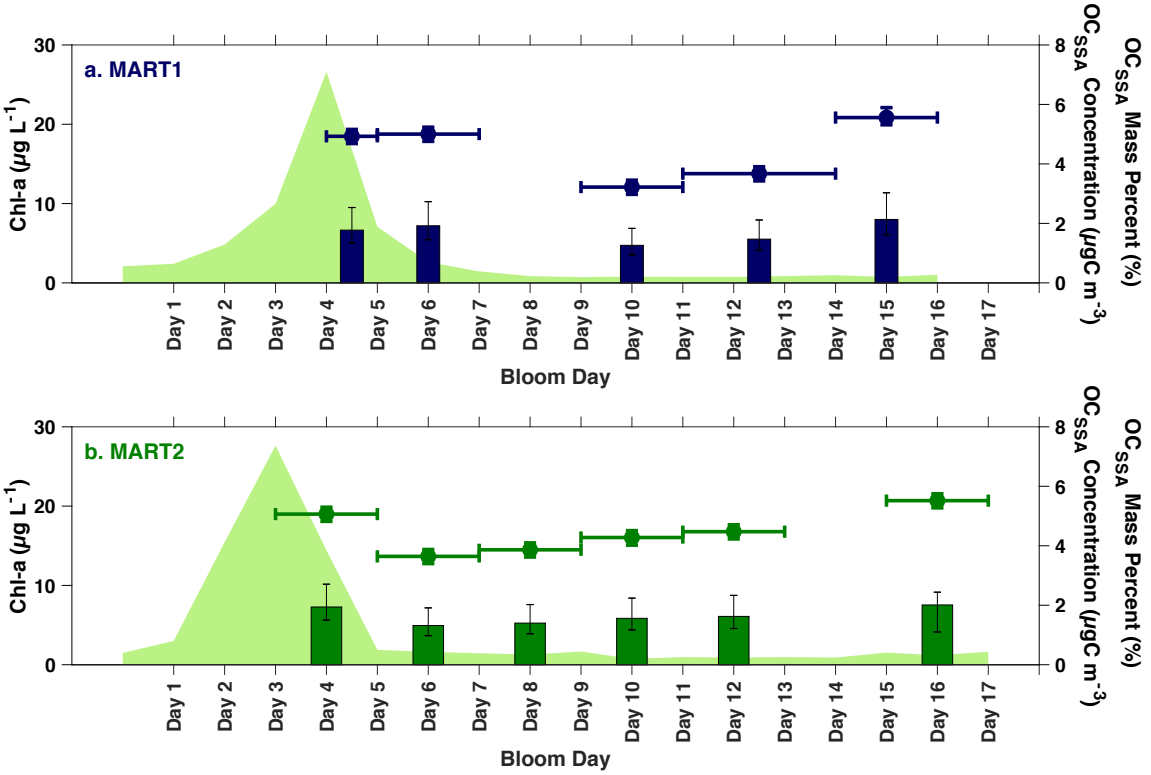

Figure 2.3 Data points represent the OC_{SSA} concentrations for a) MART1 and b) MART2. Horizontal error bars represent the collection duration for each SSA sample and the data points were placed in the middle of the sampling period. Vertical error bars are included and are about the height of the data point. The bars represent the percent contribution of OC to total SSA mass for a) MART1 and b) MART2, calculated by assuming an average total SSA mass concentration of 271 μg m^{-3} for each day. Total SSA mass was calculated from the aerosol mass distribution in Figure 2.1. Bars are placed in the middle of the sampling duration.

2.4.2 Seawater $\delta^{13}C$ Constraints on Nascent $\delta^{13}C_{SSA}$ in the Marine Environment.

Conducting experiments in an isolated environment enabled the first measurement of $\delta^{13}C_{SSA}$ on nascent SSA without any background aerosol contributions. Figure 2.4 shows that $\delta^{13}C_{SSA}$ was statistically less negative than the average $\delta^{13}C_{DOC}$ value for each SSA collection period throughout the entirety of both blooms except for MART2 Days 15-17. This establishes that $\delta^{13}C_{SSA}$ is not necessarily equivalent to $\delta^{13}C_{DOC}$, as has been widely assumed by previous researchers. Interestingly, $\delta^{13}C_{SSA}$ fell between $\delta^{13}C_{POC}$ and $\delta^{13}C_{DOC}$ for the entirety of the MART1

and MART2 experiments, suggesting the difference between $\delta^{13}C_{SSA}$ and $\delta^{13}C_{DOC}$ can be used to assess the contribution of freshly produced OC to OC_{SSA}. This observation is consistent with our earlier hypothesis that OC_{SSA} is comprised of both freshly produced and "aged" OC. As described below, validation of this initial hypothesis prompted a more detailed and quantitative examination of how these seawater carbon pools contribute to OC_{SSA} and influence marine $\delta^{13}C_{SSA}$ values.

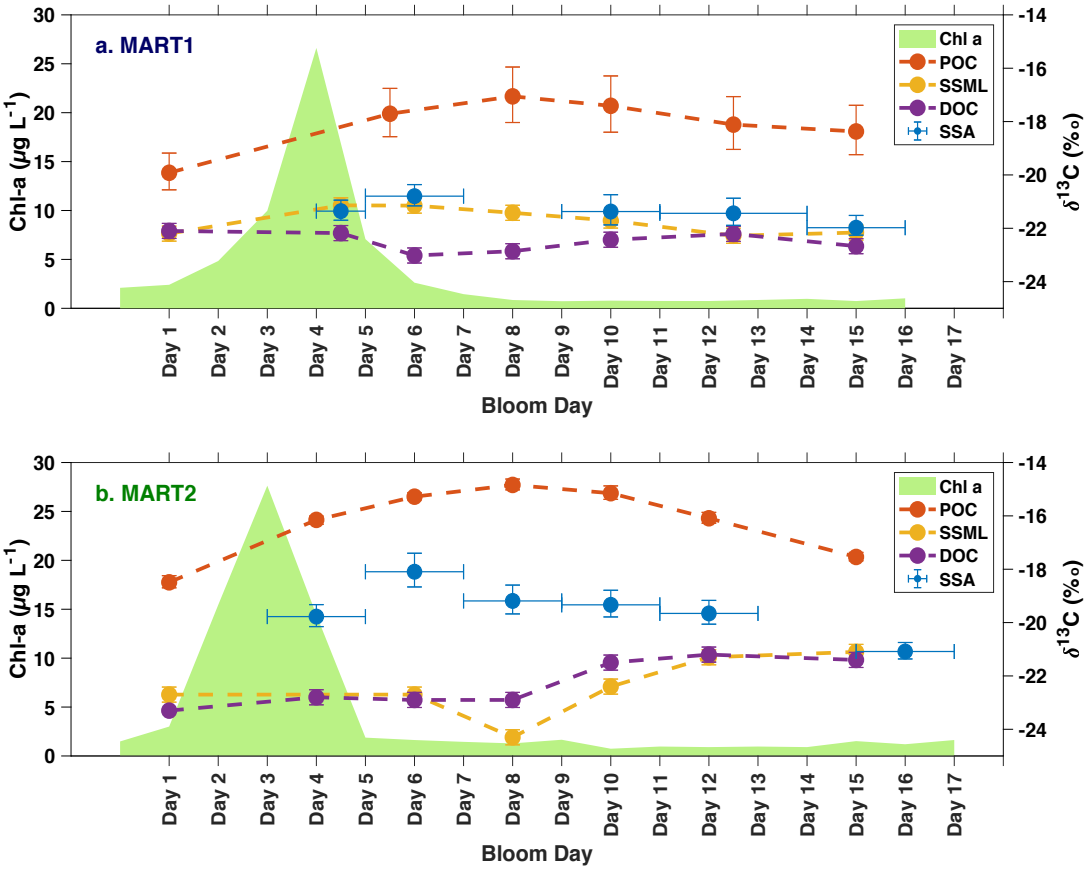

Figure 2.4 $\delta^{13}C$ values for POC, DOC, SSML, and SSA throughout a) MART1 and b) MART2, overlaid on the chl-a time series. Because SSA was sampled continuously, while POC, DOC, and SSML were only measured at individual points, Figure 2.4 plots the average of two seawater $\delta^{13}C$ values, one at the beginning and end of each SSA collection (Table 2.1), with the data points in the middle of the collection period (further details in Section 2.6.1). This facilitates an easier comparison between $\delta^{13}C_{SSA}$ and the seawater $\delta^{13}C$ values, showing that $\delta^{13}C_{SSA}$ is consistently less negative than $\delta^{13}C_{DOC}$. Horizontal error bars for SSA indicate the collection duration for each sample, and data points represent the middle of the sampling period. Vertical error bars, calculated as explained in Section 2.6.1, are shown for each species and are approximately the height of the data point for $\delta^{13}C_{DOC}$ and $\delta^{13}C_{SSML}$.

In order to estimate the contribution of freshly produced OC to OC_{SSA} using the isotopic mixing model introduced in Equation 2.1b, there are two conditions that must be met: 1) $\delta^{13}C_{POC}$ and $\delta^{13}C_{DOC}$ must have distinct isotopic values, and 2) the POC pool should be comprised primarily of freshly produced OC, while the DOC pool should be predominantly "aged" OC. As anticipated, increased amounts of isotopically less negative, freshly produced OC during the phytoplankton growth phase, most of which was POC, caused $\delta^{13}C_{POC}$ to increase by 3-4 ‰ in the two experiments (Figure 2.4). In contrast, $\delta^{13}C_{DOC}$ displayed only modest changes during the phytoplankton growth phase, and was distinctly more negative than $\delta^{13}C_{POC}$ throughout both experiments, fulfilling the first condition. Regarding the second condition, as detailed in Section 2.4.1, the POC and DOC concentrations in Figure 2.2 show most POC is freshly produced OC, while DOC is primarily "aged" OC. Since the two conditions were satisfied in both experiments, the fractional contribution of freshly produced OC to OC_{SSA} for each SSA sample, termed $Fraction_{FreshOC}$, was calculated and displayed in Figure 2.5 by approximating that freshly produced OC had isotopic values equivalent to $\delta^{13}C_{POC}$ and "aged" OC the same as $\delta^{13}C_{DOC}$.

Figure 2.5 shows the proportional contribution of freshly produced OC to OC_{SSA} necessary to account for the difference between $\delta^{13}C_{SSA}$ and $\delta^{13}C_{DOC}$ for each collection. The proportion of "freshly produced" OC ranged from 7-63%, and a contribution of freshly produced OC to OC_{SSA} was necessary to explain the measured $\delta^{13}C_{SSA}$ value for every SSA sample in both experiments, demonstrating OC_{SSA} composition in the marine environment will nominally be comprised of both freshly produced and "aged" OC. These findings directly contradict the assertion by some researchers that OC_{SSA} is comprised only of organic species from the "aged" OC pool.[15,19,20] Complementary to the findings in this work, a recent study by Beaupre et al.[63] in the Western Atlantic compared radiocarbon signatures for OC_{SSA} with dissolved inorganic carbon (DIC), a

proxy for freshly produced OC, and surface DOC, a proxy for "aged" OC. Using their surface DOC measurements as the "aged" end-member and surface DIC measurements as the freshly produced end-member, additional calculations akin to Equation 2.1b indicate freshly produced OC in the Western Atlantic comprises 19-88% of OC_{SSA}. These measurements confirm that freshly produced OC is significantly incorporated into OC_{SSA} in the marine environment and show good agreement with the contribution of freshly produced OC to SSA observed in this work. Although one might expect that higher amounts of freshly produced OC in our nutrient-enhanced biological growth experiments would lead to higher $Fraction_{FreshOC}$ values, much of this organic material may have been whole phytoplankton and cell detritus too large to be transferred into SSA. Their radiocarbon measurements were conducted on SSA from natural seawater without any stimulated biological growth, suggesting the $Fraction_{FreshOC}$ values and OC_{SSA} compositions in our experiments are similar to what would be expected in the natural marine environment.

The radiocarbon measurements showed the contribution of freshly produced OC was largest in coastal regions with elevated chl-a values, reinforcing the importance of biological activity on OC_{SSA} composition. However, it was also found to be as high as 37% in low biological activity oceanic regimes, suggesting freshly produced OC is a substantial contributor to OC_{SSA} under most oceanic conditions. The authors point out that while radiocarbon measurements reveal the age of carbon in SSA, $\delta^{13}C$ measurements would have been useful to characterize the sources of carbon contributing to OC_{SSA}. In this study, the $\delta^{13}C$ measurements identified two distinct seawater carbon pools contributing to SSA with freshly produced OC consisting mostly of POC, and "aged" OC primarily composed of DOC. Additionally, conducting these measurements throughout a phytoplankton bloom cycle revealed the temporal changes in the contribution of freshly produced OC to SSA.

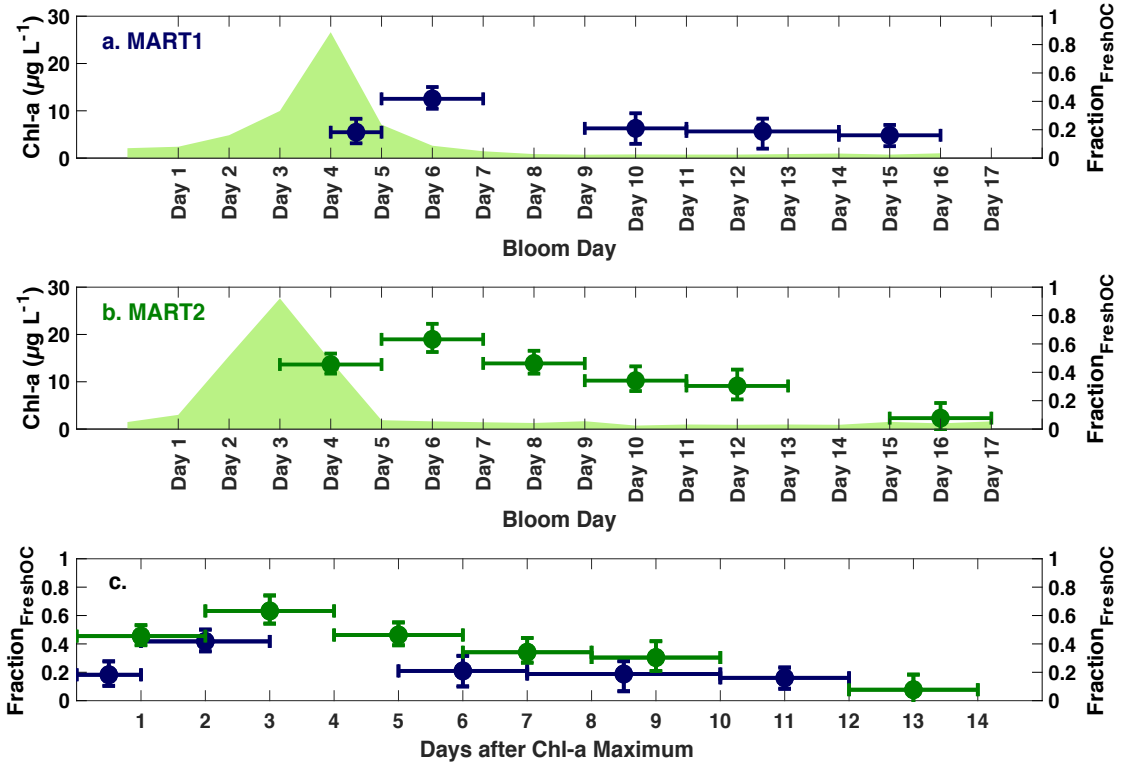

Figure 2.5 Fractional contribution of freshly produced OC to OC_{SSA}, $Fraction_{FreshOC}$, overlaid on the chl-a time series for a) MART1 and b) MART2. C) Shows the combined $Fraction_{FreshOC}$ data from MART1 and MART2 plotted in days after the chl-a maximum to help facilitate experimental comparison. Both experiments show a similar time lag between the chl-a maximum and the largest $Fraction_{FreshOC}$. This time lag, which was 2 days for MART1 and 3 days for MART2, suggests freshly produced OC may undergo bacterial processing before being efficiently transferred into SSA. $Fraction_{FreshOC}$ was calculated using Equation 2.1b and the isotopic values from Figure 2.4 (see Section 2.6.2 for more details). Vertical error bars were calculated from the $\delta^{13}C_{SSA}$ uncertainty in Figure 2.4, and the horizontal error bars represent the collection duration for each SSA sample with data points placed at the middle of the sampling period.

2.4.3 Temporal Dependence of Freshly Produced OC Contribution to OC_{SSA}.

Measuring changes in $\delta^{13}C$ over the course of both MART experiments provided a time series of the biological activity effects on seawater chemistry and nascent OC_{SSA} composition. A clear link between oceanic biological activity and OC_{SSA} composition was evident due to the fact that this study eliminated contributions from the interfering aerosol sources mentioned previously. Most notably, in Figure 2.5 both experiments exhibit the same temporal trend in $Fraction_{FreshOC}$

with the highest values delayed from the chl-a maximum by 2-3 days. Similar results were obtained in a previous MART experiment where mass spectral organic biomarkers were found to increase in the days following the chl-a maximum.[46] A time lag between the chl-a peak and the greatest contribution of freshly produced organic material to OC_{SSA} demonstrates phytoplankton abundance (chl-a) alone is not sufficient to explain changes in SSA organic enrichment, implying carbon transfer into SSA is likely influenced by microbial processing in the seawater. Interestingly, Figure 2.6 displaying the OC_{SSA} mass percent for three labile phytoplankton lipid biomarkers in MART1, $C_{16:1}$, $C_{20:5}$, and $C_{22:6}$, shows the contribution of these labile species to SSA sharply decreases after the first 24 hours. Although the MART2 SSA sample collected for the first 48 hours after the chl-a peak was not available for lipid measurements, Figure 2.6 similarly shows the OC_{SSA} contribution of these labile lipid biomarkers is low for samples collected more than 48 hours after the chl-a peak. Consistent with these measurements, a recent phytoplankton bloom mesocosm experiment found that enrichment of highly-labile, aliphatic organic matter in SSA was highest during the chl-a peak, and this enrichment mostly disappeared within 24 hours after the chl-a maximum.[30] This was attributed to rapid bacterial-enzymatic degradation of highly labile organic matter in the seawater, revealing that seawater bacterial activity, in addition to phytoplankton abundance, controls enrichment of organic matter in SSA.

This study extends the previous research on SSA organic enrichment by demonstrating that while the contribution of highly-labile organic species to SSA may be highest immediately following the chl-a peak, the largest proportional contribution of freshly produced OC to SSA is delayed from the chl-a maximum by 2-3 days. These findings suggest the highest enrichment of freshly produced OC in SSA occurs after this organic material has been partially degraded by

bacteria and imply that bacterial processing may lead to more efficient transfer of freshly produced organic material into SSA.

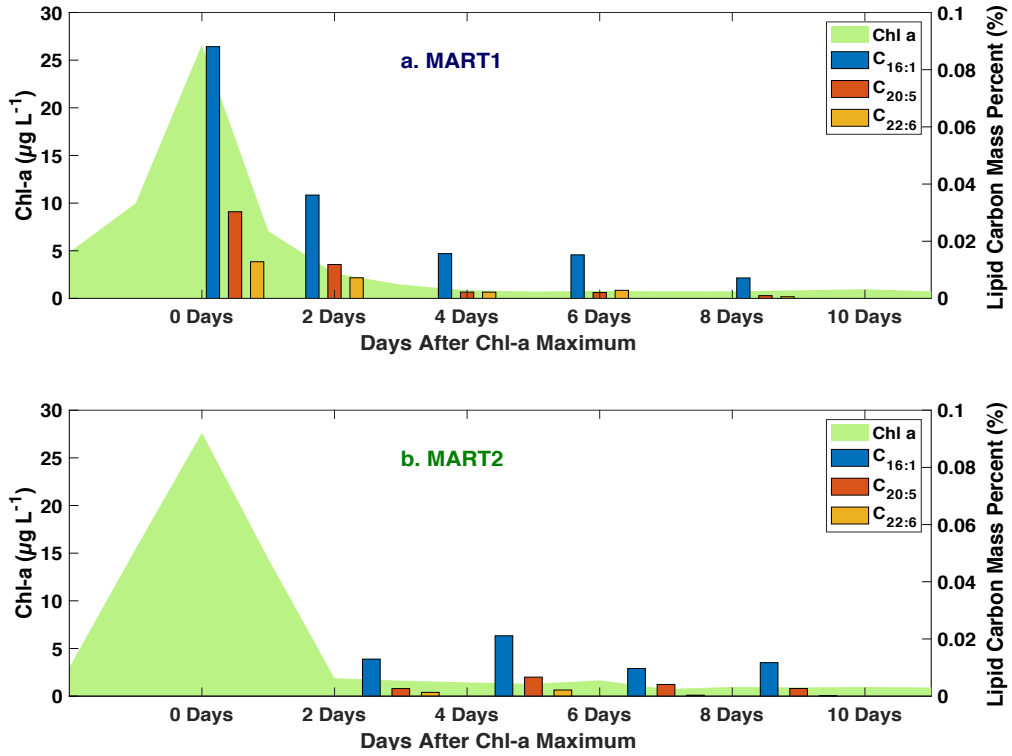

Figure 2.6 Changes in OC_{SSA} mass percent of three phytoplankton lipid biomarkers in SSA during the first 10 days of bloom decay for a) MART1 and b) MART2. The lipid biomarker concentrations were converted to lipid carbon mass percent to account for any differences in OC_{SSA} concentrations between SSA samples (see Figure 2.3). The highest values occur in the MART1 sample collected for the first 24 hours after the chl-a peak, and the lipid biomarker contributions to OC_{SSA} have decreased by more than 50% in the sample collected 24-72 hours after the chl-a peak. Measurement of the MART2 SSA sample collected in the 48 hours following the chl-a peak was not available but similar to MART1, MART2 also shows low contributions of the lipid biomarkers to all SSA samples collected more than 48 hours after the chl-a peak. The bars are placed in the middle of each SSA collection duration for every sample.

Similar to the findings in this work, Rinaldi et al.[58] have observed a time lag of 5-7 days, accounting for the air mass travel time, gives the highest correlation between chl-a and the contribution of water-insoluble organic matter (WIOM) to submicron SSA in ocean waters with high chl-a concentrations. The authors hypothesized this time lag might be due to seawater biological processes producing organic material that is more efficiently transferred into SSA but

did not directly resolve the relationship between increased WIOM enrichment in SSA and biological processes occurring in the seawater. Their field observations align well with our bloom experiments where an increased proportional contribution of more insoluble, freshly produced OC to OC_{SSA} occurred 2-3 days delayed from the maximum chl-a concentration. Because most of the freshly produced organic material formed during phytoplankton growth was in the POC pool, the time lag is likely related to the degradation of freshly produced POC into sizes small enough to efficiently transfer into SSA. In this study, freshly produced organic material during the phytoplankton growth phase, as indicated by chl-a, is likely dominated by whole, living phytoplankton, many of which are >10 μm in diameter,[64] larger than the majority of SSA particles.[3] Immediately following the chl-a peak in both experiments, the heterotrophic bacteria concentration swiftly increased resulting in the breakdown of freshly produced organic material into smaller phytoplankton exudates and detritus as well as organic aggregates. For both MART1 and MART2, bacterial abundance was highest either during or before the SSA sampling period with the largest $Fraction_{FreshOC}$, suggesting that several days after the chl-a maximum bacterial processing may have degraded freshly produced OC into small enough sizes to be more effectively enriched in SSA.

The proposed mechanism is supported by bubbling experiments on biologically active seawater that showed the ^{1}H-NMR spectra of submicron marine aerosol closely match the spectra for POC <10 μm.[24] This would also explain why the observed time lag was longer for submicron SSA compared to this study on TSP SSA, because the freshly produced OC would need to be broken down into smaller sizes to be transferred into the submicron aerosols. Although the exact physicochemical mechanisms controlling breakdown of freshly produced OC and enrichment in SSA cannot be fully resolved by these isotopic measurements, the comparable time lag between

peak chl-a and maximum freshly produced OC contribution to OC_{SSA} for both MART experiments strongly points to the important role heterotrophic bacteria play in controlling carbon transfer during separate phytoplankton blooms. The isotopic measurements highlight the influence of seawater microbiology on SSA organic composition, confirming conclusions from previous research indicating this influence depends on both phytoplankton and bacterial abundance.[30] Additionally, because freshly-produced OC has a less negative $\delta^{13}C$ value, these chemical and biological influences on OC_{SSA} composition may affect the $\delta^{13}C$ value of nascent SSA.

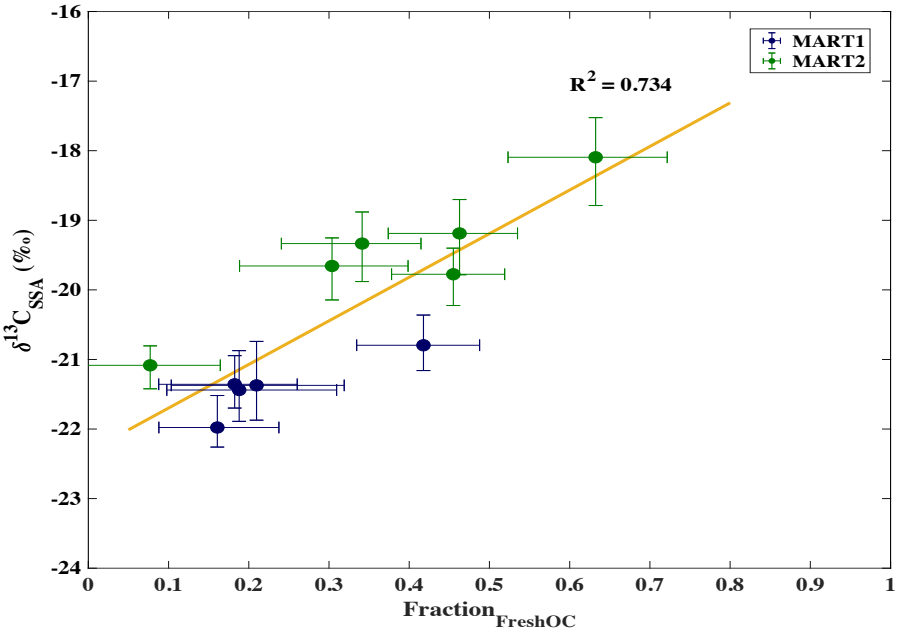

Figure 2.7 A robust positive correlation between $Fraction_{FreshOC}$ and $\delta^{13}C_{SSA}$ for the combined data from MART1 and MART2. This relationship suggests that increased incorporation of isotopically-heavy, freshly-produced OC into SSA leads to higher $\delta^{13}C_{SSA}$ values.

2.4.4 Impact of Seawater Carbon Pools on $\delta^{13}C_{SSA}$ Variability.

One of the main objectives for this study was to better understand how seawater biological activity impacts $\delta^{13}C_{SSA}$ values. Combining the isotopic data from both experiments shows that $\delta^{13}C_{SSA}$ ranged from -18 to -22 ‰ under conditions of high biological activity, less negative than

the normally assumed -20 to -23 ‰. Furthermore, Figure 2.7 shows that the less negative $\delta^{13}C_{SSA}$ values correlate with higher $Fraction_{FreshOC}$ values ($R^2 = 0.734$), suggesting that the biological influence on $\delta^{13}C_{SSA}$ derives from an increased proportional contribution of isotopically-heavy, freshly produced OC to SSA. Although the contribution of two separate carbon pools to OC_{SSA} complicates estimates of nascent $\delta^{13}C_{SSA}$, the fact that $\delta^{13}C_{SSA}$ consistently fell between $\delta^{13}C_{POC}$ and $\delta^{13}C_{DOC}$ for both experiments, indicates that seawater measurements of $\delta^{13}C_{POC}$ and $\delta^{13}C_{DOC}$ can provide upper and lower constraints on the range of likely nascent $\delta^{13}C_{SSA}$ values.

To investigate potential factors impacting the contribution of freshly produced OC to OC_{SSA}, correlation plots were made for the combined data from MART1 and MART2 to compare changes in POC, DOC, and OC_{SSML} concentrations with changes in OC_{SSA} concentration and $Fraction_{FreshOC}$ (Figure 2.8). The only significant correlation for the combined experiments, $R^2 = 0.6489$, was between OC_{SSML} concentration and $Fraction_{FreshOC}$ (Figure 2.8g), where higher OC_{SSML} concentrations corresponded to a larger $Fraction_{FreshOC}$ in SSA. One plausible explanation would be the SSML contained more freshly produced OC and higher OC_{SSML} concentrations resulted in a larger contribution of this carbon pool to SSA. However, if the OC_{SSML} was contributing more to OC_{SSA} one would expect their organic composition, and thus $\delta^{13}C_{SSML}$ and $\delta^{13}C_{SSA}$ values, should be similar. Figure 2.4b shows the two SSA samples with the highest $Fraction_{FreshOC}$ values and least negative $\delta^{13}C_{SSA}$ values, MART2 Days 6-8 and 8-10, correspond to the most negative $\delta^{13}C_{SSML}$ values. This indicates on these days the OC_{SSA} composition was actually not similar to the OC_{SSML} composition. Moreover, Figure 2.8c displays no correlation between OC_{SSML} and OC_{SSA} concentrations, suggesting increased OC_{SSML} concentrations did not lead to larger amounts of carbon transferred into SSA, but only to an increased proportional contribution of freshly produced OC to SSA. Because changes in seawater organic composition

do not seem to fully account for the differences in $Fraction_{FreshOC}$ between MART1 and MART2, we speculate below on two complementary explanations that address the primary formation mechanisms for SSA in the context of the relationship between higher OC_{SSML} concentrations and a higher contribution of freshly produced OC to SSA. These explanations are consistent with our measurements and recent research regarding the physical processes that affect carbon transfer into SSA. Recent bubble bursting experiments by Chingin et al.[65,66] indicate that adsorption of organics to the bubble surface begins as a kinetic process immediately following bubble formation, but transitions into a competitive equilibrium process as the bubble rises through the water column and its surface becomes saturated with organics. The competitive equilibrium process favors more aliphatic, insoluble organic species (e.g. lipids and biomolecules), which have a higher affinity for the bubble surface. Their research shows that for the seawater OC concentrations around 300 μM and bubble rise paths around 25 cm in our MART experiments, many bubbles will likely be saturated with organics before reaching the SSML. Because the bubble surface will already be saturated by the time the bubble rises to the SSML, the only way organic species near the seawater surface can be transferred to the bubble surface is through competitive equilibrium adsorption, which favors more aliphatic, insoluble freshly produced OC. Previous bubble bursting studies have found higher OC concentrations in surface seawater lead to bubble stabilization increasing bubble residence time at the air-sea interface, and allowing for more equilibrium adsorption.[67,68]

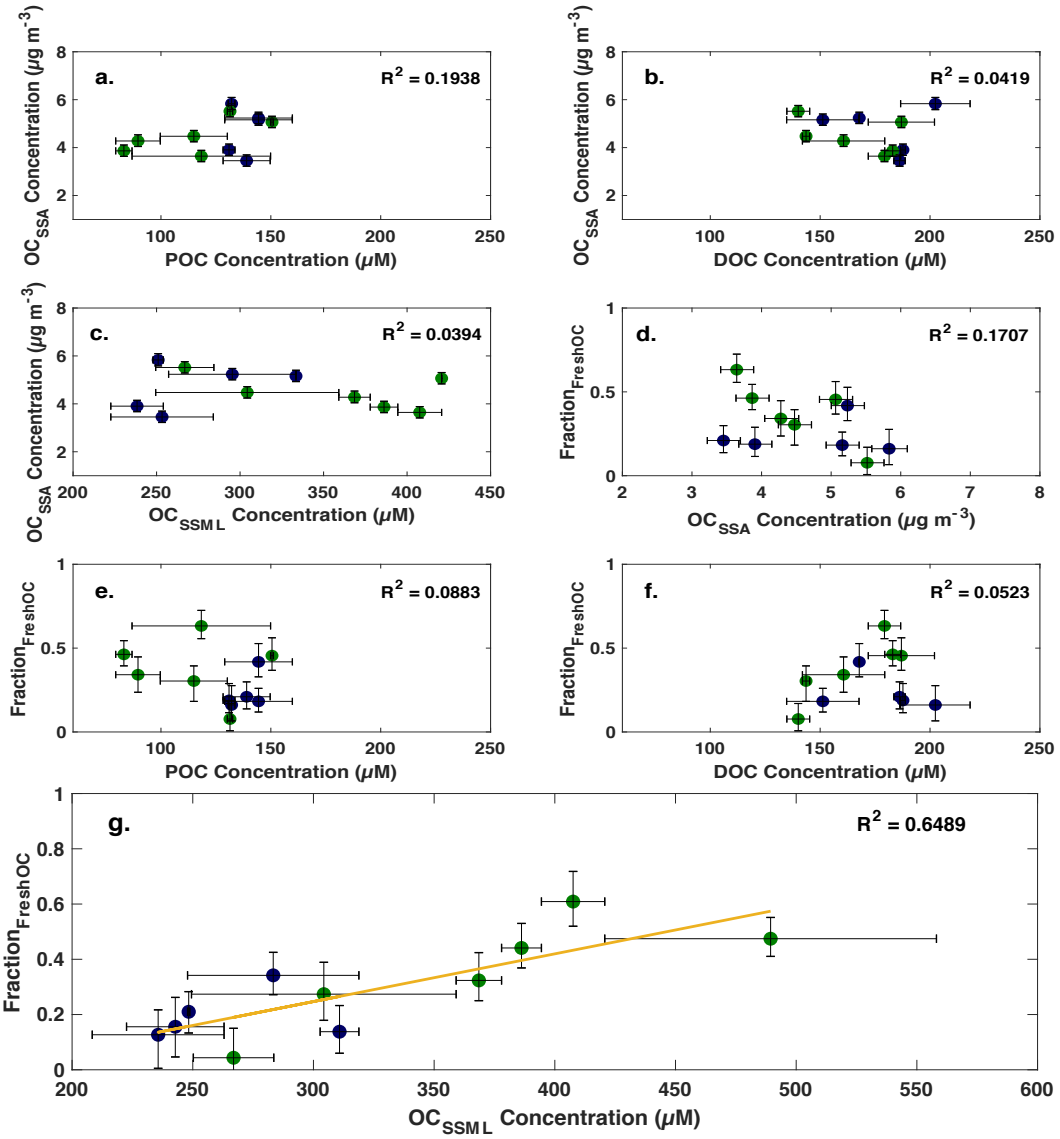

Figure 2.8 Correlation scatterplots of POC, DOC, and OC_{SSML} with OC_{SSA} (plots a-c), OC_{SSA} with $Fraction_{FreshOC}$ (plot d), and POC, DOC, and OC_{SSML} with $Fraction_{FreshOC}$ (plots e-g) for the combined data from MART1 (dark blue dots) and MART2 (green dots). The only significant correlation was between OC_{SSML} concentration and $Fraction_{FreshOC}$ (plot g), with higher OC_{SSML} concentrations leading to the increased proportional transfer of freshly produced OC into SSA. Vertical error bars are included for all data points and horizontal error bars represent the likely range of concentrations during each SSA collection period.

Supermicron SSA is primarily comprised of jet drops, which form from bulk seawater below the SSML,[16] so their organic composition is not expected to reflect the composition of the SSML. Because supermicron SSA includes organic material from the base of the bubble, the competitive equilibrium adsorption could lead to an increased proportion of freshly produced OC in supermicron SSA. An increased proportion of freshly produced OC in supermicron SSA would explain why the $Fraction_{FreshOC}$ increases, but the OC_{SSA} composition is not similar to the OC_{SSML}. On the other hand, submicron SSA are mostly formed from the bubble film when the bubble bursts. Longer bubble residence at the air-sea interface has been found to increase drainage of more soluble OC from the bubble film back into the seawater,[68] resulting in a larger proportion of aliphatic, freshly produced OC remaining on the bubble surface before bursting to form SSA. This provides a rationale for how the proportion of freshly produced OC could be higher in submicron SSA at higher OC_{SSML} concentrations.

These two MART experiments highlighting the important influence of the SSML on carbon transfer and OC_{SSA} composition suggest more comprehensive SSML organic concentration and composition measurements during field studies may be useful to characterize OC_{SSA} composition in the marine environment. Additionally, while our isotopic data cannot definitively establish that changes in bubble dynamics directly affected the contribution of freshly produced OC to SSA, future research focusing on the potentially significant impact of bubble persistence and drainage, as well as size dependence of OC_{SSA} composition, could be important to elucidating the fundamental mechanisms controlling carbon transfer into SSA.

2.5 Conclusions and Atmospheric Implications

This study performed two phytoplankton blooms in a highly characterized laboratory environment to evaluate the $\delta^{13}C$ value of isolated, nascent SSA and examine how $\delta^{13}C_{SSA}$ is influenced by seawater biological activity. The two phytoplankton bloom experiments revealed $\delta^{13}C_{SSA}$ is consistently less negative than $\delta^{13}C_{DOC}$ during high biological activity regimes, because of a significant contribution of isotopically less negative freshly produced OC to OC_{SSA}. Figure 2.9 depicts a simplified representation of how biological activity affects the seawater POC and DOC pools and shows the processes by which these carbon pools influence OC_{SSA} composition. The range of $\delta^{13}C$ values observed in the high biological activity regimes from this work are presented in Figure 2.9 for POC, DOC, SSML, and SSA. Some open ocean $\delta^{13}C$ measurements made over a wider range of biological activity levels are included from previous studies for comparison. To our knowledge this work provides the first $\delta^{13}C_{SSML}$ measurements and the first measurements for pure, nascent $\delta^{13}C_{SSA}$.

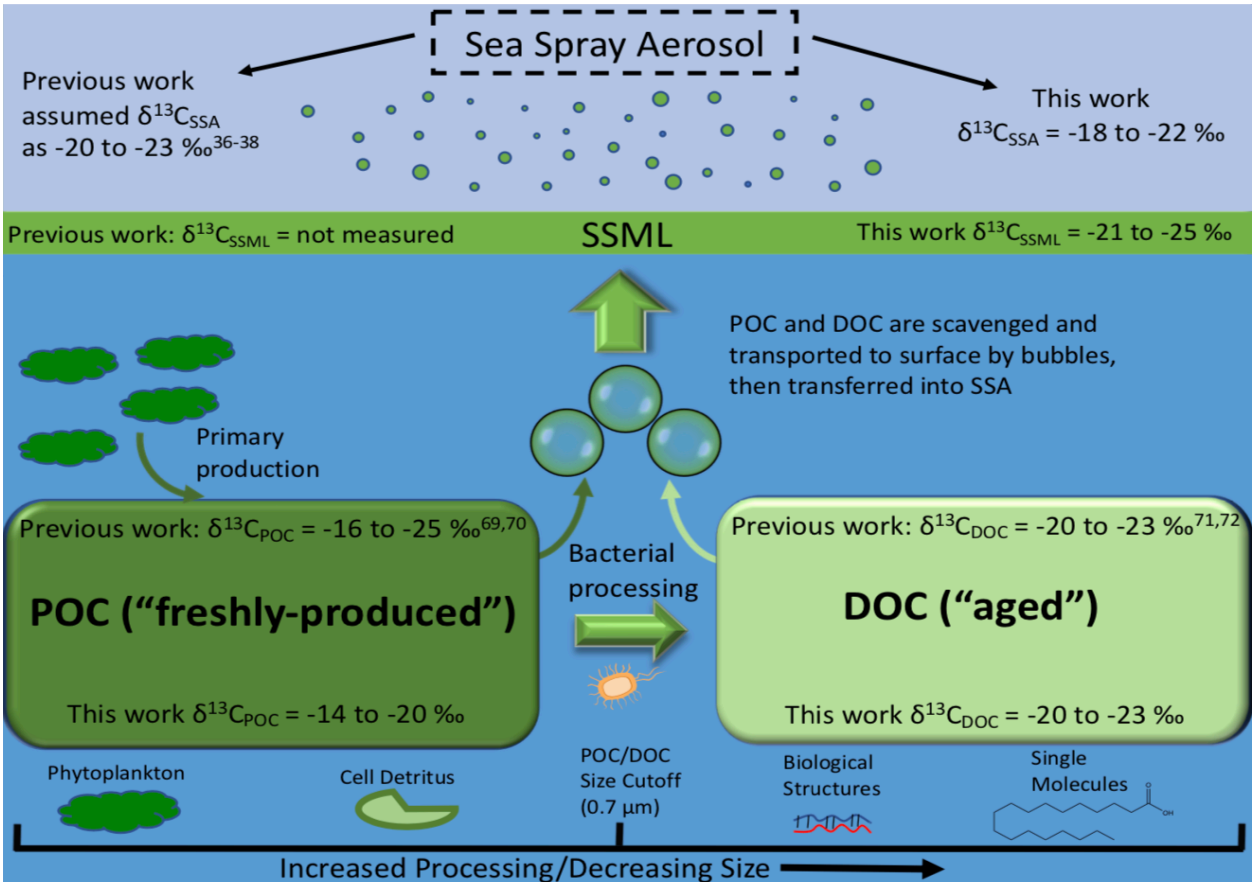

Figure 2.9 A schematic depicting the relationship between the different seawater carbon pools and their transfer processes into SSA. POC formed by primary production can be converted to DOC by microbial processing, and both POC and DOC are scavenged by bubbles, brought to the SSML and subsequently enriched in SSA. The size spectrum at the bottom of the schematic shows typical organisms and molecules in the seawater along with the operational 0.7 µm size cutoff used in this manuscript for POC and DOC. Also included are the $\delta^{13}C_{POC}$, $\delta^{13}C_{DOC}$, $\delta^{13}C_{SSML}$, and $\delta^{13}C_{SSA}$ ranges from this work observed during periods of high biological activity as well as open ocean values from previous works (with references) for comparison.[69–72]

Accounting for the biologically induced $\delta^{13}C_{SSA}$ variability exhibited in our experiments may help improve source apportionment of marine aerosols in oceanic regimes with elevated biological activity. The importance of considering biological influences on $\delta^{13}C_{SSA}$ in marine aerosol source apportionment calculations is illustrated by Figure 2.10. For given $\delta^{13}C_{marine}$ values, this figure shows the difference between the f_{anth} values calculated from Equation 1.3 when assuming a $\delta^{13}C_{SSA}$ of -21 ‰ versus using the actual $\delta^{13}C_{SSA}$ values of -18 to -22‰ observed in

our experiment. The f_{anth} difference, multiplied by 100 to obtain a percent value, is displayed as the colormap on Figure 2.10 and demonstrates that assuming a constant $\delta^{13}C_{SSA}$ of -21‰[37–39] can lead to over a 30% underestimate in the anthropogenic contribution to aerosol carbon in marine environments.

Studies looking to use our $\delta^{13}C_{SSA}$ measurements to improve marine aerosol source apportionment should consider that these measurements apply to nascent $\delta^{13}C_{SSA}$ before any atmospheric aging occurred. This has important implications for the OC_{SSA} composition and $\delta^{13}C$ values observed in this study as compared to marine aerosols. Photochemical aging of primary OC_{SSA} often leads to $\delta^{13}C$ increases during atmospheric transport.[73–75] Dasari et al.[75] have used the isotopic shift between source and receptor sites as a proxy to model the extent of aerosol aging. Field studies often collect SSA from air masses that have been traveling several days, so this study provides an isotopic source characterization of nascent SSA that can be integrated with marine measurements to evaluate aging of SSA. Aerosol aging can cause climatically significant changes in absorptivity and hygroscopicity,[73,75–77] so measuring $\delta^{13}C$ for nascent, unaltered SSA provides a critical reference point to understand the impact of aging on climatically relevant SSA properties.

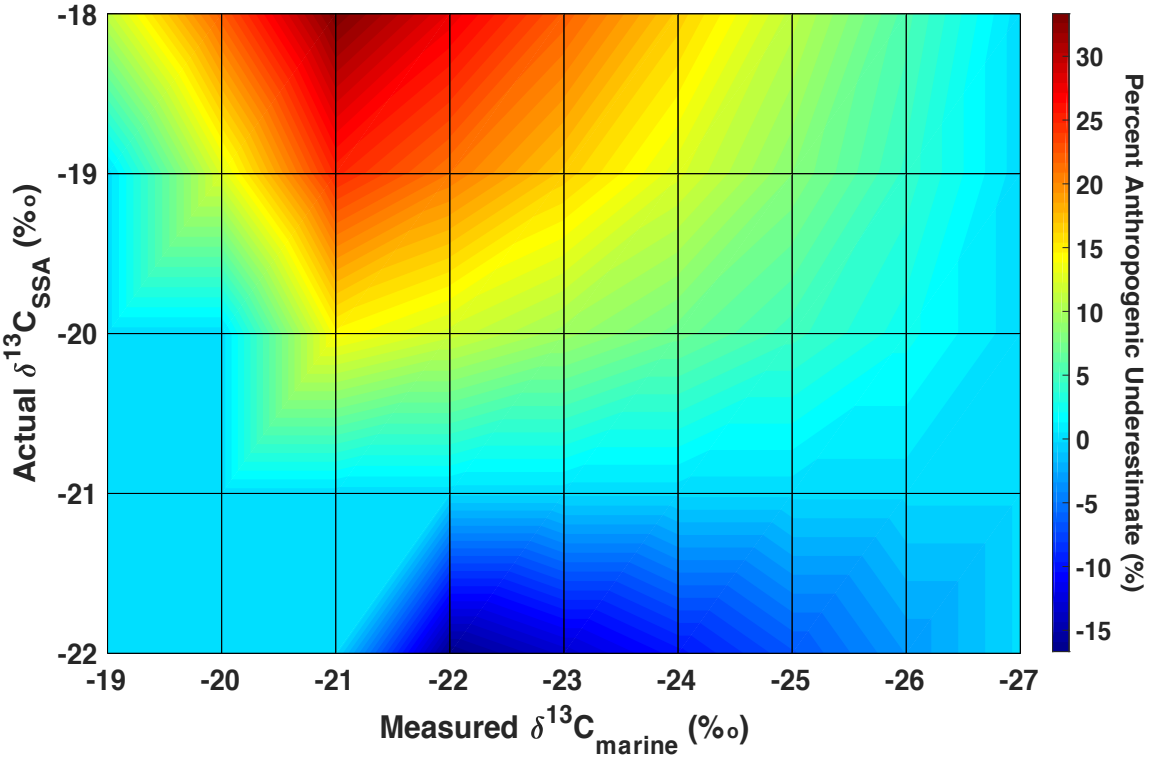

Figure 2.10 For each $\delta^{13}C_{marine}$ value, shows the difference in the percent anthropogenic contribution, f_{anth}(x100), calculated from Equation 1.3 when assuming a $\delta^{13}C_{SSA}$ of -21 ‰ versus using the actual $\delta^{13}C_{SSA}$ values of -18 to -22‰ observed in our experiment. A $\delta^{13}C_{anth}$ endmember of -27 ‰ was used based on previous marine source apportionment studies.[33,37] When $\delta^{13}C_{SSA}$ is -18 ‰, the highest value observed in our experiments, assuming a $\delta^{13}C_{SSA}$ of -21 ‰ results in a maximum underestimate of 33% at a measured $\delta^{13}C_{marine}$ value of -21 ‰.

In addition to aging of primary SSA, atmospheric oxidation of gas phase species can lead to formation of secondary marine aerosol (SMA). SMA is expected to have a more negative $\delta^{13}C$ value than primary SSA,[62-64] so source apportionment studies will need to account for the contribution of marine SMA to total marine aerosol carbon before applying the $\delta^{13}C_{SSA}$ values measured in these experiments. Dual-isotopic mixing is only able to distinguish between marine and terrestrial aerosol contributions, but atmospheric source apportionment studies would benefit greatly from the ability to separate primary and secondary marine aerosol carbon. These two experiments provide constraints on the $\delta^{13}C$ values for primary SSA, and applying these values to

aerosols in the remote marine environment (with minimal terrestrial contributions) can help future atmospheric studies differentiate between primary and secondary marine aerosols.

Hitherto, many marine field studies have focused on simple measurements of OC_{SSA} concentrations and enrichment factors to characterize SSA carbon. This is understandable as identification of unaltered, freshly produced organic species is complicated by rapid degradation of this highly labile organic material in the ocean and photochemical alteration during atmospheric transport. Nevertheless, it is highly recommended that future field studies supplement bulk OC_{SSA} measurements by including direct measurements of chemical or isotopic composition for seawater POC, seawater DOC, OC_{SSML} and OC_{SSA} to address the transfer of freshly produced OC into SSA. Our isotopic measurements indicate the most significant biological influence on OC_{SSA} occurred 2-3 days after the chl-a peak and suggest the contribution of freshly produced OC to OC_{SSA} is strongly dependent on the degradation processes and timescales for incorporation of this organic material into nascent SSA as it forms at the ocean surface. These findings imply that accurate knowledge of seawater enzymatic activity and kinetics for microbial degradation of freshly produced organic material are integral to understanding biological impacts on OC_{SSA} composition, and measurements of these properties should be a focus of future marine field studies.

2.6 Supporting Information

2.6.1 Determination of Filter Blanks and Measurement Uncertainties.

All isotopic corrections for the POC and SSA filter blanks were made using Equation 2.2 for isotopic mass balance to calculate $\delta^{13}C_{SSA}$ or $\delta^{13}C_{POC}$:

$$\delta^{13}C_{Sample} = (f_{blank})(\delta^{13}C_{blank}) + (f_{SSAorPOC})(\delta^{13}C_{SSAorPOC}) \quad \text{(Equation 2.2)}$$

For determination of the POC filter blank mass fraction, f_{blank}, four combusted GF/F filters were analyzed simultaneously with the POC samples. The carbon amount and isotopes from these four blank samples were averaged and the measurement uncertainty used was the standard deviation of the four blanks' values for both isotopes and amount.

For SSA samples, the carbon amount (OC_{SSA}) and $\delta^{13}C_{SSA}$ f_{blank} values were separated into an offline analysis carbon blank and a MART sampling carbon blank. The offline analysis carbon blank ("field blank") was determined by individually attaching four QMA filters to the MART and immediately removing without any air collection. The MART sampling carbon blank was determined by separately attaching three QMA filters to a sealed MART containing 120 L of seawater with particle-free air pumping through the headspace. Air was collected onto the QMA filters for 3 days each, nine days in total, by pumping at 5 L min^{-1}, but without any aerosol production from the plunging waterfall. The difference between the "field blank" and three-day collection blanks gave the MART sampling carbon blank, which is important as QMA filters have been shown to absorb some gaseous species in addition to aerosols.[1,2] The MART sampling carbon blank was further corrected to account for differing 1-3 day SSA sampling durations before use in Equation 2.2.

2.6.2 Averaging of Seawater $\delta^{13}C$ for Calculation of $Fraction_{FreshOC}$ and OC Correlations.

To facilitate comparison of $\delta^{13}C_{SSA}$ with $\delta^{13}C_{POC}$, $\delta^{13}C_{DOC}$, and $\delta^{13}C_{SSML}$, the values measured at the beginning and end of each SSA collection period were averaged and these average values are plotted in Figure 2.4. All averaged data points for the three seawater species are placed in the middle of the time period between the two measurements used in the average. If one of the seawater $\delta^{13}C$ values was not measured on a specific day, the nearest two measurements were used

to calculate the average value. For example, no measurements for POC, DOC, or SSML were made for MART2 Day 15, so the data points for $\delta^{13}C_{POC}$, $\delta^{13}C_{DOC}$, and $\delta^{13}C_{SSML}$ on MART2 Day 15 are an average of the Day 13 and Day 17 seawater $\delta^{13}C$ values, as these were the nearest measured data points. Likewise, the Day 4 and Day 7 $\delta^{13}C_{POC}$ values were averaged and included both the Day 4-5 and Day 5-7 SSA samples. This averaged $\delta^{13}C_{POC}$ value was compared to both SSA samples for any further calculations. These are the two instances where a seawater value did not directly line up with a $\delta^{13}C_{SSA}$ measurement.

The same averaging technique was used to calculate the $Fraction_{FreshOC}$ displayed in Figure 2.5. For averaged DOC, POC, or SSML values that did not perfectly overlap with the SSA collection period, the closest averaged value was used to compare to the SSA, same as the explanation above.

2.7 Acknowledgements

This material is based on work supported by the National Science Foundation through the Centers for Chemical Innovation Program under Grant CHE-1801971. We thank Kathryn Mayer for assistance with aerosol sizing measurements and Bruce Deck for assistance with POC isotope measurements. We also thank Subrata Chakraborty, Lihini Aluwihare, Francesca Malfatti, and Nicole Peiris for helpful discussions.

Chapter 2, in part, is a reprint of the material as published in ACS Earth and Space Chemistry, 2020. Crocker, D. R.; Hernandez, R.; Huang D. H.; Pendergraft, M. A.; Cao, R.; Dai, J.; Morris, C. K.; Deane, G. B.; Prather, K. A.; Thiemens M. H. The dissertation author was the primary investigator and author of this paper.

2.8 References

(1) Quinn, P. K.; Collins, D. B.; Grassian, V. H.; Prather, K. A.; Bates, T. S. Chemistry and Related Properties of Freshly Emitted Sea Spray Aerosol. *Chem. Rev.* **2015**, *115* (10), 4383–4399. https://doi.org/10.1021/cr500713g.

(2) De Leeuw, G.; Andreas, E. L.; Anguelova, M. D.; Fairall, C. W.; Lewis, E. R.; O'Dowd, C.; Schulz, M.; Schwartz, S. E. Production Flux of Sea Spray Aerosol. *Rev. Geophys.* **2011**, *49* (2), 1–39. https://doi.org/10.1029/2010RG000349.

(3) Prather, K. A.; Bertram, T. H.; Grassian, V. H.; Deane, G. B.; Stokes, M. D.; DeMott, P. J.; Aluwihare, L. I.; Palenik, B. P.; Azam, F.; Seinfeld, J. H.; Moffet, R. C.; Molina, M. J.; Cappa, C. D.; Geiger, F. M.; Roberts, G. C.; Russell, L. M.; Ault, A. P.; Baltrusaitis, J.; Collins, D. B.; Corrigan, C. E.; Cuadra-Rodriguez, L. A.; Ebben, C. J.; Forestieri, S. D.; Guasco, T. L.; Hersey, S. P.; Kim, M. J.; Lambert, W. F.; Modini, R. L.; Mui, W.; Pedler, B. E.; Ruppel, M. J.; Ryder, O. S.; Schoepp, N. G.; Sullivan, R. C.; Zhao, D. Bringing the Ocean into the Laboratory to Probe the Chemical Complexity of Sea Spray Aerosol. *PNAS* **2013**, *110* (19), 7550–7555. https://doi.org/10.1073/pnas.1300262110.

(4) Bertram, T. H.; Cochran, R. E.; Grassian, V. H.; Stone, E. A. Sea Spray Aerosol Chemical Composition: Elemental and Molecular Mimics for Laboratory Studies of Heterogeneous and Multiphase Reactions. *Chem. Soc. Rev.* **2018**, *47* (7), 2374–2400. https://doi.org/10.1039/c7cs00008a.

(5) Ovadnevaite, J.; O'Dowd, C.; Dall'Osto, M.; Ceburnis, D.; Worsnop, D. R.; Berresheim, H. Detecting High Contributions of Primary Organic Matter to Marine Aerosol: A Case Study. *Geophys. Res. Lett.* **2011**, *38* (2), 2–6. https://doi.org/10.1029/2010GL046083.

(6) Patterson, J. P.; Collins, D. B.; Michaud, J. M.; Axson, J. L.; Sultana, C. M.; Moser, T.; Dommer, A. C.; Conner, J.; Grassian, V. H.; Stokes, M. D.; Deane, G. B.; Evans, J. E.; Burkart, M. D.; Prather, K. A.; Gianneschi, N. C. Sea Spray Aerosol Structure and Composition Using Cryogenic Transmission Electron Microscopy. *ACS Cent. Sci.* **2016**, *2* (1), 40–47. https://doi.org/10.1021/acscentsci.5b00344.

(7) Brooks, S. D.; Thornton, D. C. O. Marine Aerosols and Clouds. *Ann. Rev. Mar. Sci.* **2018**, *10*, 289–313. https://doi.org/10.1146/annurev-marine-121916-063148.

(8) Keene, W. C.; Maring, H.; Maben, J. R.; Kieber, D. J.; Pszenny, A. A. P.; Dahl, E. E.; Izaguirre, M. A.; Davis, A. J.; Long, M. S.; Zhou, X.; Smoydzin, L.; Sander, R. Chemical and Physical Characteristics of Nascent Aerosols Produced by Bursting Bubbles at a Model Air-Sea Interface. *J. Geophys. Res. Atmos.* **2007**, *112* (21), 1–16. https://doi.org/10.1029/2007JD008464.

(9) Sellegri, K.; O'Dowd, C. D.; Yoon, Y. J.; Jennings, S. G.; de Leeuw, G. Surfactants and Submicron Sea Spray Generation. *J. Geophys. Res. Atmos.* **2006**, *111* (22), 1–12. https://doi.org/10.1029/2005JD006658.

(10) Forestieri, S. D.; Cornwell, G. C.; Helgestad, T. M.; Moore, K. A.; Lee, C.; Novak, G. A.; Sultana, C. M.; Wang, X.; Bertram, T. H.; Prather, K. A.; Cappa, C. D. Linking Variations in Sea Spray Aerosol Particle Hygroscopicity to Composition during Two Microcosm Experiments. *Atmos. Chem. Phys.* **2016**, *16* (14), 9003–9018. https://doi.org/10.5194/acp-16-9003-2016.

(11) DeMott, P. J.; Hill, T. C. J.; McCluskey, C. S.; Prather, K. A.; Collins, D. B.; Sullivan, R. C.; Ruppel, M. J.; Mason, R. H.; Irish, V. E.; Lee, T.; Hwang, C. Y.; Rhee, T. S.; Snider, J. R.; McMeeking, G. R.; Dhaniyala, S.; Lewis, E. R.; Wentzell, J. J. B.; Abbatt, J.; Lee, C.; Sultana, C. M.; Ault, A. P.; Axson, J. L.; Martinez, M. D.; Venero, I.; Santos-Figueroa, G.; Stokes, M. D.; Deane, G. B.; Mayol-Bracero, O. L.; Grassian, V. H.; Bertram, T. H.; Bertram, A. K.; Moffett, B. F.; Franc, G. D. Sea Spray Aerosol as a Unique Source of Ice Nucleating Particles. *PNAS* **2016**, *113* (21), 5797–5803. https://doi.org/10.1073/pnas.1514034112.

(12) McCluskey, C. S.; Hill, E. T. C. J.; Sultana, C. M.; Laskina, O.; Trueblood, J.; Santander, M. V.; Beall, C. M.; Michaud, J. M.; Kreidenweis, S. M.; Prather, K. A.; Grassian, V.; Demott, P. J. A Mesocosm Double Feature: Insights into the Chemical Makeup of Marine Ice Nucleating Particles. *J. Atmos. Sci.* **2018**, *75* (7), 2405–2423. https://doi.org/10.1175/JAS-D-17-0155.1.

(13) Blanchard, D. Sea-to-Air Transport of Surface Active Material. *Science (80-.).* **1964**, *146* (3642), 396–397.

(14) Schmitt-Kopplin, P.; Liger-Belair, G.; Koch, B. P.; Flerus, R.; Kattner, G.; Harir, M.; Kanawati, B.; Lucio, M.; Tziotis, D.; Hertkorn, N.; Gebefügi, I. Dissolved Organic Matter in Sea Spray: A Transfer Study from Marine Surface Water to Aerosols. *Biogeosciences* **2012**, *9* (4), 1571–1582. https://doi.org/10.5194/bg-9-1571-2012.

(15) Quinn, P. K.; Bates, T. S.; Schulz, K. S.; Coffman, D. J.; Frossard, A. A.; Russell, L. M.; Keene, W. C.; Kieber, D. J. Contribution of Sea Surface Carbon Pool to Organic Matter Enrichment in Sea Spray Aerosol. *Nat. Geosci.* **2014**, *7* (3), 228–232. https://doi.org/10.1038/ngeo2092.

(16) Wang, X.; Deane, G. B.; Moore, K. A.; Ryder, O. S.; Stokes, M. D.; Beall, C. M.; Collins, D. B.; Santander, M. V.; Burrows, S. M.; Sultana, C. M.; Prather, K. A. The Role of Jet and Film Drops in Controlling the Mixing State of Submicron Sea Spray Aerosol Particles. *PNAS* **2017**, *114* (27), 6978–6983. https://doi.org/10.1073/pnas.1702420114.

(17) Van Pinxteren, M.; Müller, C.; Iinuma, Y.; Stolle, C.; Herrmann, H. Chemical Characterization of Dissolved Organic Compounds from Coastal Sea Surface Microlayers (Baltic Sea, Germany). *Environ. Sci. Technol.* **2012**, *46* (19), 10455–10462. https://doi.org/10.1021/es204492b.

(18) Cunliffe, M.; Engel, A.; Frka, S.; Gašparović, B. Ž.; Guitart, C.; Murrell, J. C.; Salter, M.; Stolle, C.; Upstill-Goddard, R.; Wurl, O. Sea Surface Microlayers: A Unified

Physicochemical and Biological Perspective of the Air-Ocean Interface. *Prog. Oceanogr.* **2013**, *109*, 104–116. https://doi.org/10.1016/j.pocean.2012.08.004.

(19) Kieber, D. J.; Keene, W. C.; Frossard, A. A.; Long, M. S.; Maben, J. R.; Russell, L. M.; Kinsey, J. D.; Tyssebotn, I. M. B.; Quinn, P. K.; Bates, T. S. Coupled Ocean-Atmosphere Loss of Marine Refractory Dissolved Organic Carbon. *Geophys. Reserach Lett.* **2016**, *43* (6), 2765–2772. https://doi.org/10.1002/2016GL068273.Received.

(20) Bates, T. S.; Quinn, P. K.; Coffman, D. J.; Johnson, J. E.; Upchurch, L.; Saliba, G.; Lewis, S.; Graff, J.; Russell, L. M.; Behrenfeld, M. J. Variability in Marine Plankton Ecosystems Are Not Observed in Freshly Emitted Sea Spray Aerosol Over the North Atlantic Ocean. *Geophys. Res. Lett.* **2020**, *47* (1). https://doi.org/10.1029/2019GL085938.

(21) O'Dowd, C. D.; Facchini, M. C.; Cavalli, F.; Ceburnis, D.; Mircea, M.; Decesari, S.; Fuzzi, S.; Young, J. Y.; Putaud, J. P. Biogenically Driven Organic Contribution to Marine Aerosol. *Nature* **2004**, *431* (7009), 676–680. https://doi.org/10.1038/nature02959.

(22) Cavalli, F.; Facchini, M. C.; Decesari, S.; Mircea, M.; Emblico, L.; Fuzzi, S.; Ceburnis, D.; Yoon, Y. J.; O'Dowd, C. D.; Putaud, J. P.; Dell'Acqua, A. Advances in Characterization of Size-Resolved Organic Matter in Marine Aerosol over the North Atlantic. *J. Geophys. Res. D Atmos.* **2004**, *109* (24), 1–14. https://doi.org/10.1029/2004JD005137.

(23) Yoon, Y. J.; Ceburnis, D.; Cavalli, F.; Jourdan, O.; Putaud, J. P.; Facchini, M. C.; Decesari, S.; Fuzzi, S.; Sellegri, K.; Jennings, S. G.; O'Dowd, C. D. Seasonal Characteristics of the Physicochemical Properties of North Atlantic Marine Atmospheric Aerosols. *J. Geophys. Res. Atmos.* **2007**, *112* (4), 1–14. https://doi.org/10.1029/2005JD007044.

(24) Facchini, M. C.; Rinaldi, M.; Decesari, S.; Carbone, C.; Finessi, E.; Mircea, M.; Fuzzi, S.; Ceburnis, D.; Flanagan, R.; Nilsson, E. D.; de Leeuw, G.; Martino, M.; Woeltjen, J.; O'Dowd, C. D. Primary Submicron Marine Aerosol Dominated by Insoluble Organic Colloids and Aggregates. *Geophys. Res. Lett.* **2008**, *35* (17). https://doi.org/10.1029/2008GL034210.

(25) Pomeroy, L. R.; le Williams, P. J. B.; Azam, F.; Hobbie, J. E. The Microbial Loop. *Oceanography* **2007**, *20* (SPL.ISS. 2), 28–33. https://doi.org/10.5670/oceanog.2007.45.

(26) Smith, D.; Simon, M.; Alldredge, A.; Azam, F. Intense Hydrolytic Enzyme Activity on Marine Aggregates and Implications for Rapid Particle Dissolution. *Nature* **1992**, *359* (6391), 139–142. https://doi.org/10.1038/246170a0.

(27) Tremblay, L.; Caparros, J.; Leblanc, K.; Obernosterer, I. Origin and Fate of Particulate and Dissolved Organic Matter in a Naturally Iron-Fertilized Region of the Southern Ocean. *Biogeosciences* **2015**, *12* (2), 607–621. https://doi.org/10.5194/bg-12-607-2015.

(28) Cochran, R. E.; Laskina, O.; Jayarathne, T.; Laskin, A.; Laskin, J.; Lin, P.; Sultana, C.; Lee, C.; Moore, K. A.; Cappa, C. D.; Bertram, T. H.; Prather, K. A.; Grassian, V. H.; Stone, E.

A. Analysis of Organic Anionic Surfactants in Fine and Coarse Fractions of Freshly Emitted Sea Spray Aerosol. *Environ. Sci. Technol.* **2016**, *50* (5), 2477–2486. https://doi.org/10.1021/acs.est.5b04053.

(29) Shank, L. M.; Howell, S.; Clarke, A. D.; Freitag, S.; Brekhovskikh, V.; Kapustin, V.; McNaughton, C.; Campos, T.; Wood, R. Organic Matter and Non-Refractory Aerosol over the Remote Southeast Pacific: Oceanic and Combustion Sources. *Atmos. Chem. Phys.* **2012**, *12* (1), 557–576. https://doi.org/10.5194/acp-12-557-2012.

(30) Wang, X.; Sultana, C. M.; Trueblood, J.; Hill, T. C. J.; Malfatti, F.; Lee, C.; Laskina, O.; Moore, K. A.; Beall, C. M.; McCluskey, C. S.; Cornwell, G. C.; Zhou, Y.; Cox, J. L.; Pendergraft, M. A.; Santander, M. V.; Bertram, T. H.; Cappa, C. D.; Azam, F.; DeMott, P. J.; Grassian, V. H.; Prather, K. A. Microbial Control of Sea Spray Aerosol Composition: A Tale of Two Blooms. *ACS Cent. Sci.* **2015**, *1* (3), 124–131. https://doi.org/10.1021/acscentsci.5b00148.

(31) Gantt, B.; Meskhidze, N. The Physical and Chemical Characteristics of Marine Primary Organic Aerosol: A Review. *Atmos. Chem. Phys.* **2013**, *13* (8), 3979–3996. https://doi.org/10.5194/acp-13-3979-2013.

(32) Malfatti, F.; Lee, C.; Tinta, T.; Pendergraft, M. A.; Celussi, M.; Zhou, Y.; Sultana, C. M.; Rotter, A.; Axson, J. L.; Collins, D. B.; Santander, M. V.; Anides Morales, A. L.; Aluwihare, L. I.; Riemer, N.; Grassian, V. H.; Azam, F.; Prather, K. A. Detection of Active Microbial Enzymes in Nascent Sea Spray Aerosol: Implications for Atmospheric Chemistry and Climate. *Environ. Sci. Technol. Lett.* **2019**, *6* (3), 171–177. https://doi.org/10.1021/acs.estlett.8b00699.

(33) Kundu, S.; Kawamura, K. Seasonal Variations of Stable Carbon Isotopic Composition of Bulk Aerosol Carbon from Gosan Site, Jeju Island in the East China Sea. *Atmos. Environ.* **2014**, *94*, 316–322. https://doi.org/10.1016/j.atmosenv.2014.05.045.

(34) Ceburnis, D.; Garbaras, A.; Szidat, S.; Rinaldi, M.; Fahrni, S.; Perron, N.; Wacker, L.; Leinert, S.; Remeikis, V.; Facchini, M. C.; Prevot, A. S. H.; Jennings, S. G.; Ramonet, M.; O'Dowd, C. D. Quantification of the Carbonaceous Matter Origin in Submicron Marine Aerosol by 13C and 14C Isotope Analysis. *Atmos. Chem. Phys.* **2011**, *11* (16), 8593–8606. https://doi.org/10.5194/acp-11-8593-2011.

(35) Cachier, H.; Buat-Menard, P.; Fontugne, M.; Chesselet, R. Long-range Transport of Continentally-derived Particulate Carbon in the Marine Atmosphere: Evidence from Stable Carbon Isotope Studies. *Tellus B* **1986**, *38 B* (3–4), 161–177. https://doi.org/10.1111/j.1600-0889.1986.tb00184.x.

(36) Miyazaki, Y.; Coburn, S.; Ono, K.; Ho, D. T.; Pierce, R. B.; Kawamura, K.; Volkamer, R. Contribution of Dissolved Organic Matter to Submicron Water-Soluble Organic Aerosols in the Marine Boundary Layer over the Eastern Equatorial Pacific. *Atmos. Chem. Phys.* **2016**, *16* (12), 7695–7707. https://doi.org/10.5194/acp-16-7695-2016.

(37) Turekian, V. C.; Macko, S. A.; Keene, W. C. Concentrations, Isotopic Compositions, and Sources of Size-Resolved, Particulate Organic Carbon and Oxalate in near-Surface Marine Air at Bermuda during Spring. *J. Geophys. Res. Atmos.* **2003**, *108* (5). https://doi.org/10.1029/2002jd002053.

(38) Miyazaki, Y.; Kawamura, K.; Sawano, M. Size Distributions of Organic Nitrogen and Carbon in Remote Marine Aerosols: Evidence of Marine Biological Origin Based on Their Isotopic Ratios. *Geophys. Res. Lett.* **2010**, *37* (6). https://doi.org/10.1029/2010GL042483.

(39) Chesselet, R.; Fontugne, M.; Buat-Menard, P.; Esat, U.; Lambert, C. E. The Origin of Particulate Organic Carbon in the Marine Atmosphere as Indicated by Its Stable Carbon Isotopic Composition. **1981**, *8* (4), 345–348.

(40) Ceburnis, D.; Masalaite, A.; Ovadnevaite, J.; Garbaras, A.; Remeikis, V.; Maenhaut, W.; Claeys, M.; Sciare, J.; Baisnée, D.; O'Dowd, C. D. Stable Isotopes Measurements Reveal Dual Carbon Pools Contributing to Organic Matter Enrichment in Marine Aerosol. *Sci. Rep.* **2016**, *6* (July), 1–6. https://doi.org/10.1038/srep36675.

(41) Ostrom, N. E.; Macko, S. A.; Deibel, D.; Thompson, R. Seasonal Variation in the Stable Carbon and Nitrogen Isotope Biogeochemistry of a Coastal Cold Ocean Environment. **1997**, *61* (14), 2929–2942.

(42) Savoye, N.; Aminot, A.; Tréguer, P.; Fontugne, M.; Naulet, N.; Kérouel, R. Dynamics of Particulate Organic Matter Δ15N and Δ13C during Spring Phytoplankton Blooms in a Macrotidal Ecosystem (Bay of Seine, France). *Mar. Ecol. Prog. Ser.* **2003**, *255*, 27–41. https://doi.org/10.3354/meps255027.

(43) Kukert, H.; Riebesell, U. Phytoplankton Carbon Isotope Fractionation during a Diatom Spring Bloom in a Norwegian Fjord. *Mar. Ecol. Prog. Ser.* **1998**, *173*, 127–137. https://doi.org/10.3354/meps173127.

(44) Stokes, M. D.; Deane, G. B.; Prather, K.; Bertram, T. H.; Ruppel, M. J.; Ryder, O. S.; Brady, J. M.; Zhao, D. A Marine Aerosol Reference Tank System as a Breaking Wave Analogue for the Production of Foam and Sea-Spray Aerosols. *Atmos. Meas. Tech.* **2013**, *6* (4), 1085–1094. https://doi.org/10.5194/amt-6-1085-2013.

(45) Guillard, R. R. L.; Ryther, J. H. Studies of Marine Planktonic Diatoms. I. Cyclotella Nana. *Can. J. Microbiol.* **1962**, *8*, 229–239.

(46) Lee, C.; Sultana, C. M.; Collins, D. B.; Santander, M. V.; Axson, J. L.; Malfatti, F.; Cornwell, G. C.; Grandquist, J. R.; Deane, G. B.; Stokes, M. D.; Azam, F.; Grassian, V. H.; Prather, K. A. Advancing Model Systems for Fundamental Laboratory Studies of Sea Spray Aerosol Using the Microbial Loop. *J. Phys. Chem. A* **2015**, *119* (33), 8860–8870. https://doi.org/10.1021/acs.jpca.5b03488.

(47) Cunliffe, M.; Wurl, O. Sampling the Sea Surface Microlayer; 2015; pp 255–261. https://doi.org/10.1007/8623_2015_83.

(48) Wurl, O.; Wurl, E.; Miller, L.; Johnson, K.; Vagle, S. Formation and Global Distribution of Sea-Surface Microlayers. *Biogeosciences* **2011**, *8* (1), 121–135. https://doi.org/10.5194/bg-8-121-2011.

(49) McKinney, C. R.; McCrea, J. M.; Epstein, S.; Allen, H. A.; Urey, H. C. Improvements in Mass Spectrometers for the Measurement of Small Differences in Isotope Abundance Ratios. *Rev. Sci. Instrum.* **1950**, *21* (8), 724–730.

(50) Craig, H. Isotopic Standards for Carbon and Oxygen and Correction Factors for Mass-Spectrometric Analysis of Carbon Dioxide. *Geochim. Cosmochim. Acta* **1957**, *12* (1–2), 133–149. https://doi.org/10.1016/0016-7037(57)90024-8.

(51) Lalonde, K.; Middlestead, P.; Gélinas, Y. Automation of 13C/12C Ratio Measurement for Freshwater and Seawater DOC Using High Temperature Combustion. *Limnol. Oceanogr. Methods* **2014**, *12* (DEC), 816–829. https://doi.org/10.4319/lom.2014.12.816.

(52) Kuwata, M.; Kondo, Y. Measurements of Particle Masses of Inorganic Salt Particles for Calibration of Cloud Condensation Nuclei Counters. *Atmos. Chem. Phys.* **2009**, *9*, 5921–5932. https://doi.org/10.1201/b12873-13.

(53) Kelly, W. P.; McMurry, P. H. Measurement of Particle Density by Inertial Classification of Differential Mobility Analyzer–Generated Monodisperse Aerosols. *Aerosol Sci. Technol.* **1992**, *17* (3), 199–212. https://doi.org/10.1080/02786829208959571.

(54) Bligh, E. G.; Dyer, W. J. A RAPID METHOD OF TOTAL LIPID EXTRACTION AND PURIFICATION. *Can. J. Biochem. Physiol.* **1959**, *37* (8).

(55) Quehenberger, O.; Armando, A. M.; Brown, A. H.; Milne, S. B.; Myers, D. S.; Merrill, A. H.; Bandyopadhyay, S.; Jones, K. N.; Kelly, S.; Shaner, R. L.; Sullards, C. M.; Wang, E.; Murphy, R. C.; Barkley, R. M.; Leiker, T. J.; Raetz, C. R. H.; Guan, Z.; Laird, G. M.; Six, D. A.; Russell, D. W.; McDonald, J. G.; Subramaniam, S.; Fahy, E.; Dennis, E. A. Lipidomics Reveals a Remarkable Diversity of Lipids in Human Plasma. *J. Lipid Res.* **2010**, *51* (11), 3299–3305. https://doi.org/10.1194/jlr.M009449.

(56) Yuras, G.; Ulloa, O.; Hormazábal, S. On the Annual Cycle of Coastal and Open Ocean Satellite Chlorophyll off Chile (18°-40°s). *Geophys. Res. Lett.* **2005**, *32* (23), 1–4. https://doi.org/10.1029/2005GL023946.

(57) O'Reilly, J. E.; Maritorena, S.; Mitchell, B. G.; Siegel, D. A.; Carder, K. L.; Garver, S. A.; Kahru, M.; McClain, C. Ocean Color Chlorophyll Algorithms for SeaWiFS. *J. Geophys. Res. Ocean.* **1998**, *103* (C11), 24937–24953. https://doi.org/10.1029/98JC02160.

(58) Rinaldi, M.; Fuzzi, S.; Decesari, S.; Marullo, S.; Santoleri, R.; Provenzale, A.; Von

Hardenberg, J.; Ceburnis, D.; Vaishya, A.; O'Dowd, C. D.; Facchini, M. C. Is Chlorophyll-a the Best Surrogate for Organic Matter Enrichment in Submicron Primary Marine Aerosol? *J. Geophys. Res. Atmos.* **2013**, *118* (10), 4964–4973. https://doi.org/10.1002/jgrd.50417.

(59) O'Dowd, C.; Ceburnis, D.; Ovadnevaite, J.; Bialek, J.; Stengel, D. B.; Zacharias, M.; Nitschke, U.; Connan, S.; Rinaldi, M.; Fuzzi, S.; Decesari, S.; Cristina Facchini, M.; Marullo, S.; Santoleri, R.; Dell'anno, A.; Corinaldesi, C.; Tangherlini, M.; Danovaro, R. Connecting Marine Productivity to Sea-Spray via Nanoscale Biological Processes: Phytoplankton Dance or Death Disco? *Sci. Rep.* **2015**, *5* (September), 1–11. https://doi.org/10.1038/srep14883.

(60) Bird, D. F.; Kalff, J. Empirical Relationships between Bacterial Abundance and Chlorophyll Concentration in Fresh and Marine Waters. *Can. J. Fish. Aquat. Sci.* **1984**, *41* (7), 1015–1023. https://doi.org/10.1139/f84-118.

(61) Sanders, R. W.; Caron, D. A.; Berninger, U. G. Relationships between Bacteria and Heterotrophic Nanoplankton in Marine and Fresh Waters: An Inter-Ecosystem Comparison. *Mar. Ecol. Prog. Ser.* **1992**, *86* (1), 1–14. https://doi.org/10.3354/meps086001.

(62) Kawamura, K.; Ishimura, Y.; Yamazaki, K. Four Years' Observations of Terrestrial Lipid Class Compounds in Marine Aerosols from the Western North Pacific. *Global Biogeochem. Cycles* **2003**, *17* (1), 3-1-3–19. https://doi.org/10.1029/2001gb001810.

(63) Beaupré, S. R.; Kieber, D. J.; Keene, W. C.; Long, M. S.; Maben, J. R.; Lu, X.; Zhu, Y.; Frossard, A. A.; Kinsey, J. D.; Duplessis, P.; Chang, R. Y. W.; Bisgrove, J. Oceanic Efflux of Ancient Marine Dissolved Organic Carbon in Primary Marine Aerosol. *Sci. Adv.* **2019**, *5* (10). https://doi.org/10.1126/sciadv.aax6535.

(64) Tomas, C. R.; Hasle, G. R.; Syvertsen, E. E.; Throndsen, J.; Steidinger, K.; Tangen, K.; Heimdal, B. *Identifying Marine Phytoplankton*; Academic Press: San Diego, 1997.

(65) Chingin, K.; Yan, R.; Zhong, D.; Chen, H. Enrichment of Surface-Active Compounds in Bursting Bubble Aerosols. *ACS Omega* **2018**, *3* (8), 8709–8717. https://doi.org/10.1021/acsomega.8b01157.

(66) Chingin, K.; Cai, Y.; Liang, J.; Chen, H. Simultaneous Preconcentration and Desalting of Organic Solutes in Aqueous Solutions by Bubble Bursting. *Anal. Chem.* **2016**, *88* (10), 5033–5036. https://doi.org/10.1021/acs.analchem.6b00582.

(67) Modini, R. L.; Russell, L. M.; Deane, G. B.; Stokes, M. D. Effect of Soluble Surfactant on Bubble Persistence and Bubble-Produced Aerosol Particles. *J. Geophys. Res. Atmos.* **2013**, *118* (3), 1388–1400. https://doi.org/10.1002/jgrd.50186.

(68) Walls, P. L. L.; Bird, J. C. Enriching Particles on a Bubble through Drainage: Measuring and Modeling the Concentration of Microbial Particles in a Bubble Film at Rupture. *Elementa* **2017**, *5*. https://doi.org/10.1525/elementa.230.

(69) Williams, P.; Druffel, E. R. M. Radiocarbon in Dissolved Organic Matter in the Central North Pacific Ocean. *Nature* **1987**, *330* (19), 246–248.

(70) Fry, B.; Hopkinson, C. S.; Nolin, A.; Wainright, S. C. 13C/12C Composition of Marine Dissolved Organic Carbon. *Chem. Geol.* **1998**, *152* (1–2), 113–118. https://doi.org/10.1016/S0009-2541(98)00100-4.

(71) Goericke, R.; Fry, B. Variations of Marine Plankton D13C with Latitude, Temperature, and Dissolved CO2 in the World Ocean. **1994**, *8* (1), 85–90.

(72) Hofmann, M.; Wolf-Gladrow, D. A.; Takahashi, T.; Sutherland, S. C.; Six, K. D.; Maier-Reimer, E. Stable Carbon Isotope Distribution of Particulate Organic Matter in the Ocean: A Model Study. *Mar. Chem.* **2000**, *72* (2–4), 131–150. https://doi.org/10.1016/S0304-4203(00)00078-5.

(73) Bosch, C.; Andersson, A.; Kirillova, E. N.; Budhavant, K.; Tiwari, S.; Praveen, P. S.; Russell, L. M.; Beres, N. D.; Ramanathan, V.; Gustafsson, Ö. Source-Diagnostic Dual-Isotope Composition and Optical Properties of Water-Soluble Organic Carbon and Elemental Carbon in the South Asian Outflow Intercepted over the Indian Ocean. *J. Geophys. Res.* **2014**, *119* (20), 11,743-11,759. https://doi.org/10.1002/2014JD022127.

(74) Kirillova, E. N.; Andersson, A.; Sheesley, R. J.; Kruså, M.; Praveen, P. S.; Budhavant, K.; Safai, P. D.; Rao, P. S. P.; Gustafsson, Ö. 13C- And 14C-Based Study of Sources and Atmospheric Processing of Water-Soluble Organic Carbon (WSOC) in South Asian Aerosols. *J. Geophys. Res. Atmos.* **2013**, *118* (2), 614–626. https://doi.org/10.1002/jgrd.50130.

(75) Dasari, S.; Andersson, A.; Bikkina, S.; Holmstrand, H.; Budhavant, K.; Satheesh, S.; Asmi, E.; Kesti, J.; Backman, J.; Salam, A.; Bisht, D. S.; Tiwari, S.; Hameed, Z.; Gustafsson, Ö. Photochemical Degradation Affects the Light Absorption of Water-Soluble Brown Carbon in the South Asian Outflow. *Sci. Adv.* **2019**, *5* (1), 1–11. https://doi.org/10.1126/sciadv.aau8066.

(76) Tritscher, T.; Dommen, J.; Decarlo, P. F.; Gysel, M.; Barmet, P. B.; Praplan, A. P.; Weingartner, E.; Prévt, A. S. H.; Riipinen, I.; Donahue, N. M.; Baltensperger, U. Volatility and Hygroscopicity of Aging Secondary Organic Aerosol in a Smog Chamber. *Atmos. Chem. Phys.* **2011**, *11* (22), 11477–11496. https://doi.org/10.5194/acp-11-11477-2011.

(77) Farmer, D. K.; Cappa, C. D.; Kreidenweis, S. M. Atmospheric Processes and Their Controlling Influence on Cloud Condensation Nuclei Activity. *Chem. Rev.* **2015**, *115* (10), 4199–4217. https://doi.org/10.1021/cr5006292.

(78) Rudolph, J.; Czuba, E.; Huang, L. The Stable Carbon Isotope Fractionation for Reactions of Selected Hydrocarbons with OH-Radicals and Its Relevance for Atmospheric Chemistry. *J. Geophys. Res. Atmos.* **2000**, *105* (D24), 29329–29346.

https://doi.org/10.1029/2000JD900447.

(79) Fisseha, R.; Saurer, M.; Jäggi, M.; Siegwolf, R. T. W.; Dommen, J.; Szidat, S.; Samburova, V.; Baltensperger, U. Determination of Primary and Secondary Sources of Organic Acids and Carbonaceous Aerosols Using Stable Carbon Isotopes. *Atmos. Environ.* **2009**, *43* (2), 431–437. https://doi.org/10.1016/j.atmosenv.2008.08.041.

Chapter 3: Isotopic Insights into Organic Composition Differences between Supermicron and Submicron Sea Spray Aerosol

3.1 Abstract

To elucidate the biological and physicochemical factors driving differences in organic composition between supermicron and submicron sea spray aerosol (SSA_{super} and SSA_{sub}), carbon isotopic composition ($\delta^{13}C$) measurements were performed on size-segregated, nascent SSA collected during a phytoplankton bloom mesocosm experiment. The $\delta^{13}C$ measurements indicate that SSA_{super} organic composition resembles a mixture of particulate and dissolved organic material in the bulk seawater. After phytoplankton growth, a greater amount of freshly produced carbon was observed in SSA_{super} with the proportional contribution being modulated by bacterial activity, emphasizing the importance of the microbial loop in controlling the organic composition of SSA_{super}. In contrast, SSA_{sub} exhibited no apparent relationship with biological activity, but correlated closely with surface tension measurements probing the topmost ~0.2-1.5 μm of the sea surface microlayer. Because this probing depth is similar to the bubble film thickness at the ocean surface, the correlation suggests that SSA_{sub} organic composition strongly depends on surfactants present at the air-sea interface that are transferred into SSA_{sub} by bubble bursting. Our findings illustrate the substantial impact of seawater dynamics on the pronounced organic compositional differences between SSA_{super} and SSA_{sub}, and demonstrate that these two SSA populations should be considered separately when assessing their contribution to marine aerosols and climate.

3.2 Introduction

Atmospheric aerosols affect Earth's radiative budget directly, by reflecting and absorbing incoming solar radiation, and indirectly, by serving as nuclei for water and ice cloud formation.[1]

There is currently a large amount of uncertainty in aerosol radiative forcing estimates for the marine environment arising from the contribution of both naturally and anthropogenically produced aerosols to the direct and indirect aerosol effects.[2,3] Sea spray aerosol (SSA), formed by bubbles bursting at the ocean surface, is often the most abundant primary aerosol type in the marine atmosphere.[4–6] However, as anthropogenic aerosol emissions have continued to increase above pre-industrial levels, so has their contribution to marine aerosols.[7,8] The important role that SSA and anthropogenic aerosol play in marine cloud formation and climate necessitates methods that effectively characterize aerosol sources in the marine environment.[9,10]

Carbon isotope analysis ($\delta^{13}C$) is one of the most commonly employed techniques in marine aerosol source apportionment studies to distinguish between the fractional contribution of natural and anthropogenic aerosol carbon (f_{SSA} and f_{anth}, Equation 1.3):[11–15] This technique is excellent for differentiating two carbon sources with distinct isotopic values but requires accurate knowledge of the $\delta^{13}C$ endmember values for both SSA ($\delta^{13}C_{SSA}$) and anthropogenic aerosol ($\delta^{13}C_{anth}$). Unfortunately, the value of pure, nascent $\delta^{13}C_{SSA}$ has been difficult to establish in the ambient environment due to background contributions from anthropogenic and terrestrial aerosols as well as photochemical processing of primary SSA organic carbon (OC) during atmospheric transport.[16,17] This has prompted a plethora of research aimed at understanding the factors influencing variability in nascent $\delta^{13}C_{SSA}$.

Lacking a better option, initial source apportionment studies assumed that $\delta^{13}C_{SSA}$ was equivalent to the $\delta^{13}C$ for oceanic dissolved organic carbon, around -21‰.[12,13,15] More recent research contradicts this assumption, showing that marine aerosols have higher (less negative) $\delta^{13}C$ values in oceanic regimes with elevated seawater biological activity.[11,14] These higher $\delta^{13}C_{SSA}$ values can be explained by biologically induced isotopic differences between the two seawater

carbon pools that contribute to SSA, dissolved and particulate organic carbon (DOC and POC). Oftentimes during large phytoplankton blooms freshly produced OC is isotopically-heavy (less negative $\delta^{13}C$) because the lack of CO_2 availability leads to less ^{12}C discrimination during CO_2 fixation.[18,19] The majority of this freshly produced OC is usually incorporated into phytoplankton biomass as POC,[20] leading to the conclusion that the seawater carbon transferred into SSA is likely a mixture of older, "aged" DOC and newer, "freshly produced" POC.[21] This conclusion is supported by laboratory experiments on nascent SSA that combined $\delta^{13}C_{SSA}$ measurements with seawater $\delta^{13}C_{POC}$ and $\delta^{13}C_{DOC}$ measurements to reveal that increased biological activity leads to a greater incorporation of freshly produced OC in SSA, resulting in less negative $\delta^{13}C_{SSA}$ values.[22] The same study further illustrated the importance of accounting for variability in $\delta^{13}C_{SSA}$ values by demonstrating that assuming a constant $\delta^{13}C_{SSA}$ value of -21‰ can result in up to a 33% underestimate in the contribution of anthropogenic aerosol carbon to the marine environment.[22]

One remaining issue to address when comparing marine aerosol source apportionment studies is that some studies have measured total suspended particles (TSP),[14,23] a combination of submicron and supermicron particles, while others have focused only on submicron particles.[11] This distinction is important because submicron SSA (SSA_{sub}) and supermicron SSA (SSA_{super}) often have dissimilar organic compositions due to their different formation mechanisms at the ocean surface.[24,25] The majority of SSA_{sub} are film drops produced when the bubble film cap bursts at the air-sea interface, whereas SSA_{super} are produced from an unstable jet formed at the bubble's base when the bubble cavity collapses.[4] SSA_{sub} generally contains aliphatic, surface-active organic material,[26,27] in accordance with its composition being heavily influenced by the sea surface microlayer (SSML), the top 1-1000 μm of the ocean surface containing elevated organic surfactant concentrations.[28,29] The organic composition of SSA_{super} is usually more comparable to the bulk

seawater, and often includes a large proportion of freshly produced biological material.[22,25,30] Logically, these organic composition differences may result in different $\delta^{13}C$ values for SSA_{sub} and SSA_{super} ($\delta^{13}C_{sub}$ and $\delta^{13}C_{super}$), but this possibility has yet to be explored for pure, nascent SSA.

Herein, we report values of $\delta^{13}C_{sub}$ and $\delta^{13}C_{super}$ for nascent SSA measured over the course of a phytoplankton bloom mesocosm experiment. The mesocosm experiment was part of the 2019 Sea Spray Chemistry and Particle Evolution (SeaSCAPE) intensive conducted in a unique ocean-atmosphere facility at the Scripps Institution of Oceanography (SIO).[31] The goal of this work is to identify the physicochemical and biological factors controlling the differences in organic composition and $\delta^{13}C$ values between SSA_{sub} and SSA_{super}.

3.3 Experimental Methods

3.3.1 The Wave Channel Mesocosm Experiment.

This work reports on a mesocosm phytoplankton bloom experiment conducted in an ocean-atmosphere wave channel at the SIO Hydraulics Lab. A comprehensive description of this experiment can be found in Sauer et al.[31] so only the important experimental details will be described here. On July 23rd, 11,800 L of coastal Pacific Ocean seawater was collected from Scripps Pier, filtered with 50 μm Nitex mesh, and added to the wave channel. From July 25th-26th, an f/20 algae nutrient mixture with sodium metasilicate was added dropwise to the wave channel to stimulate phytoplankton growth.[32] Solar simulator lamps were lined along the entire outside of the wave channel to provide photosynthetically-active radiation for phytoplankton growth, and the lamps were run on a 14-hour/10-hour day/night diel cycle. Chlorophyll-a (chl-a) was continuously measured *in situ* to monitor phytoplankton growth in the wave channel (see section 3.3.2 below).

On July 28th, a separate 1,135 L carboy was filled with natural seawater, collected and filtered in the same manner as the wave channel seawater above. Algae growth nutrients (f/2) with sodium metasilicate were immediately added to this seawater and it was left outdoors where it could receive a greater radiation flux. Once the carboy bloom reached exponential growth phase on August 1st, as indicated by chl-a (Aquafluor, Turner Designs), 1,135 L of the wave channel seawater was removed, and the carboy was added as a 10% inoculation. Simultaneously, algae nutrients were added to the wave channel to bring the total wave channel nutrient concentration to f/2.[32] The goal of this inoculation was to grow a robust phytoplankton bloom that would enable the investigation of biologically induced changes to the chemical composition of SSA.

3.3.2 In Situ Measurement of Chl-a and Dissolved CO_2 Concentrations.

A flow-through sensor/analyzer suite was used for *in situ* measurements bulk seawater properties including seawater temperature, dissolved oxygen, salinity, and chl-a (SeaBird Scientific SBE16 and SBE63 with Eco-Triplet BBFL2). The *in situ* chl-a data was calibrated using measurements of chl-a extracted from GF/F filtered bulk seawater and quantified by fluorometric analysis according to CalCOFI methods.[33] More details on the chl-a measurements can be found in Sauer et al.[31]

A separate continuous flow system was used for determination of the dissolved CO_2 concentration. This system measured pH (Honeywell Durafet), dissolved oxygen (Aanderaa Data Instruments 3835 Optode), and pCO_2 and total dissolved inorganic carbon using a "Burke-o-lator" custom IR analyzer.[34,35] The seawater carbonate speciation and dissolved CO_2 concentration were calculated from these measurements with corrections made for seawater temperature and salinity.

3.3.3 Collection of Communal Bulk Seawater and SSML Samples.

Each morning between 9 and 11 am the bulk seawater and SSML were collected from the back of the wave channel in a designated seawater sampling section (see Sauer et al.[31] for wave channel depiction). The bulk seawater was siphoned into two 8 L plastic carboys with a 2 m long Teflon tube placed about 20 cm below the seawater surface. All materials were acid washed with 10% HCl each day before collection. In the laboratory, all bulk seawater analyses used aliquots from these carboys to ensure that every measurement was made on comparable seawater samples.

The SSML was collected from the same seawater sampling section of the wave channel by employing the glass plate method.[36] The glass plate was carefully lowered into the water at a rate of 5-6 cm/s and withdrawn at the same rate, which corresponds to a sampled SSML thickness of around 50 μm.[36,37] After withdrawal from the seawater, the glass plate was suspended for 20 seconds to allow any bulk seawater to drain back into the wave channel. The remaining mixture of seawater and organics on the plate was considered the SSML and scraped into a combusted glass bottle using a Teflon scraper. This process was repeated until about 200 mL of SSML had been collected. This 200 mL SSML sample was used for all SSML measurements in the experiment to ensure consistency between analyses.

3.3.4 Seawater Analyses of DOC, POC, and Bacteria Concentrations

For collection of DOC, two 40 mL aliquots were taken from the communal carboys and GF/F filtered (Whatman, 0.7 μm pore size) into combusted glass vials. The DOC samples were immediately acidified to ~pH 2 with concentrated HCl and stored in a covered box at room temperature.

One liter of bulk seawater from the carboys was used to collect POC samples segregated into two size classes, 1.0-2.7 μm and 2.7-10 μm, by three successive filtrations. First, the seawater was filtered through an Isopore polycarbonate membrane (EMD Millipore, 10 μm pore size) to remove the POC too large to be transferred into most SSA. Then the seawater was GF/D filtered (Whatman, 2.7 μm pore size) to retain the 2.7-10 μm fraction and GF/B filtered (EMD Millipore, 1.0 μm pore size) to retain the 1.0-2.7 μm fraction. Each filtration step was made into a separate, combusted filter flask, and the filtration apparatus was rinsed with 1% HCl and MQ H_2O between successive filtrations. The POC filters were collected into plastic petri dishes and stored frozen at -12˚C.

For quantification of bacteria cells, bulk seawater samples were prepared according to standard protocols.[38,39] Samples were preserved with 5% glutaraldehyde, flash frozen with liquid nitrogen, and stored at -80˚C.[40] The bacteria samples were then diluted 10-fold in 1x TE buffer at pH 8 and stained for 10 minutes with SYBR Green I in the dark at room temperature.[38] Finally, bacteria cells enumeration was carried out using a BD FACSCanto II™ flow cytometer.

3.3.5 Bacterial Production Measurements and Bacterial Carbon Demand

Bacterial production was measured daily in bulk seawater samples by [^{3}H]-leucine incorporation[41] modified for microcentrifugation.[42] Triplicate 1.7 mL aliquots were incubated with [^{3}H]-leucine (20 nM final concentration) for 1 hour. Samples with 100% trichloroacetic acid added prior to [^{3}H]-leucine addition served as blanks. Leucine incorporation was converted to carbon production assuming 3.1 kg C (mol leucine)$^{-1}$.[43]

$$\text{Bacterial Respiration} = 3.70 \times (\text{Bacterial Production})^{0.41} \quad \text{(Equation 3.1)}$$

The bacterial carbon demand (BCD) is the sum of the carbon incorporated into bacterial biomass (bacterial productivity) and the carbon respired by bacteria back into CO_2 (bacterial respiration). An equation to estimate bacterial respiration from measured bacterial production was developed by del Giorgio and Cole (Equation 3.1).[44] We used Equation 3.1 to estimate BR from each daily BP measurement, and added these two values together to obtain the total BCD.

3.3.6 Tensiometer and Atomic Force Microscopy SSML Surface Tension Measurements.

Surface tension measurements on SSML samples collected daily were performed using Kibron AquaPi force tensiometer (Kibron, Finland) with the Du Noüy-Padday method.[45,46] Samples were not diluted before measurements, and at least three replicate measurements were performed on each liquid sample. Surface tension values are reported as the mean with one standard deviation.

Force spectroscopy (i.e., force plots) measurements were performed using Molecular force probe 3D atomic force microscopy (AFM, Asylum Research, Santa Barbara, CA) in contact mode at ambient pressure and temperature (25°C).[45,47] High aspect ratio, constant diameter Ag_2Ga nanoneedles (NN-HAR-FM60, Nauga Needles) with a nominal spring constant of 2.7-3.3 N/m and typical radius of 25–100 nm were used for surface tension measurements. The nanoneedle radius was calibrated by performing force measurements on a reference ultra-pure water droplet with known surface tension (72.0 mN/m at 25 °C) before and after each surface tension measurement.[48] If the calibrated radius differed by more than 10%, the data was discarded, and the experiment was repeated with a new nanoneedle. The resultant value was also compared with scanning electron microscopy image of each nanoneedle. For AFM surface tension measurement, an SSML droplet (typically 5-7 mm width and 2-3 mm height) was placed on a silicon wafer substrate. Evaporation

of the SSML droplets was minimized using a custom-made sealed humidity cell. Force measurements were collected over the approximate center of each SSML droplet with a 1 Hz scan rate. The nanoneedle was indented several hundreds of nanometers (range of 0.2–1.5 μm) into the SSML droplet, paused within the droplet for 2 seconds of dwell time, and then retracted away from the droplet with a constant pulling rate of 2 μm/s.[45] At least five consecutive force plots were collected for each sample, and the maximum retention force was used to quantify the droplet surface tension. AFM surface tension data is reported as the mean with one standard deviation.

3.3.7 Size-Segregated SSA Collection and Analysis.

For size-segregated SSA collection, a sampling setup made entirely of stainless steel tubing was connected to the headspace of the wave channel. The tubing contained a y-splitter that split the flow in two directions to collect both SSA_{sub} particles and total suspended SSA particles (SSA_{TSP}) onto precombusted quartz fiber filters (Whatman QM-A, 47 mm). Most SSA samples were collected for >40 hours to ensure sufficient carbon amounts for isotopic analysis. Additionally, field blank filters were collected every couple of days to correct for sample handling and analysis. Sample handling and analysis were likely the largest contributor to carbon blanks, as the background particle concentrations in the wave channel remained below 5 cm^{-3} throughout almost the entire experiment.[31] The SSA and field blank filters were collected into plastic petri dishes and stored frozen at -12˚C until analysis.

Collection of SSA_{sub} was achieved using an URG-2000-30EH cyclone, which allows particles smaller than the cutpoint to pass through to the filter while retaining particles larger than the cutpoint. According to manufacturer settings, this cyclone has a 50% cutpoint diameter of 1.0 μm at the flow rate of 50 LPM used for sample collection. Therefore, SSA was collected out

of the wave channel at a total flow rate of 100 LPM, and rotameters were used to keep the flow in both directions the same at 50 LPM, which ensured uniform particle distributions in both directions. A drier was not included before either filter, so particles were deposited wet; thus, the 1.0 μm cutpoint for SSA_{sub} applies to the wet particle diameter. Relative humidity (RH) was not directly measured for this sampling setup, but based on measurements for similar offline sampling setups during SeaSCAPE, SSA particles were likely collected around an RH of 75-85%.[49]

All SSA samples and field blanks were analyzed via a combustion method previously developed in the Thiemens Stable Isotope Laboratory.[22] To convert all carbon species to CO_2, filters were combusted for 3 hours at 850˚C in an evacuated quartz tube containing 250 mg of CuO. The total CO_2 yield was measured by capacitance manometry and $\delta^{13}C$ was analyzed on a MAT 253 Isotope-Ratio Mass Spectrometer. SSA samples were not acidified to remove carbonates so OC in SSA refers to the combination of carbonates and organic carbon; however, the SSA collected in this study had a pH of 4 or below,[49] so the contribution of carbonates was likely insignificant.

After field blank correction of the SSA_{sub} and SSA_{TSP} OC amounts and $\delta^{13}C$ values, the SSA_{super} OC amount was subsequently calculated by taking the difference between the blank-corrected SSA_{TSP} and SSA_{sub} OC amounts. Likewise, the $\delta^{13}C_{super}$ was calculated analogous to Equation 1.3 by realizing that $\delta^{13}C_{TSP}$ is a weighted combination of $\delta^{13}C_{super}$ and $\delta^{13}C_{sub}$.

3.3.8 Concentration and Isotope Analysis for POC and DOC.

Before isotopic analysis, the POC filter samples were processed according to CCE-CalCOFI methods adapted from Bodungen et al.[50] Inorganic carbonate was removed from the samples by acid fumigation in a dessicator for 12 hours. The POC filters were then dried in an

oven at 60˚C for 48 hours. Subsequently, the POC amount and $\delta^{13}C$ value were analyzed at the SIO Stable Isotope Facility on a Thermo Finnigan DeltaPlus Isotope-Ratio mass spectrometer interfaced with a Costech 4010 elemental combustion analyzer.

Liquid DOC samples were sent to the Jan Veizer Stable Isotope Laboratory in Ottawa, Canada for $\delta^{13}C$ and concentration analysis. The samples were analyzed on an OI Analytical Aurora Model 1030W total organic carbon (TOC) Analyzer interfaced to a Finnigan DeltaPlus XP Isotope-Ratio mass spectrometer with a 1σ analytical precision of ± 0.2‰.[51]

3.3.9 TD-GCxGC-EI-ToF-MS Measurements of Speciated Organics

Submicron aerosols were collected onto tissuequartz filters (Pallflex) from a sampling port directly past the wave breaking region. Supermicron aerosols were excluded using a greaseless cyclone (BGI Mesa Labs). Extraction of dissolved phase seawater organics was carried out via methodology adapted from Dittmar et al.[52] Briefly, 20 L seawater samples were collected into a cleaned polypropylene jug and pumped through a series of filters: 10 micron, 0.7 micron, and 0.2 micron, using a peristaltic pump with PTFE-lined tubing at a flowrate of 100 mL/min to minimize backpressure and avoid cell lysing. Following this, the seawater was gravity filtered through a pre-cleaned SPE-PPL cartridge overnight at a rate of 3 drops/sec or less. Samples were washed and eluted with methanol three times, immediately dried down to a solid, and stored in a freezer at -18°C. Plasticware was cleaned with 3x methanol followed by 3x Milli-Q water rinses before usage.

Prior to organic speciation analysis, dried dissolved samples were reconstituted in methanol and introduced onto filter material (Pallflex tissuequartz) for maximized methodological similarity to aerosol compositional analysis. Dissolved and aerosol-phase organics were analyzed

by thermal desorption two-dimensional gas chromatography coupled with high resolution electron ionization time of flight mass spectrometry (TD-GCxGC-EI-ToF-MS). This instrument thermally desorbs organics from the filter material, focuses them on a cooled inlet, and separates them by both volatility and polarity using two sequential GC columns. Recovery of polar organics is enhanced by derivatization. Separated organics between between C12 and C36 n-alkane volatility equivalents are detected by 70 ev EI MS (Tofwerk), enabling the production of clean mass spectra for each individual organic compound. These spectra can then be compared to authentic standards and NIST/NIH/EPA mass spectral databases for identification and categorization of known organics. Additional instrumental and methodological details can be found in Worton et al.[53]

3.4 Results and Discussion

3.4.1 Biological Progression and Seawater Carbon Dynamics

When discussing the biological progression during the mesocosm study it is helpful to organize the experiment into three parts based on the experimental phases that occurred: 1) prior to the 10% inoculation (before 8/1), 2) highest phytoplankton abundance (8/1-8/4), and 3) bloom senescence and bacterial growth after the wall scraping (8/5-8/7 and thereafter). Little phytoplankton growth (chl-a increase) was observed throughout the first period following the initial addition of f/20 algae nutrients on July 25th, prompting addition of the outdoor carboy on August 1st (solid line in Figure 3.1a). After inoculation with the outdoor carboy bloom and simultaneous augmentation of the algae nutrients to f/2, phytoplankton abundance (chl-a) in the wave channel sharply increased to above 20 μg L^{-1}, and was sustained around this level for the next two days before declining on August 3rd and 4th. The substantial phytoplankton growth during this period also led to a large drawdown in the dissolved CO_2 concentration (Figure 3.1a), which

has important consequences for the isotopic compositions of freshly produced OC in the seawater and SSA.

From August 1st-August 4th, the biological growth (i.e. phytoplankton and bacteria) was so intense that it coated the wave channel walls and began to block out the photosynthetic light supplied by the solar simulator lamps. Therefore, on August 5th the sides of the wave channel were scraped to remove the biomass accumulation and enable a greater flux of light for continued growth (asterisk in Figure 3.1a). Rapid bacterial growth occurred in the water column over the next two days probably due to feeding on the organic material scraped off the walls, resulting in the highest bacteria concentrations observed during the experiment.

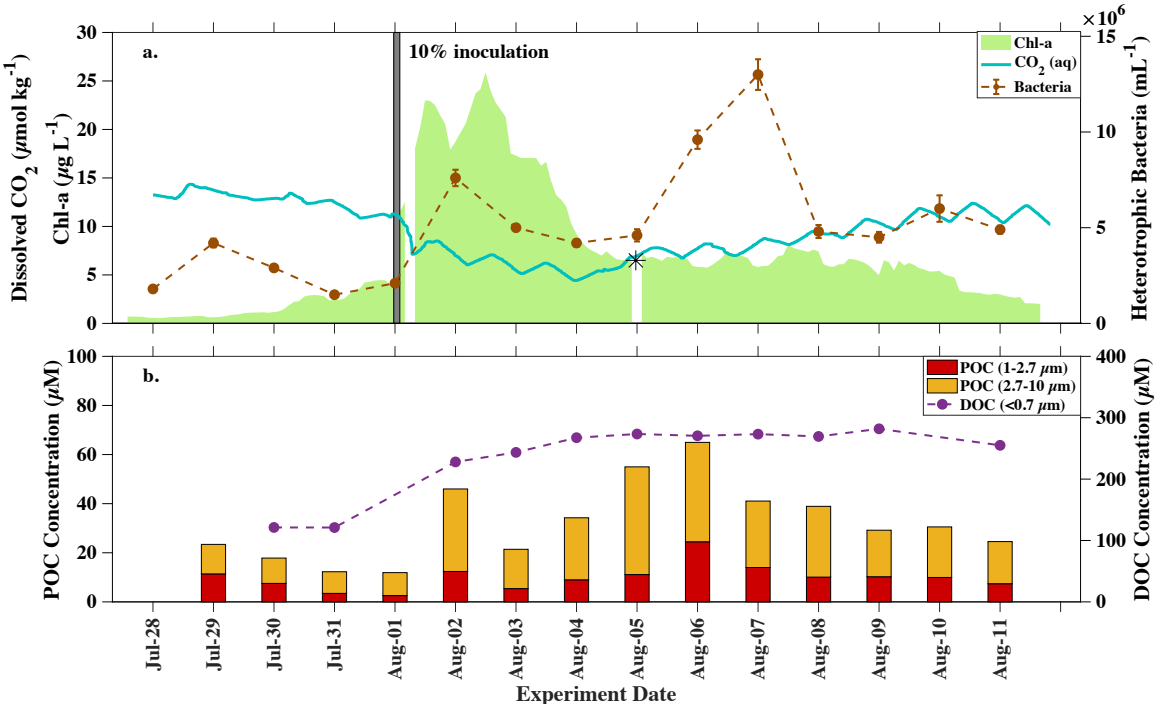

Figure 3.1 a) Chl-a, dissolved CO_2, and bacteria concentrations throughout the mesocosm experiment. The 10% inoculation on August 1st is indicated by the gray line, and the asterisk denotes when the wave channel walls were scraped on August 5th. b) The DOC and $POC_{1\text{-}10}$ concentrations during the experiment with the $POC_{1\text{-}10}$ concentration (full bar height) separated into 1-2.7 µm (red) and 2.7-10 µm (yellow) size fractions. The $POC_{1\text{-}10}$ measurement on 8/1 represents the concentration before the 10% inoculation, while no analogous measurement was available for DOC. The DOC increase between 7/31 and 8/2 is entirely due to the 108 µM C in the nutrient addition. The dashed lines represent that measurements were taken at individual time points, while solid lines indicate continuous sample measurement.

As a result of the biological growth and experimental perturbations, DOC and POC concentrations exhibited vastly different temporal evolutions over the course of the mesocosm experiment (Figure 3.1b). The DOC (purple) increased from 121 μM on 7/31 to 228 μM on 8/2, but this increase was due to the EDTA and vitamins addition from the f/2 algae nutrients, which contributed an additional 108 μM C.[54] From 8/2 onward DOC concentrations did not increase by more than 23%, indicating that most of the DOC in the wave channel was present in the initial Pacific Ocean source seawater or was contributed by the nutrient addition.

On the other hand, concentrations of POC with 1-10 μm diameters ($POC_{1\text{-}10}$) were 80-545% higher throughout phytoplankton growth and senescence as compared to the concentration on 8/1 right before the 10% inoculation. This indicates that a significant portion of the $POC_{1\text{-}10}$ was freshly produced by biological growth during the experiment. The goal of measuring POC with 1-10 μm diameters was to assess the amount of seawater particulate material small enough to transfer into SSA particles, the majority of which have diameters less than 10 μm.[30] In Figure 3.1b, the $POC_{1\text{-}10}$ concentrations are reported in stacked bars separated into two size fractions, 1.0-2.7 μm (red) and 2.7-10 μm (yellow), to show how the biological dynamics impacted different particulate sizes. A portion of the 1.0-2.7 μm POC was likely intact bacteria cells as this particulate fraction showed a moderate positive correlation with bacterial abundance ($R^2 = 0.55$, Figure 3.2a). The 2.7-10 μm POC is larger than most bacteria and likely comprised of pico- and nano-plankton, algal detritus, and particulate aggregates.[55] The highest 2.7-10 μm POC concentrations occurred on 8/5 and 8/6, probably resulting from the wall scraping introducing larger particulate material into the water column.

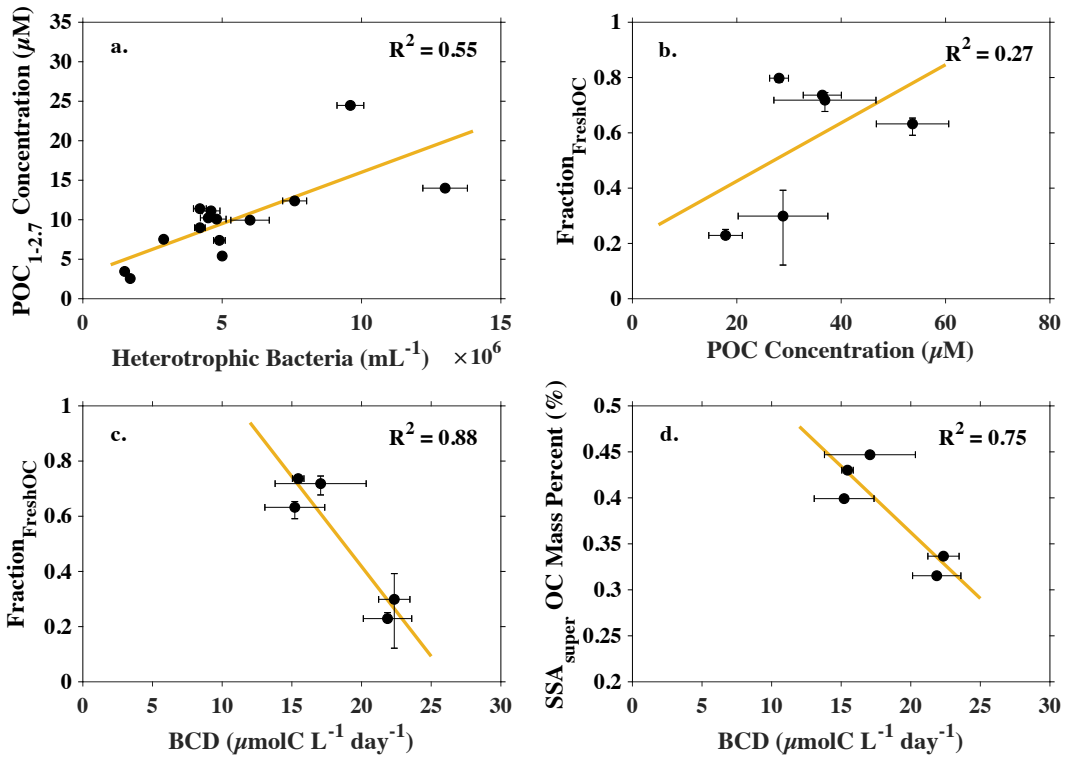

Figure 3.2 a) Correlation plot showing a moderate positive correlation between heterotrophic bacteria and concentration of POC between 1-2.7 µm. b) Correlation between $POC_{1\text{-}10}$ concentration and $Fraction_{FreshOC}$ showing that increased $POC_{1\text{-}10}$ only has a weak influence on the amount of freshly produced OC transferred into SSA_{super}. c) Strong negative correlation between bacterial carbon demand and $Fraction_{FreshOC}$ suggesting that increased bacterial productivity and respiration may remove some of the freshly produced OC before it can be transferred into SSA. d) Strong negative correlation between bacterial carbon demand and the OC mass percent of SSA_{super} consistent with increased bacterial utilization of carbon leading to less freshly produced OC transferred into SSA_{super}.

3.4.2 Strong Dissimilarity between $\delta^{13}C_{super}$ and $\delta^{13}C_{sub}$

A comparison of $\delta^{13}C_{super}$ and $\delta^{13}C_{sub}$ in Figure 3.3 shows that they exhibit distinct isotopic values throughout the entire experiment. The dissimilar $\delta^{13}C$ values indicate that SSA_{super} and SSA_{sub} differ in their overall organic composition. Furthermore, the disparate temporal evolution of $\delta^{13}C_{super}$ and $\delta^{13}C_{sub}$ during the biological experiment suggests the SSA_{super} and SSA_{sub} organic compositions are influenced by separate seawater biological and chemical factors. Because

$\delta^{13}C_{super}$ increased sharply after the chl-a peak, it appears likely the SSA_{super} organic composition is impacted by biological activity. Additionally, $\delta^{13}C_{super}$ consistently fell within or near the range of previously observed $\delta^{13}C$ values for nascent SSA_{TSP} in a similar biological experiment (Figure 3.3). Unlike $\delta^{13}C_{super}$, $\delta^{13}C_{sub}$ does not exhibit any obvious relationship with seawater biological activity levels throughout the bloom and lies well below the typical values observed for nascent SSA_{TSP}. In the sections below our discussion will focus on the biological and physicochemical drivers that give rise to the distinct differences in $\delta^{13}C$ and organic composition between SSA_{super} and SSA_{sub}.

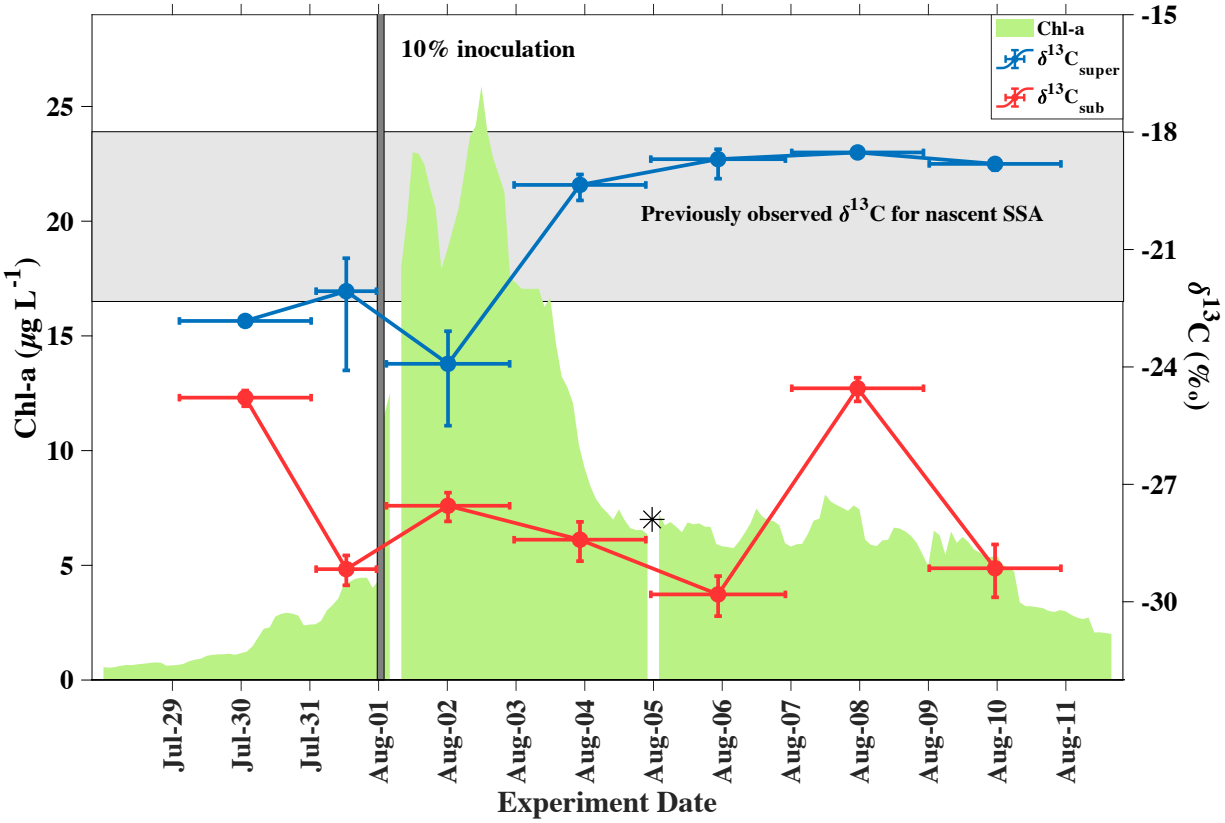

Figure 3.3 Time series of $\delta^{13}C_{super}$ and $\delta^{13}C_{sub}$ displaying their distinctly different values throughout the entire experiment. The $\delta^{13}C_{super}$ falls within or near the range of $\delta^{13}C$ values previously observed for nascent SSA (gray shaded region),[22] and exhibits a large increase after the peak in biological activity (chl-a). The $\delta^{13}C_{sub}$ is much more negative than the previously observed $\delta^{13}C$ range and does not seem to be significantly influenced by the biological activity.

3.4.3 A Substantial Biological Influence on SSA_{super}.

Examining the temporal evolution of $\delta^{13}C$ for POC and DOC, the two seawater carbon pools that contribute to SSA_{super}, provides a good starting point to assess the impact of seawater biological activity on SSA_{super} (Figure 3.4a). The experimental time series of $\delta^{13}C_{DOC}$ and $\delta^{13}C_{POC}$ provides insight into variations in bulk organic composition associated with the changes in POC and DOC concentrations. For $\delta^{13}C_{DOC}$, the only significant change was a decrease following the nutrient addition on 8/1, but this is likely because commercial EDTA usually has a more negative isotopic value.[56] Little variation in $\delta^{13}C_{DOC}$ or DOC concentration was observed after the peak in primary production (chl-a), indicating the DOC pool was mostly comprised of carbon initially present in the Pacific Ocean source seawater or contributed by the nutrient addition. Conversely, $\delta^{13}C_{POC}$ was higher (less negative) after phytoplankton growth accelerated on 8/1. This is consistent with the augmented biological formation of freshly produced POC with higher $\delta^{13}C$ values, which often occurs during large blooms when CO_2 availability is lower (Figure 3.1a).[18,57]

The $\delta^{13}C_{super}$ values have been plotted along with $\delta^{13}C_{POC}$ and $\delta^{13}C_{DOC}$ in Figure 3.4a to compare the organic composition of SSA_{super} with the seawater carbon pools. As expected for SSA_{super} containing a mixture of seawater POC and DOC, $\delta^{13}C_{super}$ lies in between $\delta^{13}C_{POC}$ and $\delta^{13}C_{DOC}$ for each collection period. This same trend has been previously observed for $\delta^{13}C_{TSP}$ measured during two similar phytoplankton bloom experiments (Chapter 2).[22] Following the approach of Chapter 2, $\delta^{13}C_{DOC}$ and $\delta^{13}C_{POC}$ were used as approximate endmembers for "aged" and "fresh" OC in an isotopic mixing model to estimate the contribution of freshly produced OC to SSA, $Fraction_{FreshOC}$ (Equation 2.1).[22] In this study we have done the same for SSA_{super} with the caveat that "aged" OC refers to the combination of carbon in the initial source seawater and contributed by the nutrient addition.

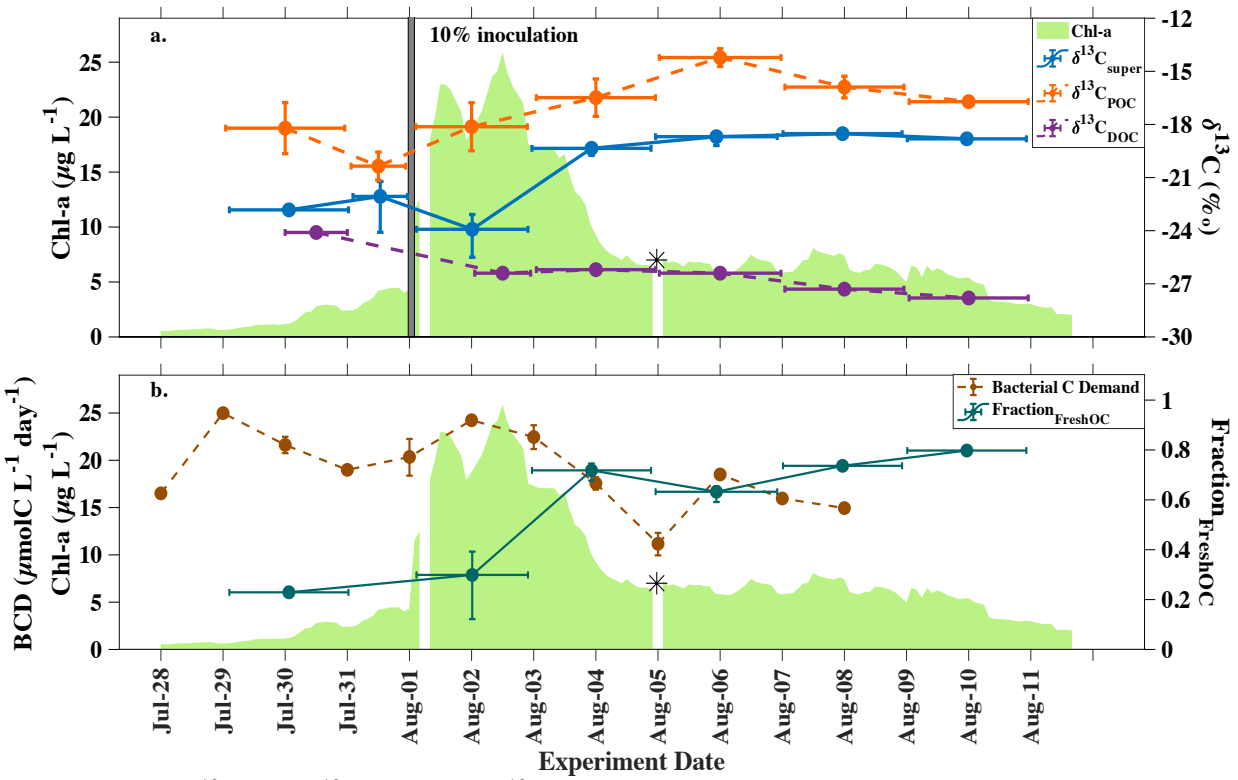

Figure 3.4 a) $\delta^{13}C_{POC}$, $\delta^{13}C_{DOC}$, and $\delta^{13}C_{super}$ overlaid on the chl-a time series. Importantly, $\delta^{13}C_{super}$ lies between $\delta^{13}C_{POC}$ and $\delta^{13}C_{DOC}$ for each collection period suggesting the SSA_{super} organic composition is similar to a mixture of seawater DOC and POC. b) The inverse relationship between bacterial carbon demand (BCD) and $Fraction_{FreshOC}$ overlaid on the chl-a time series. For both plots, solid lines indicate samples were collected throughout the entire sampling duration, while the dashed lines signify that the samples were taken at individual time points. Horizontal error bars indicate the collection period or averaging duration for each sample, with the data point placed in the center.

The biological influence on SSA_{super} is immediately apparent from the higher $Fraction_{FreshOC}$ values after the chl-a peak (Figure 3.4b), but interestingly the increased contribution of freshly produced OC to SSA_{super} is delayed from the chl-a peak by about 2 days. This offset between maximum primary productivity (chl-a) and incorporation of freshly produced OC into SSA has been observed before in multiple studies.[22,54,58] Previous studies have posited that the delay may be related to the degradation timescale for freshly produced POC into smaller sizes that efficiently transfer into SSA,[22,59] so in this experiment we specifically measured POC from 1-10 μm, similar to the majority of SSA_{super} particle diameters.[30] Unexpectedly, despite most of the

$POC_{1\text{-}10}$ being freshly produced (Section 3.4.1), the $POC_{1\text{-}10}$ concentration in the water column only weakly correlated with the $Fraction_{FreshOC}$ (Figure 3.2b). The lack of correlation between the amount of freshly produced OC in the water column and the proportion in SSA_{super}, suggests that secondary biological processing of freshly produced organic material may influence the amount transferred into SSA_{super}.

We used bacterial carbon demand (BCD) to assess secondary processing of freshly produced organic material. BCD is the sum of bacterial production, the carbon incorporated into bacterial biomass, and bacterial respiration, the carbon respired by bacteria back into CO_2.[44,60] Direct measurements of bacterial production were used to estimate bacterial respiration via Equation 3.1,[44] and these two values were summed to obtain the BCD values shown in Figure 3.4b. In this experiment, a strong inverse relationship existed between the BCD and the $Fraction_{FreshOC}$ values (Figure 3.2c, $R^2 = 0.88$). This points to alteration of freshly produced organic material by incorporation into bacterial biomass, and especially enhanced remineralization to CO_2, as important mechanisms that may limit the amount of freshly produced OC transported to the ocean surface and transferred into SSA. This bacterial influence on the amount of freshly produced OC available to transfer into SSA_{super} is supported by two additional observations. First, all three peaks in the BCD values, 7/29, 8/2, and 8/6 (Figure 3.4b), were followed by decreases in the $POC_{1\text{-}10}$ concentrations the next day (Figure 3.1b). Second, the BCD also exhibits an inverse correlation with the SSA_{super} OC mass percent (Figure 3.2d), consistent with a lower amount of organic material transferred into SSA_{super} when more OC is being utilized by bacteria in the water column. Taken altogether, these findings suggest that transfer of freshly produced organic material into SSA_{super} is controlled not just by the amount of freshly produced OC formed from primary productivity, but also by the bacterial assimilation, transformation, and remineralization rates of

this freshly produced OC. This demonstrates the importance of the complete microbial loop in controlling the organic composition of SSA_{super} and the value of $\delta^{13}C_{super}$.

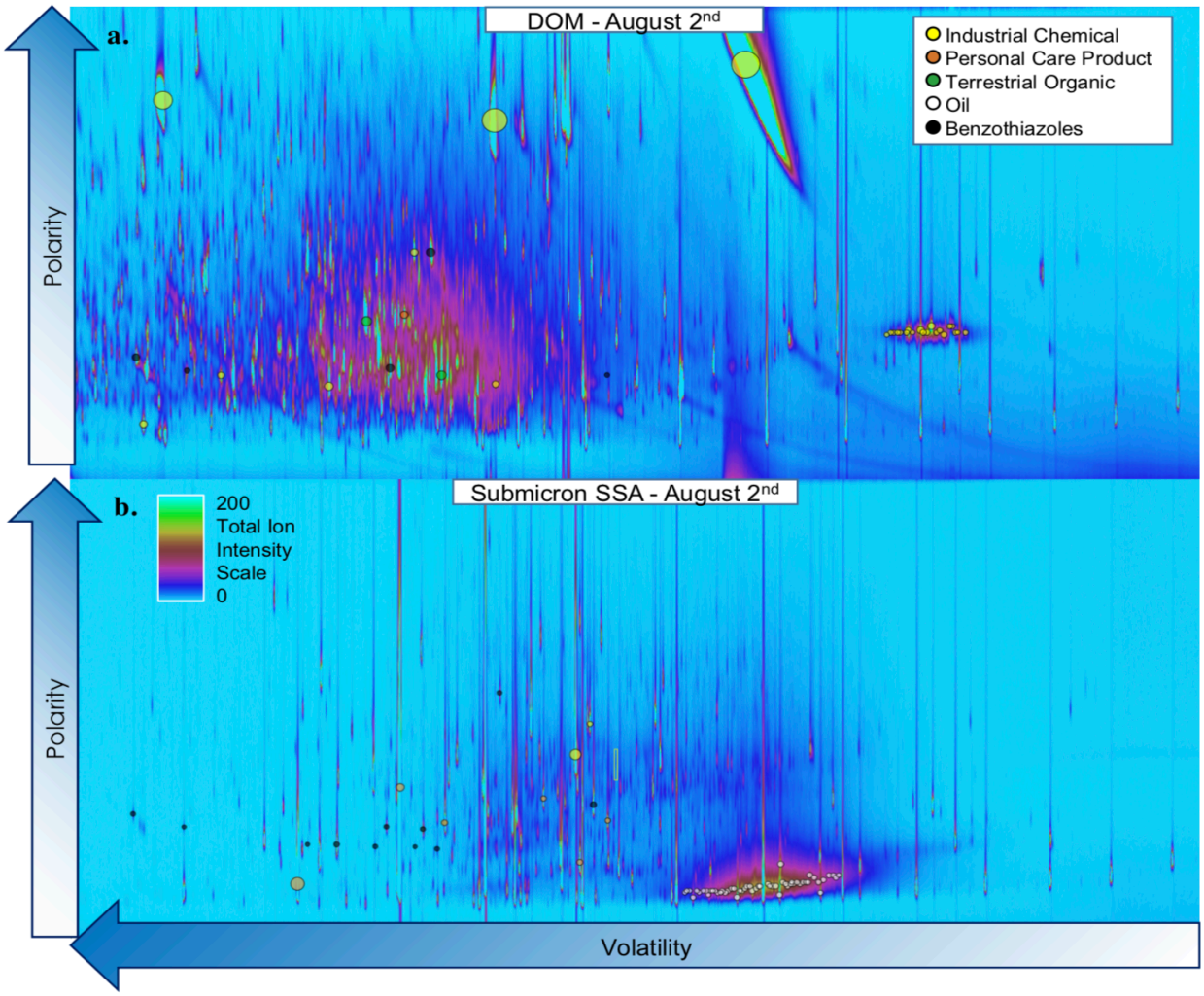

Figure 3.5 TD-GCxGC-EI-ToF-MS chromatograms demonstrating the differing speciation of organic material in the a) DOC (<0.2 μm) and b) SSA_{sub} from August 2nd of the SeaSCAPE mesocosm experiment. Some examples of confidently identified anthropogenic or terrestrial organic compounds have been indicated for both samples and classified as follows: commonly reported industrial chemicals (yellow circles), personal care products (pink circles), terrestrial biomass burning products (green circles), oils and petrochemicals (white circles), and benzothiazoles (black circles). Thus, despite their differing composition, both DOC and SSA_{sub} contain anthropogenic organic species, even when the biological growth was highest after the 10% inoculation on August 1st.

3.4.4 Selective Enrichment of Organics in the SSML and SSA_{sub}

In stark contrast to $\delta^{13}C_{super}$, the lower $\delta^{13}C_{sub}$ values were more negative than typical marine, biogenic organic compounds,[61] and resemble $\delta^{13}C$ values for anthropogenic or terrestrial organic compounds.[62] Multiple classes of highly surface-active anthropogenic compounds, including plasticizers, sunscreen products, and industrial waste,[28] were identified in DOC (<0.2 μm) samples from the initial, Pacific Ocean source seawater[31] and persisted in the seawater even after inoculation with the biologically-active carboy (Figure 3.5a). This helps explain why anthropogenic pollutants were also present in SSA_{sub} during the experiment (Figure 3.5b), although the overall organic speciation of SSA_{sub} was patently different than that of the bulk DOC, suggesting that the processes controlling organic transfer into SSA_{sub} are selective for certain chemical species.[63,64]

Along these lines, Figure 3.6 shows that $\delta^{13}C_{sub}$ exhibits a clear correlation with the SSML surface tension as measured by atomic force microscopy (AFM). Surface tension measurement by AFM is a newly developed technique capable of probing the topmost 0.2-1.5 μm of a liquid sample, which differs from the traditional tensiometer technique that measures to a much greater depth in the sample (>1000 μm).[45] Lower SSML surface tension is generally indicative of higher surfactant concentrations, and in this experiment decreased AFM-measured SSML surface tension correlated with lower $\delta^{13}C_{sub}$ values. Taken as a whole, the correlation between lower AFM-measured surface tension and lower $\delta^{13}C_{sub}$ values may be attributable to elevated anthropogenic or terrestrial surfactant concentrations in the topmost ~1 μm of the SSML, which were then transferred into SSA_{sub} by bubble bursting.

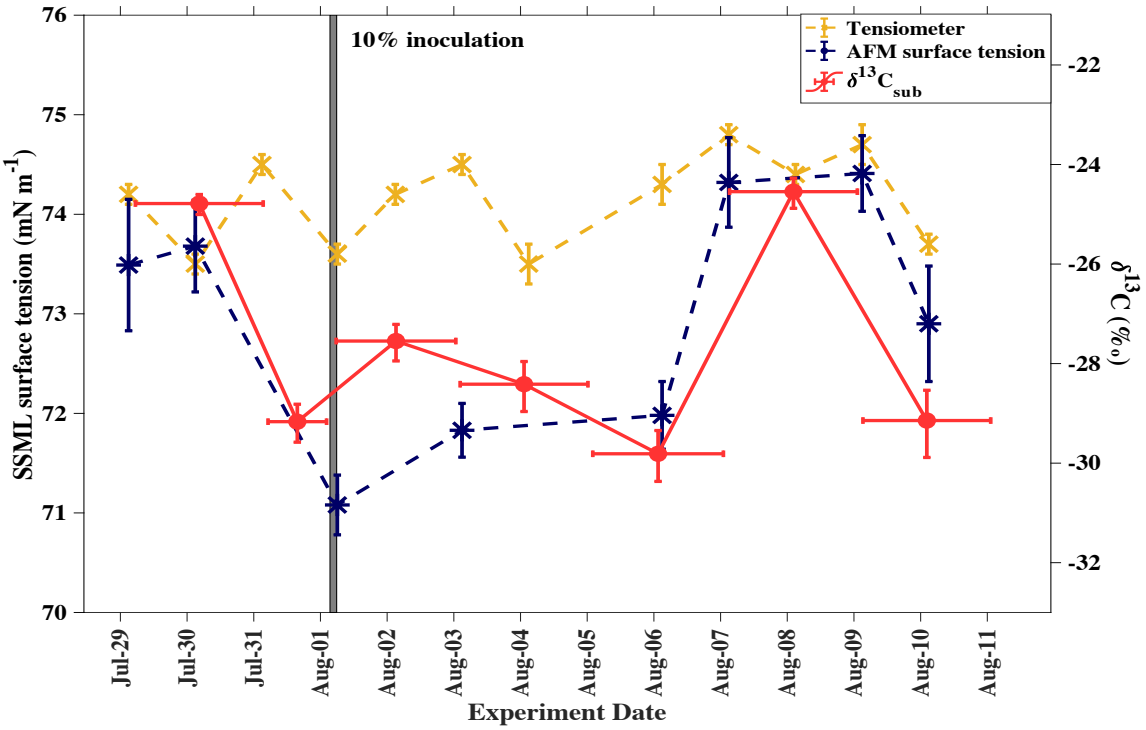

Figure 3.6 $\delta^{13}C_{sub}$ plotted with SSML surface tension measurements made by both the AFM and tensiometer techniques. Dashed lines indicate the samples were taken at individual time points, while solid lines signify that samples were collected throughout the entire sampling duration. Horizontal error bars indicate the collection period or averaging duration for each sample, with the data point placed in the center. The tensiometer measures to an SSML sample depth greater than 1000 µm and does not correlate with $\delta^{13}C_{sub}$, but the AFM-measured surface tension, which probes only the top 0.2-1.5 µm of the SSML sample, closely correlates with $\delta^{13}C_{sub}$.[45] This suggests that the organic composition of SSA_{sub} will strongly depend on the surfactants present in the topmost ~1 µm of the SSML, a thickness similar to the bubble film cap at the ocean surface.[65]

There were two collection periods (7/29-7/31 and 8/7-8/9) where the $\delta^{13}C_{sub}$ values were higher, indicative of a smaller anthropogenic influence on SSA_{sub} (Figure 3.6). During this same period, surfactant concentrations were lower in the topmost SSML layers (higher AFM-measured surface tension), suggesting that depletion of anthropogenic surfactants in the SSML may have driven the diminished anthropogenic influence on SSA_{sub}. From this experiment alone it was unclear what processes caused the SSML surfactant depletion or whether the same processes were responsible for the depletion during both time periods. What does remain clear from our data is the strong

association between surfactant concentrations in the topmost 0.2-1.5 μm of the SSML and the organic composition of SSA_{sub} (Figure 3.6). Therefore, our understanding of organic transfer into SSA_{sub} would benefit from additional research focused on resolving the biological, chemical, and physical factors influencing surfactant concentrations at the air-sea interface. This information could then be incorporated into modelling and molecular dynamics studies to shed light on the competition between surface-active compounds at the air-sea interface that determines the selective transfer of organic species into SSA_{sub}.

3.4.5 Insights into Ocean-Aerosol Transfer of Organic Material

The isotopic measurements made on SSA_{super} and SSA_{sub} in this experiment strongly support the purported motifs for organic transfer into both SSA size fractions (Figure 3.7). The SSA_{super} organic composition was similar to a mixture of bulk DOC and POC, consistent with jet drops formed ar2 the base of the bubble producing SSA_{super} from bulk seawater. Thus, biologically induced changes in bulk seawater chemical composition, will influence the organic composition of SSA_{super} (Figure 3.2). In this experiment, the impact of seawater biology on SSA_{super} was larger than expected with freshly produced OC contributing >50% of the total SSA_{super} OC amount after the chl-a peak. This preferential incorporation of freshly produced OC into SSA_{super} occurred even though the initial seawater carbon and nutrients comprised the majority of the cumulative bulk seawater $POC_{1\text{-}10}$ and DOC (Figure 3.1b), which suggests there may be additional seawater processes that enrich freshly produced organic material in SSA_{super}. Recently, Marks et al.[66] provided experimental evidence that a combination of fluid dynamics and electrostatic attractions during bubble ascension can concentrate biological particulate material at the bubble's base, facilitating transfer into jet drop SSA. Looking forward, further research into the physicochemical

mechanisms controlling the transfer of particulate material into SSA_{super} will be important to fully elucidate how seawater biological activity impacts the organic composition of SSA_{super}.

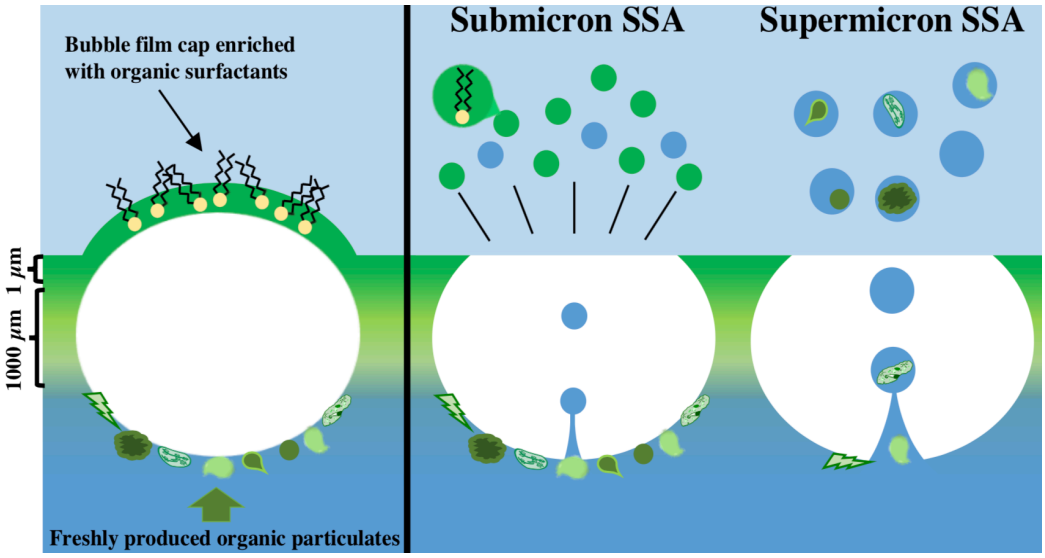

Figure 3.7 Depiction of how the different SSA formation processes influence the organic composition of SSA_{super} and SSA_{sub}. Supermicron SSA are mostly formed from the base of the bubble and contain a large proportion of freshly produced OC. Submicron SSA are primarily formed from the bubble film cap, and are thus comprised of organic surfactants present in the topmost layers of the ocean surface.

For organic transfer into SSA_{sub}, the observed relationship between AFM-measured SSML surface tension and $\delta^{13}C_{sub}$ provides experimental evidence that the organic composition of SSA_{sub} is highly sensitive to changes in the concentration or speciation of surfactants in the top ~1 μm of the SSML. Because the AFM probing depth of 0.2-1.5 μm is comparable to the thickness of a bubble's film at the ocean surface,[65] our data is consistent with conventional wisdom that surface-active organic material present in the top layer of the ocean surface is concentrated on the bubble film and entrained in SSA_{sub} when the bubble bursts. Moreover, our experimental findings provide support for earlier modelling work by Burrows et al.[67] that focused on the top 1 μm of the ocean surface when assessing ocean-aerosol organic transfer. Other ocean-aerosol organic transfer studies have concentrated on measurements of the entire SSML, typically 50-100 μm

thicknesses,[68,69] but our results indicate organic compounds located in the top ~1-2% of the SSML may be the most relevant for predicting the organic constituents in SSA_{sub}. Therefore, analytical techniques capable of probing morphological and compositional changes in the topmost nanolayers of the seawater surface, such as Brewster angle microscopy, infrared reflection absorption spectroscopy, and sum frequency generation spectroscopy,[70] should provide crucial insight into biological and chemical changes that will affect the organic composition of SSA_{sub}.

3.5 Supporting Information

3.5.1 Collection of Field Blank Filters and Calculation of Supermicron SSA OC.

Field blank filters were collected every couple of days during the experiment by placing filters in the filter holders and attaching the sampling apparatus to the wave channel for 10 seconds without turning on the pumps. The filters were collected into plastic petri dishes and stored at -12˚C, in the same manner as the actual SSA samples. Separate field blank filters were collected for the submicron SSA (SSA_{sub}) filter holder and the total suspended SSA (SSA_{TSP}) filter holder to account for any potential differences.

The field blank filters were analyzed via the same combustion method as the SSA samples.[22] The averaged OC amount from the field blanks was subtracted from the OC values for both SSA_{sub} and SSA_{TSP}. The measured SSA $\delta^{13}C$ values were corrected using the measured OC amount and $\delta^{13}C$ values from the filter field blanks ($\delta^{13}C_{blank}$) to obtain the actual $\delta^{13}C$ values for SSA_{sub} and SSA_{TSP} ($\delta^{13}C_{sub}$ and $\delta^{13}C_{TSP}$) according to Equation 2.2. The $\delta^{13}C_{sub}$ and $\delta^{13}C_{TSP}$ uncertainty was determined from the standard deviation in f_{blank} and $\delta^{13}C_{blank}$ measurements by using the highest f_{blank} and lightest $\delta^{13}C_{blank}$ and the lowest f_{blank} and heaviest $\delta^{13}C_{blank}$ to calculate the upper and lower $\delta^{13}C$ bounds, respectively.

The supermicron SSA (SSA_{super}) OC amount was calculated by taking the difference between the SSA_{sub} and SSA_{TSP} carbon amounts. The $\delta^{13}C$ value for SSA_{super} ($\delta^{13}C_{super}$) was calculated analogous to Equation 2.2 by realizing that $\delta^{13}C_{TSP}$ is a mixture of $\delta^{13}C_{sub}$ and $\delta^{13}C_{super}$ multiplied by their fractional contribution to the total OC amount. The error bars for $\delta^{13}C_{super}$ were calculated from the uncertainties in $\delta^{13}C_{sub}$ and $\delta^{13}C_{TSP}$.

The SSA_{super} OC mass percent was calculated by dividing the SSA_{super} OC amount by the total SSA_{super} mass on the filter. The total SSA_{super} mass was determined gravimetrically on a scale with a precision of ± 0.001 g. The filters were dried in a silica gel dessicator at 30˚C for at least 12 hours before being weighed to remove any adsorbed water. We are aware that quartz fiber filters are fragile and some filter materials can be removed when attaching or detaching from the filter holder setup.[71] Therefore, to correct the SSA_{super} weights each of the field blank filters was also dried and weighed. The average of the field blank filters was subtracted from each SSA_{super} sample to obtain the total SSA_{super} mass on each day. The uncertainty in the field blank filters was also used to calculate the error bars for the SSA_{super} OC mass percent (Figure 3.2d).

3.5.2 Averaging of $\delta^{13}C_{POC}$ and $\delta^{13}C_{DOC}$ and Calculation of $Fraction_{FreshOC}$

Because most SSA samples were collected for 2 days, when available the three, daily seawater $\delta^{13}C_{POC}$ and $\delta^{13}C_{DOC}$ measurements made at the beginning, middle, and end of each SSA collection period were averaged to compare with the SSA measurements. If one of the seawater OC variables was not measured on a specific day, the other two measurements were used to calculate the average value. The exception to this was the SSA sample from 7/31-8/1 that was only collected for one day. A POC sample was collected before the addition of the outdoor carboy on

8/1, but no DOC sample was available for measurement. Thus, no DOC data point is included for comparison with this SSA sample.

The $\delta^{13}C_{POC}$ and $\delta^{13}C_{DOC}$ values averaged over the SSA collection periods are shown in Figure 3.4a with the data point placed at the middle of the averaging period. The error bars are the standard error of the averaged $\delta^{13}C_{POC}$ and $\delta^{13}C_{DOC}$ values. These averaged $\delta^{13}C_{POC}$ and $\delta^{13}C_{DOC}$ values were also used to calculate the $Fraction_{FreshOC}$ values via Equation 2.1.[22] Because there was no DOC measurement before the carboy addition on 8/1, no $Fraction_{FreshOC}$ value was calculated for the 7/31-8/1 SSA sample.

3.6 Acknowledgements

This work was funded by the National Science Foundation Center for Aerosol Impacts on Chemistry of the Environment (NSF-CAICE), a Center for Chemical Innovation (CHE-1801971). The authors thank the entire SeaSCAPE team, and especially Dr. Kathryn Mayer, Dr. Jon Sauer, Prof. Timothy Bertram, and Prof. Christopher Cappa for designing and overseeing the campaign. We thank Michael Alves for collection and filtration of DOC samples for organic speciation measurements. We also thank Jiawei Yin for assistance with POC filtration and Yiling Lan for assistance with surface tension measurements. The authors declare no conflicts of interest or financial conflicts in association with this work.

Chapter 3, in part, has been submitted for publication of the material as it may appear in Environmental Science and Technology. Crocker, D. R.; Kaluarachchi, C.P.; Cao, R; Dinasquet, J.; Franklin, E. B.; Morris, C.K.; Nguyen, T.; Torres R.R.; Martz, T. D.; Malfatti, F. M.; Goldstein, A.H.; Tivanski, A. V.; Prather, K. A.; Thiemens M. H. The dissertation author was the primary investigator and author of this paper.

3.7 References

(1) McNeill, V. F. Atmospheric Aerosols: Clouds, Chemistry, and Climate. *Annu. Rev. Chem. Biomol. Eng.* **2017**, *8*, 427–444. https://doi.org/10.1146/annurev-chembioeng-060816-101538.

(2) Regayre, L.; Schmale, J.; Johnson, J.; Tatzelt, C.; Baccarini, A.; Henning, S.; Yoshioka, M.; Stratmann, F.; Gysel-Beer, M.; Carslaw, K. The Value of Remote Marine Aerosol Measurements for Constraining Radiative Forcing Uncertainty. *Atmos. Chem. Phys. Discuss.* **2019**, 1–11. https://doi.org/10.5194/acp-2019-1085.

(3) Carslaw, K. S.; Lee, L. A.; Reddington, C. L.; Pringle, K. J.; Rap, A.; Forster, P. M.; Mann, G. W.; Spracklen, D. V.; Woodhouse, M. T.; Regayre, L. A.; Pierce, J. R. Large Contribution of Natural Aerosols to Uncertainty in Indirect Forcing. *Nature* **2013**, *503* (7474), 67–71. https://doi.org/10.1038/nature12674.

(4) Quinn, P. K.; Collins, D. B.; Grassian, V. H.; Prather, K. A.; Bates, T. S. Chemistry and Related Properties of Freshly Emitted Sea Spray Aerosol. *Chem. Rev.* **2015**, *115* (10), 4383–4399. https://doi.org/10.1021/cr500713g.

(5) Vignati, E.; Facchini, M. C.; Rinaldi, M.; Scannell, C.; Ceburnis, D.; Sciare, J.; Kanakidou, M.; Myriokefalitakis, S.; Dentener, F.; O'Dowd, C. D. Global Scale Emission and Distribution of Sea-Spray Aerosol: Sea-Salt and Organic Enrichment. *Atmos. Environ.* **2010**, *44* (5), 670–677. https://doi.org/10.1016/j.atmosenv.2009.11.013.

(6) Rinaldi, M.; Decesari, S.; Finessi, E.; Giulianelli, L.; Carbone, C.; Fuzzi, S.; O'Dowd, C. D.; Ceburnis, D.; Facchini, M. C. Primary and Secondary Organic Marine Aerosol and Oceanic Biological Activity: Recent Results and New Perspectives for Future Studies. *Adv. Meteorol.* **2010**, *2010*, 1–10. https://doi.org/10.1155/2010/310682.

(7) Aswini, A. R.; Hegde, P.; Aryasree, S.; Girach, I. A.; Nair, P. R. Continental Outflow of Anthropogenic Aerosols over Arabian Sea and Indian Ocean during Wintertime: ICARB-2018 Campaign. *Sci. Total Environ.* **2020**, *712*, 135214. https://doi.org/10.1016/j.scitotenv.2019.135214.

(8) Wang, Y.; Wang, M.; Zhang, R.; Ghan, S. J.; Lin, Y.; Hu, J.; Pan, B.; Levy, M.; Jiang, J. H.; Molina, M. J. Assessing the Effects of Anthropogenic Aerosols on Pacific Storm Track Using a Multiscale Global Climate Model. *PNAS* **2014**, *111* (19), 6894–6899. https://doi.org/10.1073/pnas.1403364111.

(9) Brooks, S. D.; Thornton, D. C. O. Marine Aerosols and Clouds. *Ann. Rev. Mar. Sci.* **2018**, *10*, 289–313. https://doi.org/10.1146/annurev-marine-121916-063148.

(10) Gaston, C. J.; Cahill, J. F.; Collins, D. B.; Suski, K. J.; Ge, J. Y.; Barkley, A. E.; Prather, K. A. The Cloud Nucleating Properties and Mixing State of Marine Aerosols Sampled along the Southern California Coast. *Atmosphere (Basel).* **2018**, *9* (2).

https://doi.org/10.3390/atmos9020052.

(11) Ceburnis, D.; Garbaras, A.; Szidat, S.; Rinaldi, M.; Fahrni, S.; Perron, N.; Wacker, L.; Leinert, S.; Remeikis, V.; Facchini, M. C.; Prevot, A. S. H.; Jennings, S. G.; Ramonet, M.; O'Dowd, C. D. Quantification of the Carbonaceous Matter Origin in Submicron Marine Aerosol by 13C and 14C Isotope Analysis. *Atmos. Chem. Phys.* **2011**, *11* (16), 8593–8606. https://doi.org/10.5194/acp-11-8593-2011.

(12) Cachier, H.; Buat-Menard, P.; Fontugne, M.; Chesselet, R. Long-range Transport of Continentally-derived Particulate Carbon in the Marine Atmosphere: Evidence from Stable Carbon Isotope Studies. *Tellus B* **1986**, *38 B* (3–4), 161–177. https://doi.org/10.1111/j.1600-0889.1986.tb00184.x.

(13) Turekian, V. C.; Macko, S. A.; Keene, W. C. Concentrations, Isotopic Compositions, and Sources of Size-Resolved, Particulate Organic Carbon and Oxalate in near-Surface Marine Air at Bermuda during Spring. *J. Geophys. Res. Atmos.* **2003**, *108* (5). https://doi.org/10.1029/2002jd002053.

(14) Miyazaki, Y.; Kawamura, K.; Sawano, M. Size Distributions of Organic Nitrogen and Carbon in Remote Marine Aerosols: Evidence of Marine Biological Origin Based on Their Isotopic Ratios. *Geophys. Res. Lett.* **2010**, *37* (6). https://doi.org/10.1029/2010GL042483.

(15) Chesselet, R.; Fontugne, M.; Buat-Menard, P.; Esat, U.; Lambert, C. E. The Origin of Particulate Organic Carbon in the Marine Atmosphere as Indicated by Its Stable Carbon Isotopic Composition. **1981**, *8* (4), 345–348.

(16) Shank, L. M.; Howell, S.; Clarke, A. D.; Freitag, S.; Brekhovskikh, V.; Kapustin, V.; McNaughton, C.; Campos, T.; Wood, R. Organic Matter and Non-Refractory Aerosol over the Remote Southeast Pacific: Oceanic and Combustion Sources. *Atmos. Chem. Phys.* **2012**, *12* (1), 557–576. https://doi.org/10.5194/acp-12-557-2012.

(17) Aggarwal, S. G.; Kawamura, K. Molecular Distributions and Stable Carbon Isotopic Compositions of Dicarboxylic Acids and Related Compounds in Aerosols from Sapporo, Japan: Implications for Photochemical Aging during Long-Range Atmospheric Transport. *J. Geophys. Res. Atmos.* **2008**, *113* (14), 1–13. https://doi.org/10.1029/2007JD009365.

(18) Kukert, H.; Riebesell, U. Phytoplankton Carbon Isotope Fractionation during a Diatom Spring Bloom in a Norwegian Fjord. *Mar. Ecol. Prog. Ser.* **1998**, *173*, 127–137. https://doi.org/10.3354/meps173127.

(19) Esposito, M.; Achterberg, E. P.; Bach, L. T.; Connelly, D. P.; Riebesell, U.; Taucher, J. Application of Stable Carbon Isotopes in a Subtropical North Atlantic MesocosmStudy: A New Approach to Assess CO2 Effects on the Marine Carbon Cycle. *Front. Mar. Sci.* **2019**, *6* (October), 1–17. https://doi.org/10.3389/fmars.2019.00616.

(20) Kharbush, J. J.; Close, H. G.; Van Mooy, B. A. S.; Arnosti, C.; Smittenberg, R. H.; Le Moigne, F. A. C.; Mollenhauer, G.; Scholz-Böttcher, B.; Obreht, I.; Koch, B. P.; Becker, K. W.; Iversen, M. H.; Mohr, W. Particulate Organic Carbon Deconstructed: Molecular and

Chemical Composition of Particulate Organic Carbon in the Ocean. *Front. Mar. Sci.* **2020**, *7* (June), 1–10. https://doi.org/10.3389/fmars.2020.00518.

(21) Ceburnis, D.; Masalaite, A.; Ovadnevaite, J.; Garbaras, A.; Remeikis, V.; Maenhaut, W.; Claeys, M.; Sciare, J.; Baisnée, D.; O'Dowd, C. D. Stable Isotopes Measurements Reveal Dual Carbon Pools Contributing to Organic Matter Enrichment in Marine Aerosol. *Sci. Rep.* **2016**, *6* (July), 1–6. https://doi.org/10.1038/srep36675.

(22) Crocker, D. R.; Hernandez, R. E.; Huang, H. D.; Pendergraft, M. A.; Cao, R.; Dai, J.; Morris, C. K.; Deane, G. B.; Prather, K. A.; Thiemens, M. H. Biological Influence on D13C and Organic Composition of Nascent Sea Spray Aerosol. *ACS Earth Sp. Chem.* **2020**, *4* (9), 1686–1699. https://doi.org/10.1021/acsearthspacechem.0c00072.

(23) Miyazaki, Y.; Kawamura, K.; Jung, J.; Furutani, H.; Uematsu, M. Latitudinal Distributions of Organic Nitrogen and Organic Carbon in Marine Aerosols over the Western North Pacific. *Atmos. Chem. Phys.* **2011**, *11* (7), 3037–3049. https://doi.org/10.5194/acp-11-3037-2011.

(24) Cavalli, F.; Facchini, M. C.; Decesari, S.; Mircea, M.; Emblico, L.; Fuzzi, S.; Ceburnis, D.; Yoon, Y. J.; O'Dowd, C. D.; Putaud, J. P.; Dell'Acqua, A. Advances in Characterization of Size-Resolved Organic Matter in Marine Aerosol over the North Atlantic. *J. Geophys. Res. D Atmos.* **2004**, *109* (24), 1–14. https://doi.org/10.1029/2004JD005137.

(25) Rastelli, E.; Corinaldesi, C.; Dell'anno, A.; Lo Martire, M.; Greco, S.; Cristina Facchini, M.; Rinaldi, M.; O'Dowd, C.; Ceburnis, D.; Danovaro, R. Transfer of Labile Organic Matter and Microbes from the Ocean Surface to the Marine Aerosol: An Experimental Approach. *Sci. Rep.* **2017**, *7* (1). https://doi.org/10.1038/s41598-017-10563-z.

(26) Facchini, M. C.; Rinaldi, M.; Decesari, S.; Carbone, C.; Finessi, E.; Mircea, M.; Fuzzi, S.; Ceburnis, D.; Flanagan, R.; Nilsson, E. D.; de Leeuw, G.; Martino, M.; Woeltjen, J.; O'Dowd, C. D. Primary Submicron Marine Aerosol Dominated by Insoluble Organic Colloids and Aggregates. *Geophys. Res. Lett.* **2008**, *35* (17). https://doi.org/10.1029/2008GL034210.

(27) Wang, X.; Sultana, C. M.; Trueblood, J.; Hill, T. C. J.; Malfatti, F.; Lee, C.; Laskina, O.; Moore, K. A.; Beall, C. M.; McCluskey, C. S.; Cornwell, G. C.; Zhou, Y.; Cox, J. L.; Pendergraft, M. A.; Santander, M. V.; Bertram, T. H.; Cappa, C. D.; Azam, F.; DeMott, P. J.; Grassian, V. H.; Prather, K. A. Microbial Control of Sea Spray Aerosol Composition: A Tale of Two Blooms. *ACS Cent. Sci.* **2015**, *1* (3), 124–131. https://doi.org/10.1021/acscentsci.5b00148.

(28) Wurl, O.; Miller, L.; Röttgers, R.; Vagle, S. The Distribution and Fate of Surface-Active Substances in the Sea-Surface Microlayer and Water Column. *Mar. Chem.* **2009**, *115* (1–2), 1–9. https://doi.org/10.1016/j.marchem.2009.04.007.

(29) Mustaffa, N. I. H.; Latif, M. T.; Ali, M. M. Distribution of Surfactants in Sea-Surface

Microlayer and Atmospheric Aerosols at Selected Coastal Area of Peninsular Malaysia. *AIP Conf. Proc.* **2013**, *1571* (December 2013), 625–631. https://doi.org/10.1063/1.4858724.

(30) Prather, K. A.; Bertram, T. H.; Grassian, V. H.; Deane, G. B.; Stokes, M. D.; DeMott, P. J.; Aluwihare, L. I.; Palenik, B. P.; Azam, F.; Seinfeld, J. H.; Moffet, R. C.; Molina, M. J.; Cappa, C. D.; Geiger, F. M.; Roberts, G. C.; Russell, L. M.; Ault, A. P.; Baltrusaitis, J.; Collins, D. B.; Corrigan, C. E.; Cuadra-Rodriguez, L. A.; Ebben, C. J.; Forestieri, S. D.; Guasco, T. L.; Hersey, S. P.; Kim, M. J.; Lambert, W. F.; Modini, R. L.; Mui, W.; Pedler, B. E.; Ruppel, M. J.; Ryder, O. S.; Schoepp, N. G.; Sullivan, R. C.; Zhao, D. Bringing the Ocean into the Laboratory to Probe the Chemical Complexity of Sea Spray Aerosol. *PNAS* **2013**, *110* (19), 7550–7555. https://doi.org/10.1073/pnas.1300262110.

(31) Sauer, J. S.; Mayer, K. J.; Lee, C.; Alves, M. R.; Amiri, S.; Bahaveolos, C.; Barnes, E. B.; Crocker, D. R.; Dinasquet, J.; Garofalo, L. A.; Kaluarachchi, C. P.; Dang, D.; Kilgour, D.; Mael, L.; Mitts, B. A.; Moon, D. R.; Morris, C. K.; Moore, A. N.; Ni, C.-M.; Pendergraft, M. A.; Petras, D.; Simpson, R.; Smith, S.; Tumminello, P. R.; Walker, J. L.; DeMott, P. J.; Farmer, D. K.; Goldstein, A. H.; Grassian, V. H.; Jaffe, J. S.; Malfatti, F.; Martz, T. R.; Slade, J.; Tivanski, A. V.; Bertram, T. H.; Cappa, C. D.; Prather, K. A. The Sea Spray Chemistry and Particle Evolution Study (SeaSCAPE): Overview and Experimental Methods. *Environ. Sci. Process. Impacts* **2021**.

(32) Guillard, R. R. L.; Ryther, J. H. Studies of Marine Planktonic Diatoms. I. Cyclotella Nana. *Can. J. Microbiol.* **1962**, *8*, 229–239.

(33) Holm-Hansen, O.; Lorenzen, C. J.; Holmes, R. W.; Strickland, J. D. H. Fluorometric Determination of Chlorophyll. *ICES J. Mar. Sci.* **1965**, *30* (1), 3–15. https://doi.org/10.1093/icesjms/30.1.3.

(34) Bandstra, L.; Hales, B.; Takahashi, T. High-Frequency Measurements of Total CO2: Method Development and First Oceanographic Observations. *Mar. Chem.* **2006**, *100* (1–2), 24–38. https://doi.org/10.1016/j.marchem.2005.10.009.

(35) Hales, B.; Chipman, D.; Takahashi, T. High-Frequency Measurement of Partial Pressure and Total Concentration of Carbon Dioxide in Seawater Using Microporous Hydrophobic Membrane Contactors. *Limnol. Oceanogr. Methods* **2004**, *2* (11), 356–364. https://doi.org/10.4319/lom.2004.2.356.

(36) Cunliffe, M.; Wurl, O. Sampling the Sea Surface Microlayer; 2015; pp 255–261. https://doi.org/10.1007/8623_2015_83.

(37) Carlson, D. J. Surface Microlayer Phenolic Enrichments Indicate Sea Surface Slicks. *Nature* **1982**, *296* (5856), 426–429. https://doi.org/10.1038/296426a0.

(38) Gasol, J. M.; Del Giorgio, P. A. Using Flow Cytometry for Counting Natural Planktonic Bacteria and Understanding the Structure of Planktonic Bacterial Communities. *Sci. Mar.* **2000**, *64* (2), 197–224. https://doi.org/10.3989/scimar.2000.64n2197.

(39) Marie, D.; Partensky, F.; Jacquet, S.; Vaulot, D. Enumeration and Cell Cycle Analysis of Natural Populations of Marine Picoplankton by Flow Cytometry Using the Nucleic Acid Stain SYBR Green I. *Appl. Environ. Microbiol.* **1997**, *63* (1), 186–193. https://doi.org/10.1128/aem.63.1.186-193.1997.

(40) Noble, R. T.; Fuhrman, J. A. Use of SYBR Green I for Rapid Epifluorescence Counts of Marine Viruses and Bacteria. *Aquat. Microb. Ecol.* **1998**, *14* (2), 113–118. https://doi.org/10.3354/ame014113.

(41) Kirchman, D.; K'nees, E.; Hodson, R. Leucine Incorporation and Its Potential as a Measure of Protein Synthesis by Bacteria in Natural Aquatic Systems. *Appl. Environ. Microbiol.* **1985**, *49* (3), 599–607. https://doi.org/10.1128/aem.49.3.599-607.1985.

(42) Smith, D.; Azam, F. A Simple, Economical Method for Measuring Bacterial Protein Synthesis Rates in Seawater Using. *Mar. Microb. food webs* **1992**, *6* (2), 107–114.

(43) Simon, M.; Azam, F. Protein Content and Protein Synthesis Rates of Planktonic Marine Bacteria. *Mar. Ecol. Prog. Ser.* **1989**, *51*, 201–213. https://doi.org/10.3354/meps051201.

(44) del Giorgio, P. A.; Cole, J. J. Bacterial Growth Efficiency in Natural Aquatic Systems. *Annu. Rev. Ecol. Syst.* **1998**, *29*, 503–541. https://doi.org/10.1146/annurev.ecolsys.29.1.503.

(45) Kaluarachchi, C. P.; Lee, H. D.; Lan, Y.; Lansakara, T. I.; Tivanski, A. V. Surface Tension Measurements of Aqueous Liquid-Air Interfaces Probed with Microscopic Indentation. *Langmuir* **2021**, *37* (7), 2457–2465. https://doi.org/10.1021/acs.langmuir.0c03507.

(46) Padday, J. F.; Pitt, A. R.; Pashley, R. M. Menisci at a Free Liquid Surface: Surface Tension from the Maximum Pull on a Rod. *J. Chem. Soc. Faraday Trans. 1 Phys. Chem. Condens. Phases* **1975**, *71*, 1919–1931. https://doi.org/10.1039/F19757101919.

(47) Lee, H. D.; Estillore, A. D.; Morris, H. S.; Ray, K. K.; Alejandro, A.; Grassian, V. H.; Tivanski, A. V. Direct Surface Tension Measurements of Individual Sub-Micrometer Particles Using Atomic Force Microscopy. *J. Phys. Chem. A* **2017**, *121* (43), 8296–8305. https://doi.org/10.1021/acs.jpca.7b04041.

(48) Nikitas, P.; Pappa-Louisi, A. Thermodynamic and Modelistic Study of Surface Solutions: Aqueous Solutions Containing 2-Butanol. *J. Phys. Chem.* **1990**, *94* (1), 361–370. https://doi.org/10.1021/j100364a062.

(49) Angle, K. J.; Crocker, D. R.; Simpson, R. M. C.; Mayer, K. J.; Garofalo, L. A.; Moore, A. N.; Mora Garcia, S. L.; Or, V. W.; Srinivasan, S.; Farhan, M.; Sauer, J. S.; Lee, C.; Pothier, M. A.; Farmer, D. K.; Martz, T. R.; Bertram, T. H.; Cappa, C. D.; Prather, K. A.; Grassian, V. H. Acidity across the Interface from the Ocean Surface to Sea Spray Aerosol. *PNAS* **2021**, *118* (2). https://doi.org/10.1073/pnas.2018397118.

(50) Bodungen, B. V.; Wunsch, M.; Fürderer, H. *Sampling and Analysis of Suspended and Sinking Particles in the Northern North Atlantic*, Geophysica.; 2013. https://doi.org/10.1029/gm063p0047.

(51) Lalonde, K.; Middlestead, P.; Gélinas, Y. Automation of 13C/12C Ratio Measurement for Freshwater and Seawater DOC Using High Temperature Combustion. *Limnol. Oceanogr. Methods* **2014**, *12* (DEC), 816–829. https://doi.org/10.4319/lom.2014.12.816.

(52) Dittmar, T.; Koch, B.; Hertkorn, N.; Kattner, G. A Simple and Efficient Method for the Solid-Phase Extraction of Dissolved Organic Matter (SPE-DOM) from Seawater. *Limnol. Oceanogr. Methods* **2008**, *6* (6), 230–235. https://doi.org/10.4319/lom.2008.6.230.

(53) Worton, D. R.; Decker, M.; Isaacman-VanWertz, G.; Chan, A. W. H.; Wilson, K. R.; Goldstein, A. H. Improved Molecular Level Identification of Organic Compounds Using Comprehensive Two-Dimensional Chromatography, Dual Ionization Energies and High Resolution Mass Spectrometry. *Analyst* **2017**, *142* (13), 2395–2403. https://doi.org/10.1039/c7an00625j.

(54) Lee, C.; Sultana, C. M.; Collins, D. B.; Santander, M. V.; Axson, J. L.; Malfatti, F.; Cornwell, G. C.; Grandquist, J. R.; Deane, G. B.; Stokes, M. D.; Azam, F.; Grassian, V. H.; Prather, K. A. Advancing Model Systems for Fundamental Laboratory Studies of Sea Spray Aerosol Using the Microbial Loop. *J. Phys. Chem. A* **2015**, *119* (33), 8860–8870. https://doi.org/10.1021/acs.jpca.5b03488.

(55) Verdugo, P.; Alldredge, A. L.; Azam, F.; Kirchman, D. L.; Passow, U.; Santschi, P. H. The Oceanic Gel Phase: A Bridge in the DOM-POM Continuum. In *Marine Chemistry*; 2004; Vol. 92, pp 67–85. https://doi.org/10.1016/j.marchem.2004.06.017.

(56) Käkelä, A.; Furness, R. W.; Kelly, A.; Strandberg, U.; Waldron, S.; Käkelä, R. Fatty Acid Signatures and Stable Isotopes as Dietary Indicators in North Sea Seabirds. *Mar. Ecol. Prog. Ser.* **2007**, *342*, 291–301. https://doi.org/10.3354/meps342291.

(57) Ostrom, N. E.; Macko, S. A.; Deibel, D.; Thompson, R. Seasonal Variation in the Stable Carbon and Nitrogen Isotope Biogeochemistry of a Coastal Cold Ocean Environment. **1997**, *61* (14), 2929–2942.

(58) O'Dowd, C.; Ceburnis, D.; Ovadnevaite, J.; Bialek, J.; Stengel, D. B.; Zacharias, M.; Nitschke, U.; Connan, S.; Rinaldi, M.; Fuzzi, S.; Decesari, S.; Cristina Facchini, M.; Marullo, S.; Santoleri, R.; Dell'anno, A.; Corinaldesi, C.; Tangherlini, M.; Danovaro, R. Connecting Marine Productivity to Sea-Spray via Nanoscale Biological Processes: Phytoplankton Dance or Death Disco? *Sci. Rep.* **2015**, *5* (September), 1–11. https://doi.org/10.1038/srep14883.

(59) Rinaldi, M.; Fuzzi, S.; Decesari, S.; Marullo, S.; Santoleri, R.; Provenzale, A.; Von Hardenberg, J.; Ceburnis, D.; Vaishya, A.; O'Dowd, C. D.; Facchini, M. C. Is Chlorophyll-a the Best Surrogate for Organic Matter Enrichment in Submicron Primary Marine Aerosol? *J. Geophys. Res. Atmos.* **2013**, *118* (10), 4964–4973. https://doi.org/10.1002/jgrd.50417.

(60) Apple, J. K.; Del Giorgio, P. A.; Kemp, W. M. Temperature Regulation of Bacterial

Production, Respiration, and Growth Efficiency in a Temperate Salt-Marsh Estuary. *Aquat. Microb. Ecol.* **2006**, *43* (3), 243–254. https://doi.org/10.3354/ame043243.

(61) Loh, A. N.; Bauer, J. E.; Druffel, E. R. M. Variable Ageing and Storage of Dissolved Organic Components in the Open Ocean. *Nature* **2004**, *430* (7002), 877–881. https://doi.org/10.1038/nature02780.

(62) Mudge, S. M.; Meier-Augenstein, W.; Eadsforth, C.; DeLeo, P. What Contribution Do Detergent Fatty Alcohols Make to Sewage Discharges and the Marine Environment? *J. Environ. Monit.* **2010**, *12* (10), 1846–1856. https://doi.org/10.1039/c0em00079e.

(63) Schmitt-Kopplin, P.; Liger-Belair, G.; Koch, B. P.; Flerus, R.; Kattner, G.; Harir, M.; Kanawati, B.; Lucio, M.; Tziotis, D.; Hertkorn, N.; Gebefügi, I. Dissolved Organic Matter in Sea Spray: A Transfer Study from Marine Surface Water to Aerosols. *Biogeosciences* **2012**, *9* (4), 1571–1582. https://doi.org/10.5194/bg-9-1571-2012.

(64) Cochran, R. E.; Laskina, O.; Jayarathne, T.; Laskin, A.; Laskin, J.; Lin, P.; Sultana, C.; Lee, C.; Moore, K. A.; Cappa, C. D.; Bertram, T. H.; Prather, K. A.; Grassian, V. H.; Stone, E. A. Analysis of Organic Anionic Surfactants in Fine and Coarse Fractions of Freshly Emitted Sea Spray Aerosol. *Environ. Sci. Technol.* **2016**, *50* (5), 2477–2486. https://doi.org/10.1021/acs.est.5b04053.

(65) Modini, R. L.; Russell, L. M.; Deane, G. B.; Stokes, M. D. Effect of Soluble Surfactant on Bubble Persistence and Bubble-Produced Aerosol Particles. *J. Geophys. Res. Atmos.* **2013**, *118* (3), 1388–1400. https://doi.org/10.1002/jgrd.50186.

(66) Marks, R.; Górecka, E.; McCartney, K.; Borkowski, W. Rising Bubbles as Mechanism for Scavenging and Aerosolization of Diatoms. *J. Aerosol Sci.* **2019**, *128* (October), 79–88. https://doi.org/10.1016/j.jaerosci.2018.12.003.

(67) Burrows, S. M.; Ogunro, O.; Frossard, A. A.; Russell, L. M.; Rasch, P. J.; Elliott, S. M. A Physically Based Framework for Modeling the Organic Fractionation of Sea Spray Aerosol from Bubble Film Langmuir Equilibria. *Atmos. Chem. Phys.* **2014**, *14* (24), 13601–13629. https://doi.org/10.5194/acp-14-13601-2014.

(68) Van Pinxteren, M.; Barthel, S.; Fomba, K. W.; Müller, K.; Von Tümpling, W.; Herrmann, H. The Influence of Environmental Drivers on the Enrichment of Organic Carbon in the Sea Surface Microlayer and in Submicron Aerosol Particles – Measurements from the Atlantic Ocean. *Elementa* **2017**, *5* (2011). https://doi.org/10.1525/elementa.225.

(69) Engel, A.; Bange, H. W.; Cunliffe, M.; Burrows, S. M.; Friedrichs, G.; Galgani, L.; Herrmann, H.; Hertkorn, N.; Johnson, M.; Liss, P. S.; Quinn, P. K.; Schartau, M.; Soloviev, A.; Stolle, C.; Upstill-Goddard, R. C.; van Pinxteren, M.; Zäncker, B. The Ocean's Vital Skin: Toward an Integrated Understanding of the Sea Surface Microlayer. *Front. Mar. Sci.* **2017**, *4* (MAY), 1–14. https://doi.org/10.3389/fmars.2017.00165.

(70) Rogers, M. M.; Neal, J. F.; Saha, A.; Algarni, A. S.; Hill, T. C. J.; Allen, H. C. The Ocean's Elevator: Evolution of the Air-Seawater Interface during a Small-Scale Algal Bloom. *ACS Earth Sp. Chem.* **2020**, *4* (12), 2347–2357. https://doi.org/10.1021/acsearthspacechem.0c00239.

(71) Rehme, K.; Smith, F.; Beard, M.; Fitz-Simons, T. *Investigation of Filter Media for Use in Determination of Mass Concentrations of Ambient Particulate Matter*; 1984.

Chapter 4: Biologically Induced Changes in the Partitioning of Submicron Particulates Between Bulk Seawater and the Sea Surface Microlayer

4.1 Abstract

Studies over the last two decades have shown that submicron particulates (SMPs) can be transferred from the seawater into sea spray aerosol (SSA), potentially impacting SSA cloud seeding ability. This work reports the first concurrent bulk and sea surface microlayer (SSML) SMP (0.4-1.0 μm) measurements, made during two mesocosm phytoplankton blooms in a region devoid of active wave breaking and bubble formation, providing insight into how biological and physicochemical processes influence seawater SMP distributions. Modal analyses of the SMP size distributions revealed contributions from multiple, biologically-related particulate populations that were controlled by the microbial loop. With negligible bubble scavenging occurring, SSML enrichment of SMPs remained low throughout both experiments, suggesting this process is vital for SMP enrichment in the SSML. Because many biological SMPs can induce ice formation in SSA, our findings are discussed in the context of SMP transfer into SSA and its potential importance for SSA ice nucleation.

4.2 Introduction

Seawater submicron particulates (SMPs) are a vital component of oceanic biogeochemical processes, contributing to carbon and nutrient cycling, trophic interactions, and attenuation of sunlight.[1,2] Research over the last two decades has additionally revealed that SMPs can be entrained in sea spray aerosol (SSA).[3–5] The compositional changes that arise from SMP entrainment in SSA can have climatically important impacts on its hygroscopicity, cloud

condensation nuclei activity, and ability to serve as ice-nucleating particulates (INPs) in the atmosphere.[6–8]

The potential contribution of SMPs to seawater ice-nucleating entities (INEs) is especially intriguing, as only about 1 in every 10^5 SSA particulates serve as INPs.[9] Previous research has shown that seawater particulates (>0.2 μm) can comprise over 80% of bulk seawater INEs.[10] Micro-Raman spectroscopy on individual SSA particulates collected from this study revealed that INPs with diameters from 0.56-1.0 μm primarily contained siliceous phytoplankton material, providing evidence that biologically related SMPs contribute to SSA INPs. This size range is particularly interesting because multiple studies have reported elevated 0.4-0.7 μm SMPs in biologically active bulk seawater.[11–13] These SMPs have been correlated with chlorophyll-a (chl-a), bacteria, and heterotrophic nanoflagellate concentrations,[11] but the primary biological parameter driving their formation has not been identified. Because the 0.4-0.7 μm SMP size mode is associated with microbial activity, it will hereafter be referred to as the "microbial mode". Monitoring evolution of the microbial mode throughout an entire phytoplankton bloom would be beneficial to identify the biological contributors to the microbial mode. A number of studies have found that seawater biological INEs, including diatoms, heterotrophic bacteria, and their cell fragments, constitute a significant portion of SSA INPs.[10,14,15] Therefore, elucidating the biological components comprising microbial mode SMPs may help explain elevated seawater INE concentrations during phytoplankton blooms,[10,16] providing insight into the higher concentrations of SSA INPs produced from biologically productive seawater.[9,16,17]

Transfer of biological INEs into SSA also depends on physical processes such as bubble scavenging of organic material and the bubble bursting mechanisms that form SSA. SSA is produced both from the bubble film cap when it bursts at the air-sea interface and from the bubble's

base during subsequent collapse of the bubble cavity.[18] It follows that particulate transfer into SSA will be influenced by particulate concentrations in the SSML, the top 1-1000 μm of the ocean surface often enriched in biological components and organic material,[19–21] as well as particulate concentrations in the underlying bulk seawater. Therefore, assessing ocean-aerosol transfer of microbial mode SMPs necessitates SMP measurements in both the bulk and SSML; however, simultaneous size measurements of bulk and SSML particulates have primarily focused on supermicron particulates.[22]

This work reports the first concurrent particulate size distribution measurements for 0.4-1.0 μm SMPs in the bulk seawater and SSML made throughout two phytoplankton bloom mesocosm experiments to elucidate how biological activity influences the distribution and concentration of SMPs between the bulk seawater and SSML. The measurements were made in a region far downstream from active wave breaking and bubble formation, providing insight on SMP partitioning between the bulk and SSML when bubble scavenging was minimal. Our results are discussed in the context of ocean-aerosol SMP transfer and the potential contribution of SMPs to SSA ice nucleation.

4.3 Experimental Methods

4.3.1 The Wave Channel Mesocosm Experiments

Two mesocosm experiments were conducted in an ocean-atmosphere wave channel at the SIO Hydraulics Laboratory as part of the 2019 Sea Spray Chemistry and Particulate Evolution (SeaSCAPE) study. A wave channel depiction and detailed description of experimental and biological parameters can be found in Sauer et al.[23] For both experiments, the 11,800 L wave channel was filled with natural, filtered seawater (50 μm Nitex mesh) collected from the coastal Pacific Ocean. Experiment 1 achieved a full phytoplankton bloom growth and decay cycle from

July 1st-July 10th, after the addition of f/2 diatom growth nutrients on July 4th.[24] For Experiment 2, from July 12th-July 19th, a more dilute f/20 nutrient mixture was added, and little phytoplankton growth was observed over the course of the experiment (see Figure 4.6a). For completeness, we report SMP measurements from Experiment 2 (Figure 4.1, Figure 4.6b), however because a phytoplankton bloom did not occur, most discussion about Experiment 2 has been placed in the Supporting Information at the end of this chapter (see Section 4.6.1).

4.3.2 Seawater Sampling and Biological Measurements

During the mesocosm experiments, a homemade, continuous flow system provided a continuous time series of chl-a concentration in the wave channel to monitor phytoplankton growth. This system employed a SeaBird Scientific ECO-Triplet-BBFL2 sensor to measure chl-a using fluorescence at excitation/emission wavelengths of 470/695 nm. The *in situ* chl-a values were calibrated using measurements of extracted chl-a taken from the bulk seawater and analyzed fluorometrically according to CALCOFI methods.[25]

All seawater measurements, including *in situ* measurement of chl-a, were made at the back of the wave channel in a designated seawater sampling section.[23] Once daily in the seawater sampling section, 16 L of bulk seawater was siphoned from the wave channel and 200 mL of SSML was collected using the glass plate method.[26,27] Aliquots were taken from these samples for bacteria and virus enumeration, TEP quantification, and particulate size analysis.

For bacteria and virus quantification, bulk seawater samples were prepared according to standard protocols.[28–30] All samples were preserved with 5% glutaraldehyde, flash frozen with liquid nitrogen, and stored at -80˚C.[31] Bacteria samples were diluted 10-fold in 1x TE buffer at pH 8 and stained for 10 minutes with SYBR Green I in the dark at room temperature.[28] Virus samples

were diluted 50-fold in 1x TE buffer at pH 8 and stained for 10 minutes with SYBR Green I at 80˚C in the dark.[30] Finally, enumeration of bacteria and viruses was carried out using a BD FACSCanto II™ flow cytometer.

Transparent exopolymer particulates (TEP) were measured following the colorimetric method as described by Engel.[32] Briefly, SSML samples were filtered onto 0.4 µm polycarbonate filters (Pall Corp.) after storage at -20°C, and stained with Alcian Blue (AB, 0.02%). AB was then released with 80% sulfuric acid over a 4 hour incubation at 4°C and absorbance was measured at 787 nm. TEP concentrations were determined following a calibration with Xanthan Gum standards and blank controls with pure water and filtered seawater.

The seawater sampling section was located about 20 meters downstream from the active wave breaking region. The wave channel surface water flow is about 1 cm per minute, so surface waters would take around 30 minutes to transit from the wave breaking region to the seawater sampling section. Because of the long time duration between wave breaking and seawater sample collection, we are interpreting the particulate measurements to be reflective of seawater conditions where the effects of active wave breaking and bubble scavenging are negligible.

4.3.3 Particulate Size Measurements and Analysis

4.3.3.1 Multispectral Advanced Nanoparticulate Tracking Analysis (MANTA)

Particulates were sized using a MANTA ViewSizer® 3000 (Horiba Scientific). The MANTA Viewsizer® 3000 uses three lasers, blue (450 nm), green (532 nm), and red (635 nm), to illuminate particulates in a sample of seawater.[33] Light scattered by particulates in a 2.5 μL viewfield of the sample is projected on a charged-coupled device (CCD) array and spectrally resolved to provide an image for each spectral band. A sequence of these images is recorded and saved to the computer as a video file. For these experiments, 100 videos were taken for each sample

to ensure that enough particulates were identified to obtain an accurate size distribution. Analysis software identifies each individual particulate in an image and tracks its Brownian motion through the seawater medium in subsequent images. For each individual particulate, the mean square displacement is determined from the sequence of images and used to calculate the diffusion coefficient (D). Under the assumption that particulates are spherical, the hydrodynamic diameter (d_h) is then calculated from the measured diffusion coefficient using the Stokes-Einstein equation (Equation 4.1):[34]

$$d_h = \frac{k_B T}{3\pi\eta D} \qquad \text{(Equation 4.1)}$$

Here k_B is the Boltzmann constant, T is seawater temperature, and η is seawater viscosity. Although the MANTA specifically measures hydrodynamic diameters, this work reports equivalent spherical diameters (ESD). In addition to assuming spherical particulates, ESD assumes particulates exhibit identical hydrodynamic, optical, electrical, and aerodynamic properties, allowing for comparison between different sizing techniques.[35]

In our experiments, the MANTA reported particulates with d_h from 0.01-1.0 μm. However, detection of the smallest particulates strongly depends on the refractive index contrast between the particulate and seawater medium, which was not measured. Therefore, we focused this study on seawater particulate sizes ranging from 0.4-1.0 μm. The particulate sizes reported by the software were organized into 0.1 μm bin widths starting from a bin midpoint diameter of 0.405 μm up to 0.995 μm.

4.3.3.2 Particulate Size Distributions

The role of particulates in surface ocean processes often depends on their concentration and size distribution.[36] The particulate size distribution (PSD), represented by $N'(d)$ in Equation

4.2a, is best described as the average number of particulates per unit volume of seawater, N(d), in a given diameter range (Δd).[37]

$$N'(d) = \frac{N(d)}{\Delta d} \quad \text{(Equation 4.2a)}$$

$$N'(d) = N_o(d)^{\xi} \quad \text{(Equation 4.2b)}$$

Frequently a portion of seawater PSDs, or the entire distribution, follow a general power law distribution of the form in Equation 4.2b, where N_o is the differential number concentration, and ξ represents how quickly particulate concentrations decrease with increasing diameter.[37] In a loglog plot of d vs. $N'(d)$, ξ is equal to the PSD slope (see Section 4.4.1 below).

4.3.3.3 Modal Analyses of PSDs

Lognormal modal analyses of the PSDs were performed in MATLAB software using maximum likelihood estimates (MLE) for parameters of a normal distribution. Although particulate sizes overall do not follow a lognormal distribution, lognormal analysis has been previously used to identify modal contributions to the total PSD.[38,39] This analysis is motivated by the fact that many particulate populations such as phytoplankton, bacteria, nonliving organic matter, and mineral particulates follow lognormal distributions in the ocean.[39,40] We recognize there are many possible ways to fit modal analyses to our PSD data. Because our goal was to assess particulate populations contributing to the microbial mode, we chose to decompose each PSD into four lognormal modes with constraints placed on the means and standard deviations. Four modes were sufficient to accurately reproduce the measured PSDs while still resolving particulate populations.

4.4 Results and Discussion

4.4.1 Seawater Submicron PSDs

Comparing our PSD measurements with previous oceanic SMP studies is difficult because the oceanic PSD slopes vary widely from -3 to -10 (Figure 4.1).[11,41–45] The cause of this variability is uncertain, but may result from analytical limitations that restrict most measurements to only a portion of SMP sizes.[36] To provide better context for our measurements, the previously measured oceanic PSDs shown in Figure 1 have been averaged at 0.05 μm intervals over the 0.05-1.0 μm range and plotted as open circles along with gray dashed lines for the 95% confidence interval. The averaged values are well represented by a power law function (solid black line, $R^2 = 0.94$) with a PSD slope of -3.72, similar to the value observed for combined submicron and supermicron marine detritus (-3.36),[40] and within the commonly reported -3 to -4 range for supermicron PSDs.[37,46] Thus, despite PSD slope inconsistency over segments of the SMP size range, a power law distribution with a PSD slope similar to supermicron particulates likely provides a good approximation for oceanic SMP concentrations when assessing the full 0.05-1.0 μm range.

The bulk and SSML PSD measurements for Experiments 1 and 2, averaged using each day of both experiments, are overlaid on the bulk seawater oceanic PSDs in Figure 4.1. All four PSDs fall within the 95% confidence interval calculated from the averaged oceanic values, and are on the same order of magnitude as previous Pacific Ocean measurements in coastal San Diego (solid maroon lines).[41] The significant overlap between bulk and SSML PSDs implies little SMP enrichment in the SSML. Additionally, the microbial mode between 0.4-0.7 μm, where the PSD deviates from the typical power law decrease, is clearly visible (and labeled) in Figure 4.1 for all four PSDs in this study as well as the averaged oceanic values.

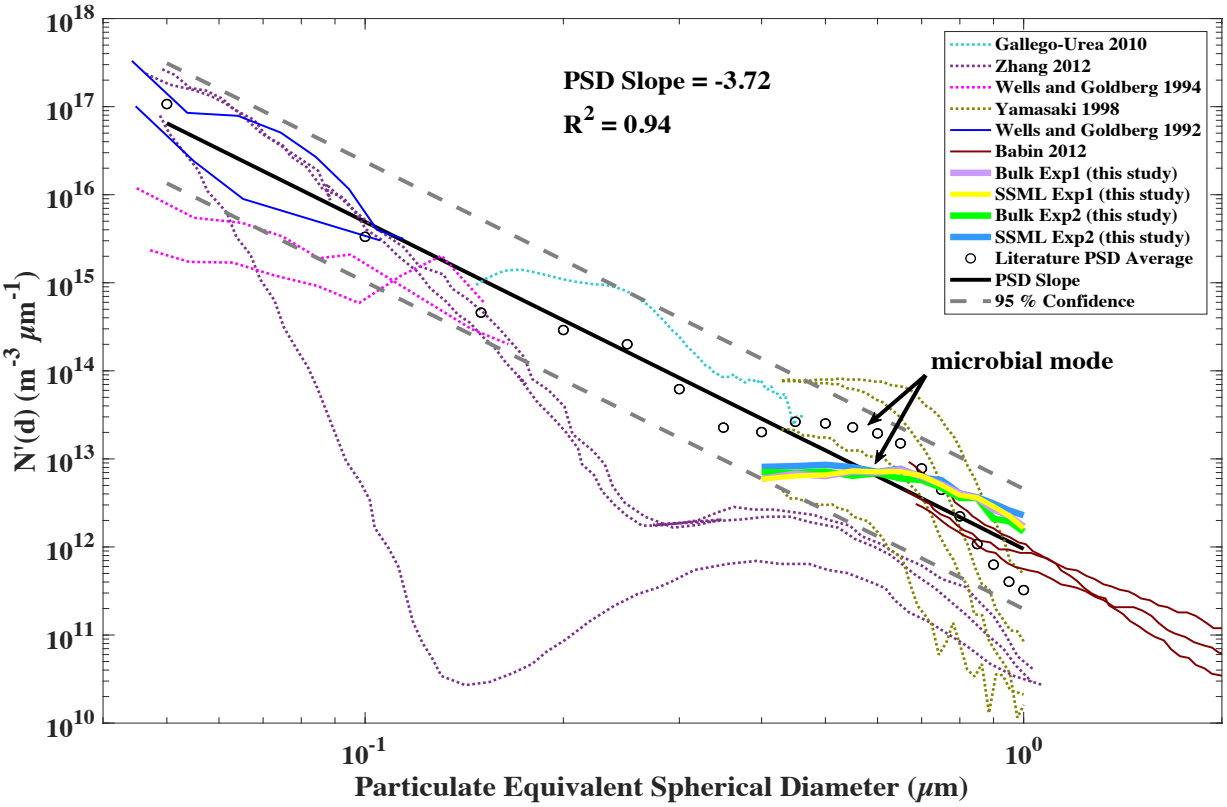

Figure 4.1 Bulk and SSML PSDs from both mesocosm experiments in this study, along with previously reported bulk seawater oceanic PSDs. Solid lines represent PSDs measured for coastal San Diego seawater, while dotted lines represent measurements in other oceanic regions. All four PSDs from this study fell within the 95% confidence interval (gray dashed lines) calculated for the averaged oceanic values.

4.4.2 Evolution of Biology and Particulate Concentrations During Experiment 1

Experiment 1 followed the typical bloom progression with phytoplankton growth (chl-a) increasing after addition of the diatom growth nutrients. Phytoplankton growth was closely followed by elevated bacteria concentrations, and then higher virus concentrations in response to the bacteria (Figure 4.2a).[47,48] To evaluate the role of biology on SMP concentrations, the experiment was separated into "pre-bloom", "growth", and "decay" phases (labeled in Figure 4.2a).

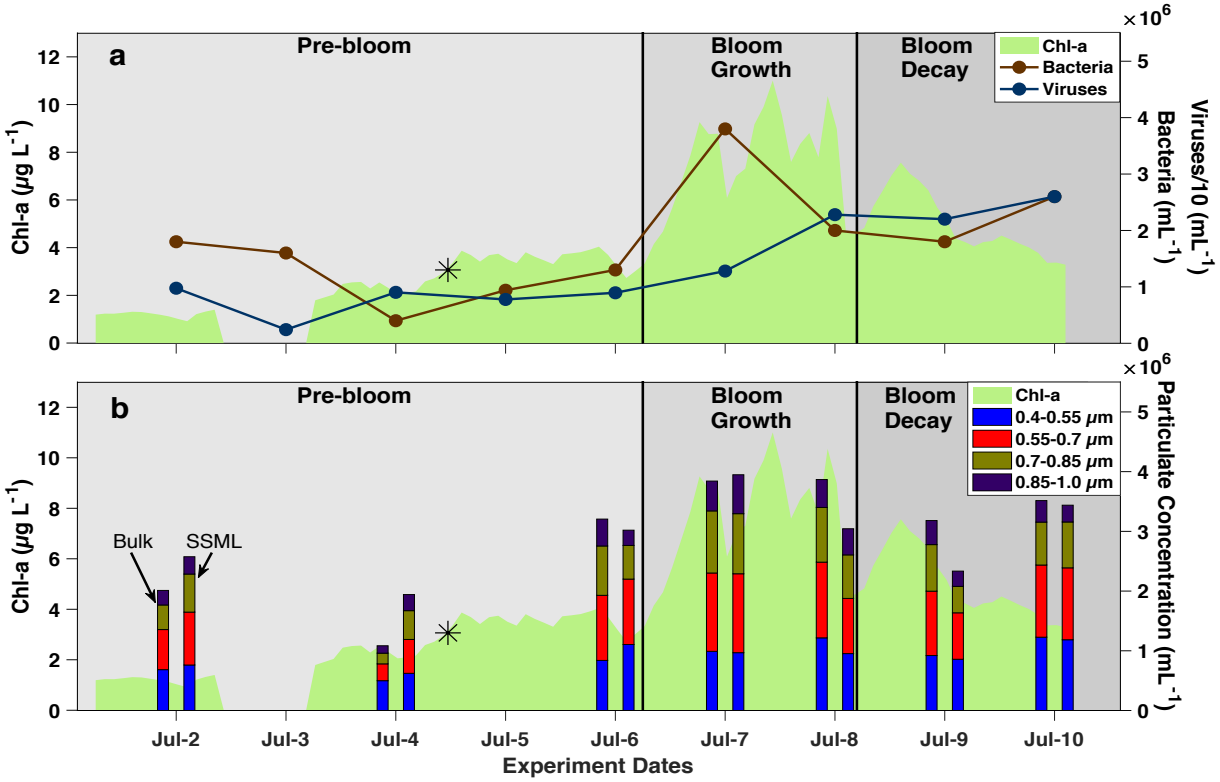

Figure 4.2 a) Development of chl-a, bacteria, and virus concentrations throughout Experiment 1 (asterisk denotes nutrient addition). b) 0.4-1.0 µm SMP concentrations for bulk (left bars) and SSML (right bars) in 0.15 µm size bins (stacked bars) with the full bar height signifying the total SMP concentration. Both plots are divided into pre-bloom, bloom growth, and bloom decay phases (solid lines) based on the beginning of exponential phytoplankton growth (chl-a), and chl-a decaying to half the peak value.

Daily bulk and SSML SMP concentrations are shown as stacked bars in Figure 4.2b. Both bulk and SSML SMP concentrations were generally higher during the growth and decay phases compared to the pre-bloom phase. To visualize how different SMP sizes are influenced by the seawater biological activity, the bars in Figure 4.2b were organized into four size regimes: 0.4-0.55 µm (blue), 0.55-0.7 µm (red), 0.7-0.85 µm (olive), and 0.85-1.0 µm (purple). Daily bulk SMP concentrations for all four size fractions moderately to strongly correlated with daily concentrations of bulk seawater bacteria and chl-a, having Pearson correlation coefficients (r) of 0.64-0.76 and 0.65-0.83, respectively (Table 4.1). This suggests that bacterial cells contributed to

SMPs of all measured sizes, including the microbial mode. Because most phytoplankton are larger than 1 μm, the correlation between SMPs and chl-a could be due to direct release of 0.4-1.0 μm algal exudates or aggregation of smaller particulates generated by primary productivity. Also relevant to the microbial mode, virus concentrations showed a strong correlation (r = 0.83) with 0.4-0.55 μm particulates (Table 4.1), suggesting viral lysis of organisms may produce microbial mode SMPs during bloom decay. Overall, the correlations with chl-a, bacteria, and viruses suggest microbial mode formation is controlled by the entire microbial loop with different particulate populations contributing during each bloom phase. To better assess changes in SMP populations throughout the bloom, modal analyses were performed on the pre-bloom, growth, and decay PSDs. Our PSD measurements do not resolve the chemical identity of SMPs, but potential contributors are discussed in the section below.

Table 4.1 Pearson correlation coefficients for Experiment 1 bulk SMPs and biological variables

Experiment 1	0.4-0.55 μm Bulk	0.55-0.7 μm Bulk	0.7-0.85 μm Bulk	0.85-1.0 μm Bulk	Chl-a	Bacteria	Virus
0.4-0.55 μm Bulk	1.00	**0.89**[a]	**0.77**	**0.74**	0.65	0.64	**0.83**
0.55-0.7 μm Bulk	--	1.00	**0.97**	**0.95**	**0.75**	**0.76**	0.58
0.7-0.85 μm Bulk	--	--	1.00	**0.99**	**0.83**	**0.74**	0.42
0.85-1.0 μm Bulk	--	--	--	1.00	**0.80**	0.68	0.38
Chl-a	--	--	--	--	1.00	0.61	0.50
Bacteria	--	--	--	--	--	1.00	0.41
Virus	--	--	--	--	--	--	1.00

[a] Coefficients (lower)higher than (-)0.7 are listed in bold and considered strong correlations.[49]

4.4.3 Potential SMP Populations Contributing to the Microbial Mode

PSD modal analysis reveals the strong resemblance between bulk and SSML PSDs throughout each bloom phase (Figure 4.3), demonstrating that similar SMP populations are contributing to the microbial mode in the SSML. Specifically, transitioning from the pre-bloom to growth phase, the bulk and SSML PSDs both display large increases in the particulate mode centered around 0.6-0.7 μm (red). The 0.6-0.7 μm particulate mode has been observed in oceanic measurements of bulk seawater SMPs,[11–13] and is patently visible as the microbial mode labeled in Figure 4.1. As mentioned above, bacteria cells are likely contributors to this particulate mode, but sonication experiments have shown that a significant proportion of microbial mode particulates are nonliving organic material.[11,13] Isao et al.[13] observed that many microbial mode SMPs were hydrated, flexible organic material that aggregated to form larger particulates. Their observations are consistent with submicron-sized nanogels, such as transparent exopolymer particulates (TEP), which are formed through self-assembly and aggregation of dissolved (<0.2 μm) exopolymeric secretions (EPS) from marine phytoplankton and bacteria.[50,51] This is substantiated by a tentative, but very strong correlation between 0.55-0.7 μm SSML particulates and SSML TEP (>0.4 μm) concentrations in Experiment 1 (Figure 4.4). Additionally, aggregates of membrane vesicles released by heterotrophic bacteria and cyanobacteria have also been observed in the bulk seawater and SSML.[52,53] Both of these SMP sources are consistent with the correlation of chl-a and bacteria concentrations to 0.55-0.7 μm bulk SMPs.

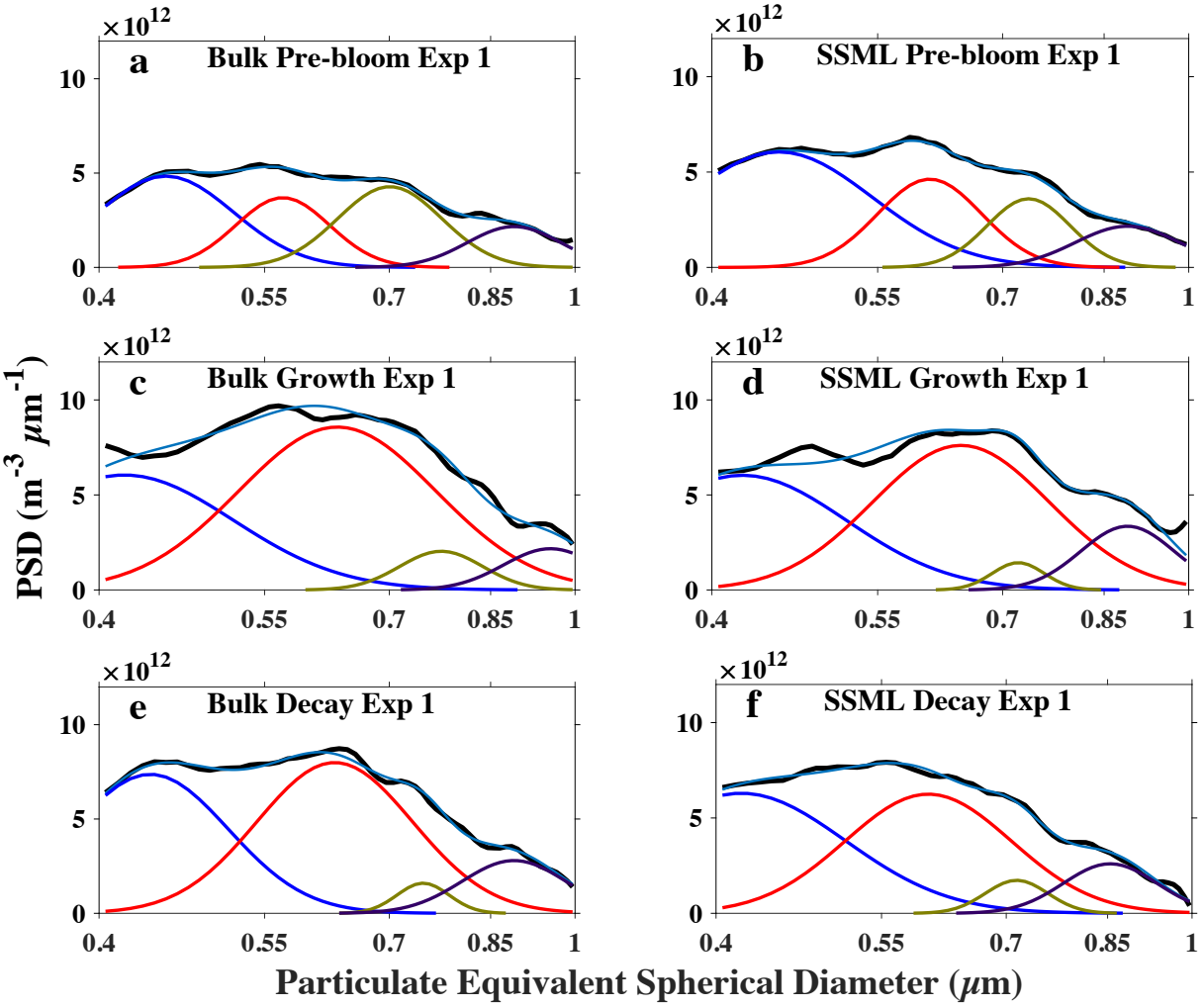

Figure 4.3 A four-component modal analysis of bulk and SSML PSDs for the pre-bloom (a,b), growth (c,d), and decay (e,f) phases. The black line is a five-point, centered moving average of the PSDs from each bloom phase. The four modes comprising each PSD are shown in blue, red, olive, and purple with a dark blue line representing the composite of these modes.

The 0.4-0.55 µm SMP concentrations increased during bloom decay and senescence (Figure 4.3e,f), and closely correlated with elevated virus concentrations. Viral lysis of large marine bacteria can produce smaller particulates with diameters between 0.4-0.7 µm,[54] which may represent a source of 0.4-0.55 µm SMPs during bloom decay. Additionally, bacterial egestion by heterotrophic nanoflagellates, which were not measured in this experiment but generally increase following bacteria growth (Nagata & Kirchman, 1992),[55] is known to produce 0.4-0.6 µm

picopellets that may contribute to this mode.[56] These observations indicate that further microbial processing of SMPs initially formed by primary production and bacterial growth may alter the identity of particulates comprising the microbial mode.

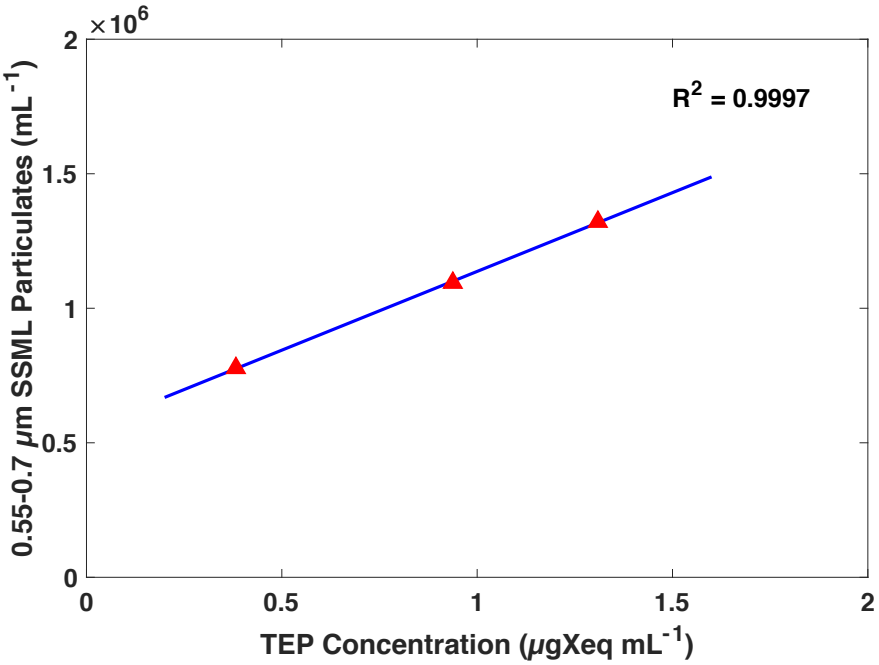

Figure 4.4 Plot of the SSML TEP (>0.4 µm) concentration, reported in micrograms of Xanthan Gum equivalents mL^{-1}, versus the concentration of 0.55-0.7 µm SSML particulates for samples measured on 7/6, 7/7, and 7/9. For these measurements there is a very strong correlation between the amount of TEP in the SSML and the concentration of 0.55-0.7 µm microbial mode particulates. The largest TEP concentration occurs on 7/7 the day with peak chl-a and bacteria concentrations.

4.4.4 SMP Partitioning in Seawater and Importance for Ocean-Aerosol Transfer

Stramski et al.[22] recently reported the first SSML particulate enrichment factors (EFs, Equation 4.3), calculated from simultaneous, oceanic bulk and SSML PSD measurements on 0.8-50 µm particulates. Their measurements were made in the presence of breaking waves and revealed size dependent SSML particulate enrichment with larger particulates (>10 µm) having the highest EFs, and enrichment generally decreasing as particulate diameter decreased. For

comparison with our SMP measurements, Figure 4.5 plots a portion of their measured EFs for three separate days in the Santa Barbara Channel (gray lines).

$$\text{Particulate Enrichment Factor (EF)} = \frac{\text{\# of SSML Particulates}}{\text{\# of Bulk Particulates}} \quad \text{(Equation 4.3)}$$

Our study extends the measured SMP EF range to 0.4 μm and separates the EFs from both experiments into their biological phases (Figure 4.5). Both pre-bloom phases displayed only slight SMP enrichment (1.0-1.4), at the low end of 0.8-1.0 μm EF measurements from the Santa Barbara Channel (1.2-2.5, Figure 4.5). With the exception of one data point, this slight enrichment disappeared during the growth and decay phases, and no SMP enrichment was observed (EF≤1.0). The underlying mechanisms causing lower SMP EFs during the growth and decay phases are uncertain, though one possibility is that the elevated concentrations of biological and organic material in the SSML led to higher particulate aggregation rates.[57,58] Faster particulate aggregation could result in a larger proportion of supermicron SSML particulates outside our measurement range.

Overall, the measured EFs (0.7-1.4) show SMP enrichment is slight to nonexistent in this study, consistent with a negligible impact from wave action and bubble formation. Bubble adsorption is a critical process for transporting particulates to the SSML,[59,60] and can lead to 5-fold increases in SSML enrichment of biological and organic particulates.[61] Furthermore, Walls & Bird[62] have found that EF values of yeast cells adsorbed to the bubble film surface increased four-fold, from 5 to 20, as water drained off the film before bursting. Their observations align particulate enrichment with previously observed EFs of 10-22 for bacteria in SSA.[20,63] Thus, the lack of enrichment observed in our study suggests future measurements in wave breaking regimes will be crucial to determine how bubble scavenging and bursting processes impact SMP enrichment in the SSML and transfer into SSA.

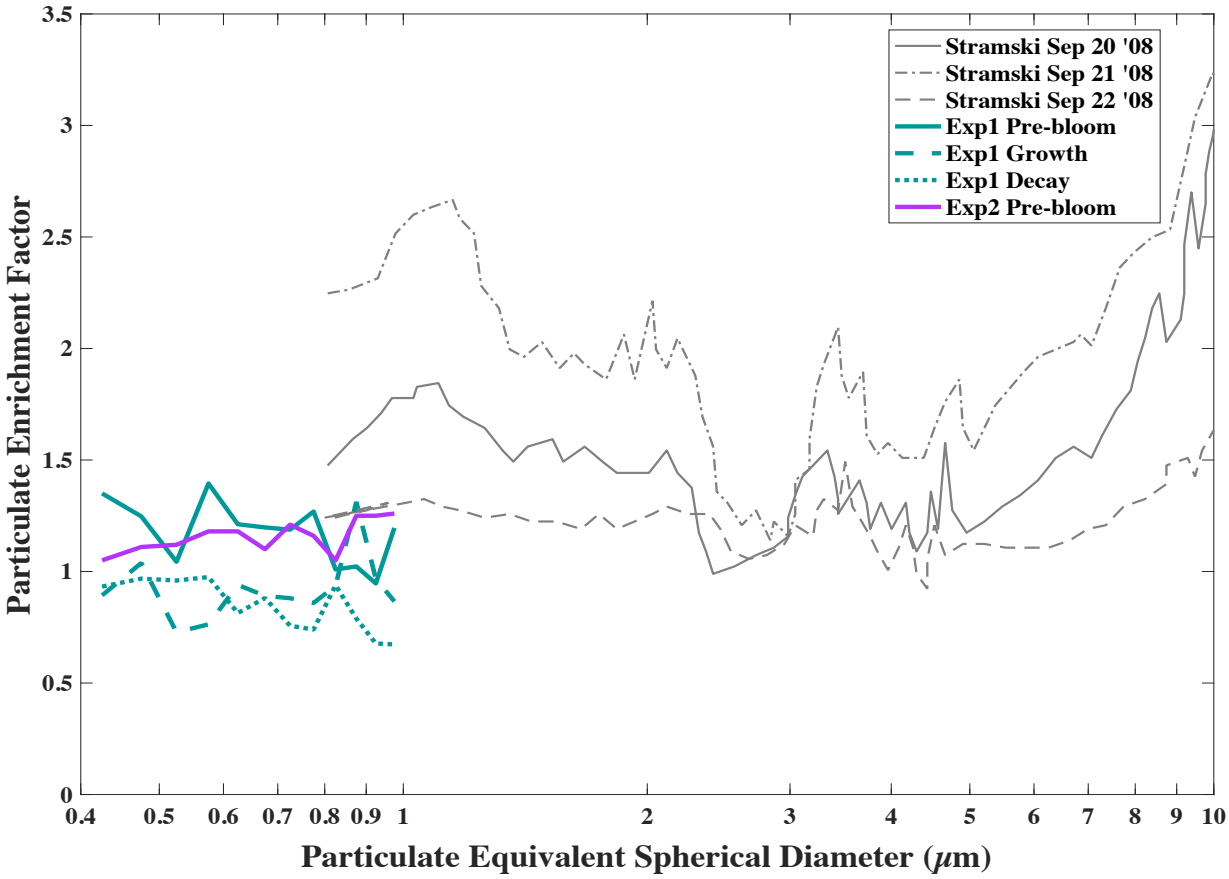

Figure 4.5 SMP enrichment factors from 0.4-1.0 µm in 0.05 µm size bins separated into bloom phases for both experiments. Included for comparison are particulate EFs measured in the Santa Barbara Channel in the presence of breaking waves (gray lines).[22]

4.5 Conclusions and Implications for SMP Entrainment in SSA

Herein, we report the first concurrent particulate size distribution measurements of 0.4-1.0 µm SMPs in the bulk seawater and SSML made over the course of two mesocosm experiments. In Experiment 1, which featured a complete phytoplankton bloom cycle, bulk and SSML SMP concentrations were generally higher during the growth and decay phases compared to the pre-bloom phase. This was primarily due to an increase in 0.4-0.7 µm microbial mode SMPs (Figure 4.2b), with potential biologically-produced particulates in this size range including bacteria cells, algal exudates, nanogels, and vesicle aggregates, among others.[52,64] PSD modal analyses further revealed that the particulate populations contributing to the microbial mode depend on the bloom

phase (Figure 4.3). During the growth phase, 0.55-0.7 μm SMPs increased in conjunction with maximum phytoplankton (chl-a) and bacterial abundance. The decay phase was distinguished by increased 0.4-0.55 μm SMPs and virus concentrations, potentially due to cellular debris from viral lysis or grazing of phytoplankton and bacteria during bloom senescence.[48]

Biologically induced changes in SMP concentrations and distributions may affect particulate entrainment in SSA, which is especially important for SMPs that possess ice nucleating ability. Similar to the SMP concentrations, higher seawater INE concentrations have been reported in biologically-active seawater.[10,16] Moreover, Micro-Raman spectroscopy has demonstrated that biologically-produced SMPs contribute to SSA INPs, and many of the likely microbial mode components have been identified as seawater particulate INEs including heterotrophic bacteria, diatom cell fragments, and potentially nanogels.[10,14,65–67] Recent research has shown that SSA INP concentrations scale with the total aerosol volume.[16] Because SSA formed from the bubble's base comprises the majority of SSA volume,[16,68] the increased bulk SMP concentrations resulting from seawater biological activity may increase the amount of SMP INEs that are transferred into SSA. This may help explain the established connection between elevated seawater biological activity and higher SSA INP concentrations.[9,16]

In summary, because seawater particulate concentrations increase with decreasing diameter (Figure 4.1), SMP INEs may constitute a significant portion of particulate INEs transferred into SSA. Therefore, the increased biological production of SMPs in our experiments, represents one factor that may contribute to higher INE entrainment in SSA during phytoplankton blooms.[9,10,16] Entrainment of submicron INEs in SSA may be further augmented in wave breaking regimes where bubble scavenging and bursting processes can enhance SMP enrichment in the SSML and transfer into SSA. To assess the contribution of SMPs to SSA INPs, we suggest future

experiments on submicron and supermicron SSA INPs that combine size-segregated seawater INE measurements with bulk and SSML PSD measurements. The knowledge gained from this further analysis will help inform climate and weather models working to assess the global radiative balance and precipitation patterns.

4.6 Supporting Information

4.6.1 Microbial Activity during Experiment 2

Very little phytoplankton (chl-a) growth was observed in Experiment 2. Throughout the entire experiment chl-a values remained similar to the Experiment 1 pre-bloom values. Despite the lack of an exponential phytoplankton growth or decay phase, we include a brief description of Experiment 2 here to demonstrate the importance of the complete microbial loop on microbial mode growth. At the beginning of the Experiment 2, the bacteria and virus concentrations increased, but bacteria concentrations only correlated with 0.4-0.55 μm particulate concentrations ($r = 0.80$) and viruses did not correlate with any of the SMP concentrations (Table 4.2). The small bacteria sizes observed in Experiment 2 are likely due to the lack of significant primary productivity, an important food source for bacteria proliferation.[69] With bacteria sizes in the 0.4-0.55 μm range, it follows that viral lysis likely produced particulates below 0.4 μm.[54] These particulates would be outside our measured size range, explaining the lack of correlation between microbial mode SMPs and virus concentrations in Experiment 2. We point out these observations from Experiment 2 to illustrate that growth of microbial mode SMPs is dependent on the interactions between multiple components of the microbial loop: phytoplankton, bacteria, and viruses.[48]

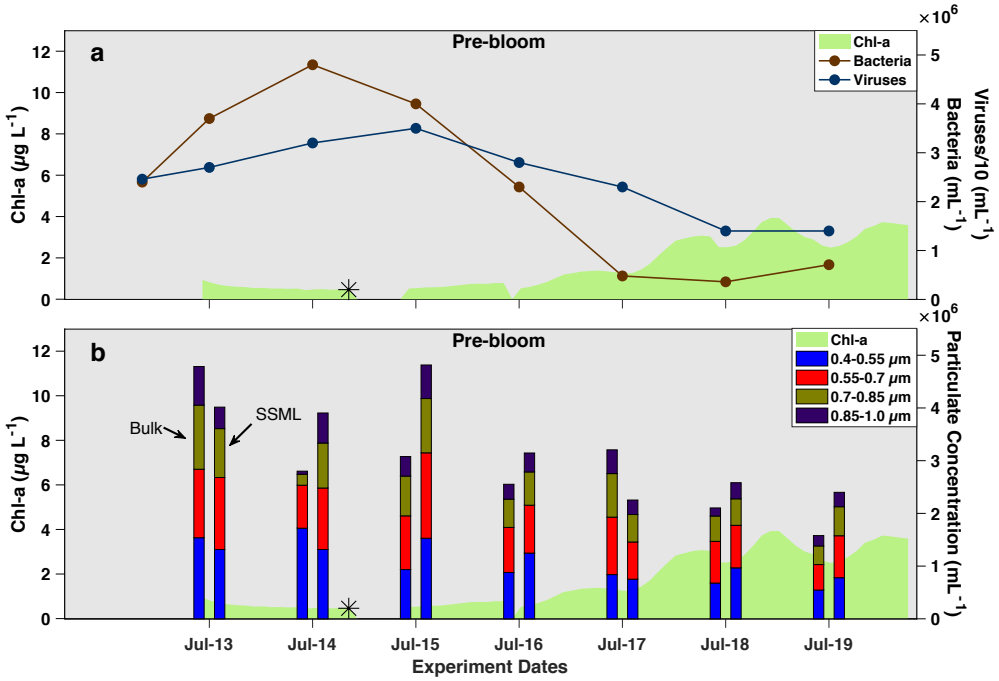

Figure 4.6 a) Development of chl-a, bacteria, and virus concentrations throughout Experiment 2. In Experiment 2, the biological progression is different from Experiment 1 with bacteria and virus concentrations increasing before algae growth nutrients were added (asterisk). b) 0.4-1.0 µm SMP concentrations for the bulk (left bars) and SSML (right bars) in Experiment 2 with stacked bars displaying SMP concentrations for equally spaced 0.15 µm size bins. Experiment 2 lacked exponential phytoplankton growth and decay periods; only exhibiting a pre-bloom phase with similar chl-a concentrations to the Experiment 1 pre-bloom phase (Figure 4.2a).

Table 4.2 Pearson correlation coefficients for Experiment 2 bulk SMPs and biological variables

Experiment 2	0.4-0.55 µm Bulk	0.55-0.7 µm Bulk	0.7-0.85 µm Bulk	0.85-1.0 µm Bulk	Chl-a	Bacteria	Virus
0.4-0.55 µm Bulk	1.00	0.50	0.18	0.21	-0.66	**0.83**[a]	0.65
0.55-0.7 µm Bulk	--	1.00	**0.87**	**0.83**	-0.57	0.37	0.53
0.7-0.85 µm Bulk	--	--	1.00	**0.98**	-0.23	0.09	0.22
0.85-1.0 µm Bulk	--	--	--	1.00	-0.24	0.12	0.23
Chl-a	--	--	--	--	1.00	**-0.79**	**-0.98**
Bacteria	--	--	--	--	--	1.00	**0.85**
Virus	--	--	--	--	--	--	1.00

[a] Coefficients (lower)higher than (-)0.7 are listed in bold and considered strong correlations.[49]

4.7 Acknowledgements

This work was funded by the National Science Foundation Center for Aerosol Impacts on Chemistry of the Environment (NSF-CAICE), a Center for Chemical Innovation (CHE-1801971). The authors thank the entire SeaSCAPE team, and especially Dr. Kathryn Mayer, Dr. Jon Sauer, Prof. Tim Bertram, and Prof. Chris Cappa for designing and overseeing the campaign. The authors declare no conflicts of interest or financial conflicts in association with this work.

Chapter 4, in part, has been submitted for publication of the material as it may appear in Geophysical Research Letters. Crocker, D. R.; Deane, G. B.; Cao, R; Santander M. V.; Morris, C. K.; Mitts, B.A.; Malfatti, F. M.; Prather, K. A.; Thiemens, M. H. The dissertation author was the primary investigator and author of this paper.

4.8 References

(1) Jonasz, M.; Fournier, G. R. *Light Scattering by Particles in Water: Theoretical and Experimental Foundations*, 1st ed.; Academic Press, 2007. https://doi.org/10.1016/B978-0-12-388751-1.X5000-5.

(2) Verdugo, P. Marine Microgels. *Ann. Rev. Mar. Sci.* **2012**, *4*, 375–400. https://doi.org/10.1146/annurev-marine-120709-142759.

(3) Facchini, M. C.; Rinaldi, M.; Decesari, S.; Carbone, C.; Finessi, E.; Mircea, M.; Fuzzi, S.; Ceburnis, D.; Flanagan, R.; Nilsson, E. D.; de Leeuw, G.; Martino, M.; Woeltjen, J.; O'Dowd, C. D. Primary Submicron Marine Aerosol Dominated by Insoluble Organic Colloids and Aggregates. *Geophys. Res. Lett.* **2008**, *35* (17). https://doi.org/10.1029/2008GL034210.

(4) Leck, C.; Bigg, E. K. Biogenic Particles in the Surface Microlayer and Overlaying Atmosphere in the Central Arctic Ocean during Summer. *Tellus, Ser. B Chem. Phys. Meteorol.* **2005**, *57* (4), 305–316. https://doi.org/10.1111/j.1600-0889.2005.00148.x.

(5) Bigg, E. K.; Leck, C. The Composition of Fragments of Bubbles Bursting at the Ocean Surface. *J. Geophys. Res. Atmos.* **2008**, *113* (11), 1–7. https://doi.org/10.1029/2007JD009078.

(6) Bigg, E. K.; Leck, C. Cloud-Active Particles over the Central Arctic Ocean. *J. Geophys.*

Res. **2001**, *106* (D23), 32,155-32,166.

(7) Orellana, M. V.; Matrai, P. A.; Leck, C.; Rauschenberg, C. D.; Lee, A. M.; Coz, E. Marine Microgels as a Source of Cloud Condensation Nuclei in the High Arctic. *PNAS* **2011**, *108* (33), 13612–13617. https://doi.org/10.1073/pnas.1102457108.

(8) Després, V. R.; Alex Huffman, J.; Burrows, S. M.; Hoose, C.; Safatov, A. S.; Buryak, G.; Fröhlich-Nowoisky, J.; Elbert, W.; Andreae, M. O.; Pöschl, U.; Jaenicke, R. Primary Biological Aerosol Particles in the Atmosphere: A Review. *Tellus, Ser. B Chem. Phys. Meteorol.* **2012**, *64* (1). https://doi.org/10.3402/tellusb.v64i0.15598.

(9) DeMott, P. J.; Hill, T. C. J.; McCluskey, C. S.; Prather, K. A.; Collins, D. B.; Sullivan, R. C.; Ruppel, M. J.; Mason, R. H.; Irish, V. E.; Lee, T.; Hwang, C. Y.; Rhee, T. S.; Snider, J. R.; McMeeking, G. R.; Dhaniyala, S.; Lewis, E. R.; Wentzell, J. J. B.; Abbatt, J.; Lee, C.; Sultana, C. M.; Ault, A. P.; Axson, J. L.; Martinez, M. D.; Venero, I.; Santos-Figueroa, G.; Stokes, M. D.; Deane, G. B.; Mayol-Bracero, O. L.; Grassian, V. H.; Bertram, T. H.; Bertram, A. K.; Moffett, B. F.; Franc, G. D. Sea Spray Aerosol as a Unique Source of Ice Nucleating Particles. *PNAS* **2016**, *113* (21), 5797–5803. https://doi.org/10.1073/pnas.1514034112.

(10) McCluskey, C. S.; Hill, E. T. C. J.; Sultana, C. M.; Laskina, O.; Trueblood, J.; Santander, M. V.; Beall, C. M.; Michaud, J. M.; Kreidenweis, S. M.; Prather, K. A.; Grassian, V.; Demott, P. J. A Mesocosm Double Feature: Insights into the Chemical Makeup of Marine Ice Nucleating Particles. *J. Atmos. Sci.* **2018**, *75* (7), 2405–2423. https://doi.org/10.1175/JAS-D-17-0155.1.

(11) Yamasaki, A.; Fukuda, H.; Fukuda, R.; Miyajima, T.; Nagata, T.; Ogawa, H.; Koike, I. Submicrometer Particles in Northwest Pacific Coastal Environments: Abundance, Size Distribution, and Biological Origins. *Limnol. Oceanogr.* **1998**, *43* (3), 536–542. https://doi.org/10.4319/lo.1998.43.3.0536.

(12) Longhurst, A. R.; Koike, I.; Li, W. K. W.; Rodriguez, J.; Dickie, P.; Kepay, P.; Partensky, F.; Bautista, B.; Ruiz, J.; Wells, M.; Bird, D. F. Sub-Micron Particles in Northwest Atlantic Shelf Water. *Deep Sea Res. Part A, Oceanogr. Res. Pap.* **1992**, *39* (1), 1–7. https://doi.org/10.1016/0198-0149(92)90016-M.

(13) Isao, K.; Hara, S.; Terauchi, K.; Kogure, K. Role of Sub-Micrometre Particles in the Ocean. *Nature* **1990**, *345* (6272), 242–244. https://doi.org/10.1038/345242a0.

(14) Knopf, D. A.; Alpert, P. A.; Wang, B.; Aller, J. Y. Stimulation of Ice Nucleation by Marine Diatoms. *Nat. Geosci.* **2011**, *4* (2), 88–90. https://doi.org/10.1038/ngeo1037.

(15) Tesson, S. V. M.; Šantl-Temkiv, T. Ice Nucleation Activity and Aeolian Dispersal Success in Airborne and Aquatic Microalgae. *Front. Microbiol.* **2018**, *9* (NOV), 1–14. https://doi.org/10.3389/fmicb.2018.02681.

(16) Mitts, B. A.; Wang, X.; Lucero, D. D.; Beall, C. M.; Deane, G. B.; DeMott, P. J.; Prather,

K. A. Importance of Supermicron Ice Nucleating Particles in Nascent Sea Spray. *Geophys. Res. Lett.* **2021**, *48* (3). https://doi.org/10.1029/2020GL089633.

(17) Wolf, M. J.; Goodell, M.; Dong, E.; Dove, L. A.; Zhang, C.; Franco, L. J.; Shen, C.; Rutkowski, E. G.; Narducci, D. N.; Mullen, S.; Babbin, A. R.; Cziczo, D. J. A Link between the Ice Nucleation Activity and the Biogeochemistry of Seawater. *Atmos. Chem. Phys.* **2020**, *20* (23), 15341–15356. https://doi.org/10.5194/acp-20-15341-2020.

(18) Wang, X.; Deane, G. B.; Moore, K. A.; Ryder, O. S.; Stokes, M. D.; Beall, C. M.; Collins, D. B.; Santander, M. V.; Burrows, S. M.; Sultana, C. M.; Prather, K. A. The Role of Jet and Film Drops in Controlling the Mixing State of Submicron Sea Spray Aerosol Particles. *PNAS* **2017**, *114* (27), 6978–6983. https://doi.org/10.1073/pnas.1702420114.

(19) Wurl, O.; Wurl, E.; Miller, L.; Johnson, K.; Vagle, S. Formation and Global Distribution of Sea-Surface Microlayers. *Biogeosciences* **2011**, *8* (1), 121–135. https://doi.org/10.5194/bg-8-121-2011.

(20) Aller, J. Y.; Kuznetsova, M. R.; Jahns, C. J.; Kemp, P. F. The Sea Surface Microlayer as a Source of Viral and Bacterial Enrichment in Marine Aerosols. *J. Aerosol Sci.* **2005**, *36* (5–6), 801–812. https://doi.org/10.1016/j.jaerosci.2004.10.012.

(21) Bigg, E. K.; Leck, C.; Tranvik, L. Particulates of the Surface Microlayer of Open Water in the Central Arctic Ocean in Summer. *Mar. Chem.* **2004**, *91* (1–4), 131–141. https://doi.org/10.1016/j.marchem.2004.06.005.

(22) Stramski, D.; Reynolds, R. A.; Gernez, P.; Röttgers, R.; Wurl, O. Inherent Optical Properties and Particle Characteristics of the Sea-Surface Microlayer. *Prog. Oceanogr.* **2019**, *176*. https://doi.org/10.1016/j.pocean.2019.05.009.

(23) Sauer, J. S.; Mayer, K. J.; Lee, C.; Alves, M. R.; Amiri, S.; Bahaveolos, C.; Barnes, E. B.; Crocker, D. R.; Dinasquet, J.; Garofalo, L. A.; Kaluarachchi, C. P.; Dang, D.; Kilgour, D.; Mael, L.; Mitts, B. A.; Moon, D. R.; Morris, C. K.; Moore, A. N.; Ni, C.-M.; Pendergraft, M. A.; Petras, D.; Simpson, R.; Smith, S.; Tumminello, P. R.; Walker, J. L.; DeMott, P. J.; Farmer, D. K.; Goldstein, A. H.; Grassian, V. H.; Jaffe, J. S.; Malfatti, F.; Martz, T. R.; Slade, J.; Tivanski, A. V.; Bertram, T. H.; Cappa, C. D.; Prather, K. A. The Sea Spray Chemistry and Particle Evolution Study (SeaSCAPE): Overview and Experimental Methods. *Environ. Sci. Process. Impacts* **2021**.

(24) Guillard, R. R. L.; Ryther, J. H. Studies of Marine Planktonic Diatoms. I. Cyclotella Nana. *Can. J. Microbiol.* **1962**, *8*, 229–239.

(25) Holm-Hansen, O.; Lorenzen, C. J.; Holmes, R. W.; Strickland, J. D. H. Fluorometric Determination of Chlorophyll. *ICES J. Mar. Sci.* **1965**, *30* (1), 3–15. https://doi.org/10.1093/icesjms/30.1.3.

(26) Cunliffe, M.; Wurl, O. Sampling the Sea Surface Microlayer; 2015; pp 255–261.

https://doi.org/10.1007/8623_2015_83.

(27) Carlson, D. J. Surface Microlayer Phenolic Enrichments Indicate Sea Surface Slicks. *Nature* **1982**, *296* (5856), 426–429. https://doi.org/10.1038/296426a0.

(28) Gasol, J. M.; Del Giorgio, P. A. Using Flow Cytometry for Counting Natural Planktonic Bacteria and Understanding the Structure of Planktonic Bacterial Communities. *Sci. Mar.* **2000**, *64* (2), 197–224. https://doi.org/10.3989/scimar.2000.64n2197.

(29) Marie, D.; Partensky, F.; Jacquet, S.; Vaulot, D. Enumeration and Cell Cycle Analysis of Natural Populations of Marine Picoplankton by Flow Cytometry Using the Nucleic Acid Stain SYBR Green I. *Appl. Environ. Microbiol.* **1997**, *63* (1), 186–193. https://doi.org/10.1128/aem.63.1.186-193.1997.

(30) Brussaard, C. P. D. Optimization of Procedures for Counting Viruses by Flow Cytometry. *Appl. Environ. Microbiol.* **2004**, *70* (3), 1506–1513. https://doi.org/10.1128/AEM.70.3.1506-1513.2004.

(31) Noble, R. T.; Fuhrman, J. A. Use of SYBR Green I for Rapid Epifluorescence Counts of Marine Viruses and Bacteria. *Aquat. Microb. Ecol.* **1998**, *14* (2), 113–118. https://doi.org/10.3354/ame014113.

(32) Engel, A. Determination of Marine Gel Particles. In *Practical Guidelines for the Analysis of Seawater*; 2009. https://doi.org/10.1201/9781420073072.ch7.

(33) Singh, P.; Bodycomb, J.; Travers, B.; Tatarkiewicz, K.; Travers, S.; Matyas, G. R.; Beck, Z. Particle Size Analyses of Polydisperse Liposome Formulations with a Novel Multispectral Advanced Nanoparticle Tracking Technology. *Int. J. Pharm.* **2019**, *566*, 680–686. https://doi.org/10.1016/j.ijpharm.2019.06.013.

(34) Einstein, A. Über Die von Der Molekularkinetischen Theorie Der Wärme Geforderte Bewegung von in Ruhenden Flüssigkeiten Suspendierten Teilchen. *Ann. Phys.* **1905**, *322* (8), 549–560. https://doi.org/10.1002/andp.19053220806.

(35) A. D. McNaught and A. Wilkinson. *IUPAC. Compendium of Chemical Terminology (the "Gold Book")*, 2nd ed.; Oxford, 2019.

(36) Groundwater, H.; Twardowski, M. S.; Dierssen, H. M.; Sciandra, A.; Freeman, S. A. Determining Size Distributions and Composition of Particles Suspended in Water: A New SEM-EDS Protocol with Validation and Comparison to Other Methods. *J. Atmos. Ocean. Technol.* **2012**, *29* (3), 433–449. https://doi.org/10.1175/JTECH-D-11-00026.1.

(37) Reynolds, R. A.; Stramski, D.; Wright, V. M.; Woźniak, S. B. Measurements and Characterization of Particle Size Distributions in Coastal Waters. *J. Geophys. Res. Ocean.* **2010**, *115* (8). https://doi.org/10.1029/2009JC005930.

(38) Jonasz, M.; Fournier, G. Approximation of the Size Distribution of Marine Particles by a Sum of Log-Normal Functions. *Limnol. Oceanogr.* **1996**, *41* (4), 744–754. https://doi.org/10.4319/lo.1996.41.4.0744.

(39) Zhang, X.; Twardowski, M.; Lewis, M. Retrieving Composition and Sizes of Oceanic Particle Subpopulations from the Volume Scattering Function. *Appl. Opt.* **2011**, *50* (9), 1240–1259. https://doi.org/10.1364/AO.50.001240.

(40) Jonasz, M.; Fournier, G. The Particle Size Distribution: Measurements and Approximations. In *Light Scattering by Particles in Water: Theoretical and Experimental Foundations*; Academic Press, 2007.

(41) Babin, M.; Stramski, D.; Reynolds, R. A.; Wright, V. M.; Leymarie, E. Determination of the Volume Scattering Function of Aqueous Particle Suspensions with a Laboratory Multi-Angle Light Scattering Instrument. *Appl. Opt.* **2012**, *51* (17), 3853–3873. https://doi.org/10.1364/AO.51.003853.

(42) Gallego-Urrea, J. A.; Tuoriniemi, J.; Pallander, T.; Hassellöv, M. Measurements of Nanoparticle Number Concentrations and Size Distributions in Contrasting Aquatic Environments Using Nanoparticle Tracking Analysis. *Environ. Chem.* **2010**, *7* (1), 67–81. https://doi.org/10.1071/EN09114.

(43) Wells, M. L.; Goldberg, E. D. Marine Submicron Particles. *Mar. Chem.* **1992**, *40* (1–2), 5–18. https://doi.org/10.1016/0304-4203(92)90045-C.

(44) Wells, M. L.; Goldberg, E. D. The Distribution of Colloids in the North Atlantic and Southern Oceans. *Limnol. Oceanogr.* **1994**, *39* (2), 286–302. https://doi.org/10.4319/lo.1994.39.2.0286.

(45) Zhang, X.; Gray, D. J.; Huot, Y.; You, Y.; Bi, L. Comparison of Optically Derived Particle Size Distributions: Scattering over the Full Angular Range versus Diffraction at near Forward Angles. *Appl. Opt.* **2012**, *51* (21), 5085–5099. https://doi.org/10.1364/AO.51.005085.

(46) Runyan, H.; Reynolds, R. A.; Stramski, D. Evaluation of Particle Size Distribution Metrics to Estimate the Relative Contributions of Different Size Fractions Based on Measurements in Arctic Waters. *J. Geophys. Res. Ocean.* **2020**, *125* (6). https://doi.org/10.1029/2020JC016218.

(47) Lee, C.; Sultana, C. M.; Collins, D. B.; Santander, M. V.; Axson, J. L.; Malfatti, F.; Cornwell, G. C.; Grandquist, J. R.; Deane, G. B.; Stokes, M. D.; Azam, F.; Grassian, V. H.; Prather, K. A. Advancing Model Systems for Fundamental Laboratory Studies of Sea Spray Aerosol Using the Microbial Loop. *J. Phys. Chem. A* **2015**, *119* (33), 8860–8870. https://doi.org/10.1021/acs.jpca.5b03488.

(48) Azam, F.; Fenchel, T.; Field, J.; Gray, J.; Meyer-Reil, L.; Thingstad, F. The Ecological Role

of Water-Column Microbes in the Sea. *Mar. Ecol. Prog. Ser.* **1983**, *10*, 257–263. https://doi.org/10.3354/meps010257.

(49) Moore, D. S.; Notz, W. I.; Flinger, M. A. *The Basic Practice of Statistics (6th Ed.) and Correlation*; 2013.

(50) Chin, W. C.; Orellana, M. V.; Verdugo, P. Spontaneous Assembly of Marine Dissolved Organic Matter into Polymer Gels. *Nature* **1998**, *391* (6667), 568–572. https://doi.org/10.1038/35345.

(51) Passow, U.; Alldredge, A. L. A Dye-binding Assay for the Spectrophotometric Measurement of Transparent Exopolymer Particles (TEP). *Limnology and Oceanography*. 1995, pp 1326–1335. https://doi.org/10.4319/lo.1995.40.7.1326.

(52) Patterson, J. P.; Collins, D. B.; Michaud, J. M.; Axson, J. L.; Sultana, C. M.; Moser, T.; Dommer, A. C.; Conner, J.; Grassian, V. H.; Stokes, M. D.; Deane, G. B.; Evans, J. E.; Burkart, M. D.; Prather, K. A.; Gianneschi, N. C. Sea Spray Aerosol Structure and Composition Using Cryogenic Transmission Electron Microscopy. *ACS Cent. Sci.* **2016**, *2* (1), 40–47. https://doi.org/10.1021/acscentsci.5b00344.

(53) Biller, S. J.; Schubotz, F.; Roggensack, S. E.; Thompson, A. W.; Summons, R. E.; Chisholm, S. W. Bacterial Vesicles in Marine Ecosystems. *Science (80-.).* **2014**, *343* (6167), 183–186. https://doi.org/10.1126/science.1243457.

(54) Shibata, A.; Kogure, K.; Koike, I.; Ohwada, K. Formation of Submicron Colloidal Particles from Marine Bacteria by Viral Infection. *Mar. Ecol. Prog. Ser.* **1997**, *155*, 303–307. https://doi.org/10.3354/meps155303.

(55) Nagata, T.; Kirchman, D. L. Release of Macromolecular Organic Complexes by Heterotrophic Marine Flagellates. *Mar. Ecol. Prog. Ser.* **1992**, *83* (2–3), 233–240. https://doi.org/10.3354/meps083233.

(56) Nagata, T. "Picopellets" Produced by Phagotrophic Nanoflagellates: Role in the Material Cycling within Marine Environments; 2000; pp 241–256. https://doi.org/10.1007/978-94-017-1319-1_12.

(57) Galgani, L.; Engel, A. Changes in Optical Characteristics of Surface Microlayers Hint to Photochemically and Microbially Mediated DOM Turnover in the Upwelling Region off the Coast of Peru. *Biogeosciences* **2016**, *13* (8), 2453–2473. https://doi.org/10.5194/bg-13-2453-2016.

(58) Verdugo, P.; Alldredge, A. L.; Azam, F.; Kirchman, D. L.; Passow, U.; Santschi, P. H. The Oceanic Gel Phase: A Bridge in the DOM-POM Continuum. In *Marine Chemistry*; 2004; Vol. 92, pp 67–85. https://doi.org/10.1016/j.marchem.2004.06.017.

(59) Zhou, J.; Mopper, K.; Passow, U. The Role of Surface-Active Carbohydrates in the Formation of Transparent Exopolymer Particles by Bubble Adsorption of Seawater. *Limnol.*

Oceanogr. **1998**, *43* (8), 1860–1871. https://doi.org/10.4319/lo.1998.43.8.1860.

(60) Crocker, D. R.; Hernandez, R. E.; Huang, H. D.; Pendergraft, M. A.; Cao, R.; Dai, J.; Morris, C. K.; Deane, G. B.; Prather, K. A.; Thiemens, M. H. Biological Influence on D13C and Organic Composition of Nascent Sea Spray Aerosol. *ACS Earth Sp. Chem.* **2020**, *4* (9), 1686–1699. https://doi.org/10.1021/acsearthspacechem.0c00072.

(61) Robinson, T. B.; Giebel, H. A.; Wurl, O. Riding the Plumes: Characterizing Bubble Scavenging Conditions for the Enrichment of the Sea-Surface Microlayer by Transparent Exopolymer Particles. *Atmosphere.* **2019**, *10* (8). https://doi.org/10.3390/atmos10080454.

(62) Walls, P. L. L.; Bird, J. C. Enriching Particles on a Bubble through Drainage: Measuring and Modeling the Concentration of Microbial Particles in a Bubble Film at Rupture. *Elementa* **2017**, *5*. https://doi.org/10.1525/elementa.230.

(63) Blanchard, D. C.; Syzdek, L. D. Water-to-Air Transfer and Enrichment of Bacteria in Drops from Bursting Bubbles. *Appl. Environ. Microbiol.* **1982**, *43* (5), 1001–1005. https://doi.org/10.1128/aem.43.5.1001-1005.1982.

(64) Alpert, P. A.; Aller, J. Y.; Knopf, D. A. Ice Nucleation from Aqueous NaCl Droplets with and without Marine Diatoms. *Atmos. Chem. Phys.* **2011**, *11* (12), 5539–5555. https://doi.org/10.5194/acp-11-5539-2011.

(65) Wilson, T. W.; Ladino, L. A.; Alpert, P. A.; Breckels, M. N.; Brooks, I. M.; Browse, J.; Burrows, S. M.; Carslaw, K. S.; Huffman, J. A.; Judd, C.; Kilthau, W. P.; Mason, R. H.; McFiggans, G.; Miller, L. A.; Najera, J. J.; Polishchuk, E.; Rae, S.; Schiller, C. L.; Si, M.; Temprado, J. V.; Whale, T. F.; Wong, J. P. S.; Wurl, O.; Yakobi-Hancock, J. D.; Abbatt, J. P. D.; Aller, J. Y.; Bertram, A. K.; Knopf, D. A.; Murray, B. J. A Marine Biogenic Source of Atmospheric Ice-Nucleating Particles. *Nature* **2015**, *525* (7568), 234–238. https://doi.org/10.1038/nature14986.

(66) McCluskey, C. S.; Hill, T. C. J.; Malfatti, F.; Sultana, C. M.; Lee, C.; Santander, M. V.; Beall, C. M.; Moore, K. A.; Cornwell, G. C.; Collins, D. B.; Prather, K. A.; Jayarathne, T.; Stone, E. A.; Azam, F.; Kreidenweis, S. M.; DeMott, P. J. A Dynamic Link between Ice Nucleating Particles Released in Nascent Sea Spray Aerosol and Oceanic Biological Activity during Two Mesocosm Experiments. *J. Atmos. Sci.* **2017**, *74* (1), 151–166. https://doi.org/10.1175/JAS-D-16-0087.1.

(67) Roy, P.; Mael, L. E.; Hill, T. C. J.; Mehndiratta, L.; Peiker, G.; House, M. L.; DeMott, P. J.; Grassian, V. H.; Dutcher, C. S. Ice Nucleating Activity and Residual Particle Morphology of Bulk Seawater and Sea Surface Microlayer. *ACS Earth Sp. Chem.* **2021**. https://doi.org/10.1021/acsearthspacechem.1c00175.

(68) Prather, K. A.; Bertram, T. H.; Grassian, V. H.; Deane, G. B.; Stokes, M. D.; DeMott, P. J.; Aluwihare, L. I.; Palenik, B. P.; Azam, F.; Seinfeld, J. H.; Moffet, R. C.; Molina, M. J.; Cappa, C. D.; Geiger, F. M.; Roberts, G. C.; Russell, L. M.; Ault, A. P.; Baltrusaitis, J.;

Collins, D. B.; Corrigan, C. E.; Cuadra-Rodriguez, L. A.; Ebben, C. J.; Forestieri, S. D.; Guasco, T. L.; Hersey, S. P.; Kim, M. J.; Lambert, W. F.; Modini, R. L.; Mui, W.; Pedler, B. E.; Ruppel, M. J.; Ryder, O. S.; Schoepp, N. G.; Sullivan, R. C.; Zhao, D. Bringing the Ocean into the Laboratory to Probe the Chemical Complexity of Sea Spray Aerosol. *PNAS* **2013**, *110* (19), 7550–7555. https://doi.org/10.1073/pnas.1300262110.

(69) Palumbo, A. V.; Ferguson, R. L.; Rublee, P. A. Size of Suspended Bacterial Cells and Association of Heterotrophic Activity with Size Fractions of Particles in Estuarine and Coastal Waters. *Appl. Environ. Microbiol.* **1984**, *48* (1), 157–164. https://doi.org/10.1128/aem.48.1.157-164.1984.

Chapter 5: Summary and Future Directions

5.1 Research Impacts on Marine Aerosol Source Apportionment and Climate

This dissertation research has focused on elucidating the seawater biological and physicochemical processes that drive changes in the organic composition of nascent SSA. Much of this work has been interpreted through the lens of biologically induced or size-dependent differences in the carbon isotopic composition of SSA, establishing a basis from which to determine the most suitable $\delta^{13}C$ values for marine-derived aerosols. The distinct $\delta^{13}C$ values for SSA_{super} and SSA_{sub} observed in this work, indicative of their dissimilar organic composition, demonstrate that SSA_{super} and SSA_{sub} should be considered separately when assessing their contributions to marine aerosols and climate. Continued advancements in marine aerosol source apportionment and SSA-climate interactions will require a better understanding of how atmospheric aging changes the composition and $\delta^{13}C$ of marine-derived aerosols, including formation of secondary marine aerosol (Figure 5.1). Below, we will describe how our findings can inform this future research to improve our understanding of SSA's contribution to the marine environment and our climate system.

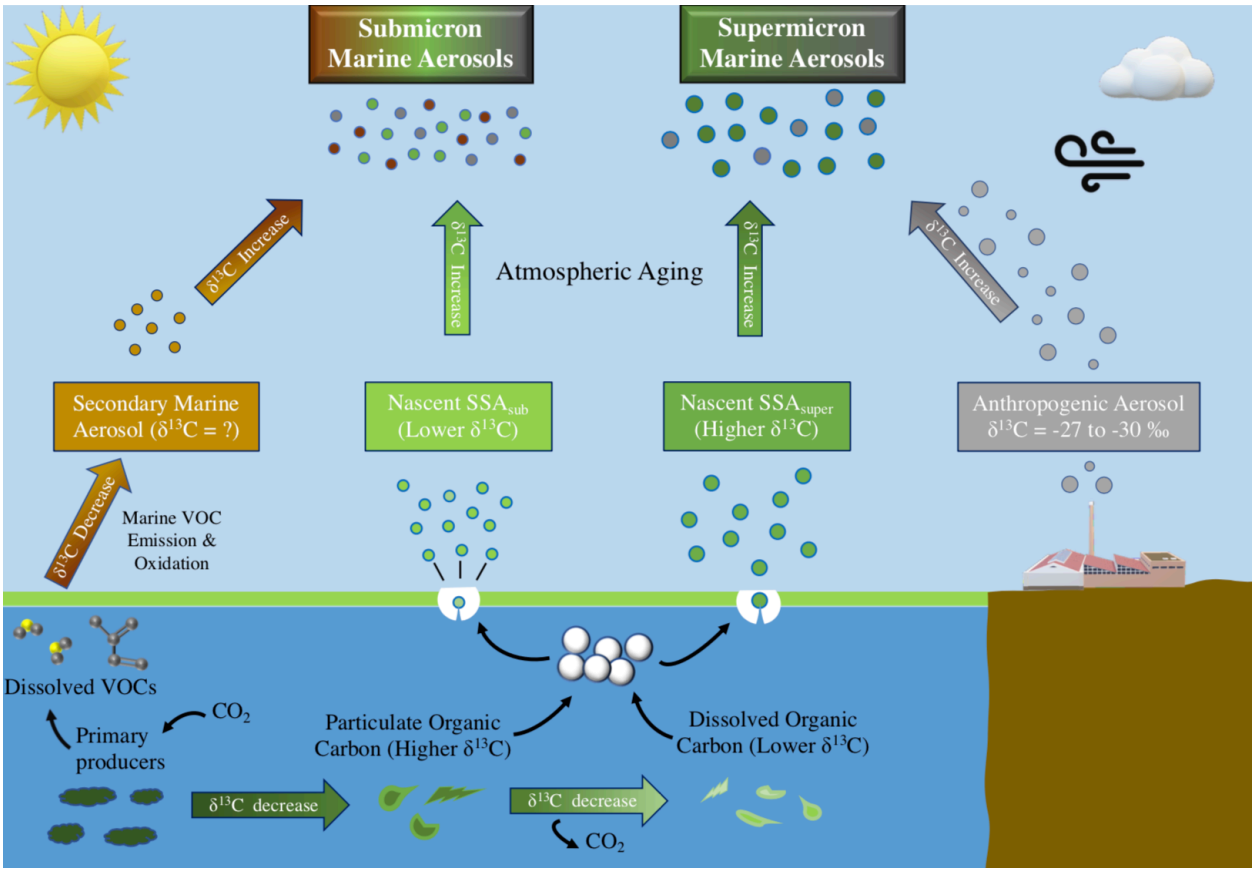

Figure 5.1 An illustration of the different aerosol types contributing to submicron and supermicron marine aerosols. Also included are the oceanic and atmospheric processes that influence the $\delta^{13}C$ values of these aerosols with darker colors to indicate $\delta^{13}C$ increases and lighter colors to indicate $\delta^{13}C$ decreases. Our study focused on one aspect of this environmental system by elucidating the seawater biological and chemical processes that result in higher $\delta^{13}C$ values for SSA_{super} and comparatively lower $\delta^{13}C$ values for SSA_{sub}. Future work remains to understand how the $\delta^{13}C$ value of nascent SSA will be impacted by photochemical aging, although studies on organic aerosols indicate that $\delta^{13}C$ will likely increase.[1–3] Additionally, more work should be aimed at constraining $\delta^{13}C$ changes during the formation and atmospheric transport of secondary marine aerosol as little attention has been given to this topic thus far.

5.2 Supermicron Marine Aerosols

The large effect of seawater biological activity on $\delta^{13}C_{super}$ prevents the application of a uniform $\delta^{13}C_{super}$ value across all oceanic regimes (Figure 3.3). Instead, because $\delta^{13}C_{super}$ consistently remained between $\delta^{13}C_{POC}$ and $\delta^{13}C_{DOC}$, complementary $\delta^{13}C$ measurements of bulk seawater POC and DOC during field studies should provide good constraints on the probable

values for nascent $\delta^{13}C_{super}$, and also nascent $\delta^{13}C_{TSP}$.[4] Before employing this $\delta^{13}C_{super}$ value in source apportionment studies, researchers must also account for potential $\delta^{13}C$ changes that occur during atmospheric transport. Photochemical processing of aerosol organics often leads to $\delta^{13}C$ increases,[1,2] so the actual $\delta^{13}C_{super}$ value for photochemically-aged SSA_{super} may indeed be less negative than the nascent $\delta^{13}C_{super}$ value. To date, research on $\delta^{13}C$ changes in marine aerosols during atmospheric transport has been limited to individual compounds, so future research regarding $\delta^{13}C$ changes for the totality of primary SSA organics would be beneficial to determine the most appropriate $\delta^{13}C_{SSA}$ values to use for marine aerosols collected from aged air masses.

Biologically induced changes in the organic composition of SSA_{super} over the course of a phytoplankton bloom may also have a substantial impact on climate and precipitation. Multiple studies have observed higher SSA ice nucleating particle (INP) concentrations originating from biologically active seawater.[5–7] Additionally, a recently study found that a majority of SSA INPs are supermicron particles,[8] and inferred that the ice nucleating entities (INEs) were likely biological material entrained in jet drop SSA_{super} particles.[8] This is relevant to the increased $Fraction_{FreshOC}$ values observed in SSA_{super} after the phytoplankton bloom peak in our experiment (Chapter 3), because many of the biological components that likely constituted freshly produced OC have also been identified as INEs (e.g. diatoms, bacteria, and their exudates/detritus).[9–11] This may also include the biologically produced submicron particulates investigated in Chapter 4, which increased during phytoplankton growth and senescence. Taken altogether, the augmented transfer of freshly produced OC into SSA_{super} during our phytoplankton bloom may help explain the higher SSA INP concentrations that have been observed during periods of elevated seawater biological activity.[5–9] To better assess a potential link between freshly produced OC and SSA INP concentrations, a continued focus should be placed on characterizing the chemical constituents

comprising INEs in the seawater and SSA, including changes in INE chemical composition during phytoplankton blooms. Ascertaining the relationship between seawater biological activity and SSA INP concentrations would be widely beneficial to modeling predictions of ice cloud formation, radiative balance, and precipitation patterns.

5.3 Submicron Marine Aerosols

Studies focusing on submicron marine aerosols need to consider that the SSA_{sub} organic composition, is highly sensitive to the surface-active organic species residing at the air-sea interface. Even in nonpolluted seawater this may lead to lower values for $\delta^{13}C_{sub}$, as biogenic surfactants (e.g. lipids)[12,13] often have more negative $\delta^{13}C$ values than the bulk organic material.[14,15] For measurements in coastal environments, such as this study, increased concentrations of anthropogenic or terrestrial surfactants in the seawater may additionally contribute to lower $\delta^{13}C_{sub}$ values. Many marine aerosol source apportionment studies use elemental carbon concentrations to identify continental air masses under the assumption that marine anthropogenic carbon originates from primary aerosol emissions on land.[16–18] However, this method may not encompass all continental influences to marine aerosols because our results indicate that anthropogenic and terrestrial organic compounds present in the seawater can be transferred into nascent SSA. Modelling studies have estimated that offshore advection of SSA_{sub} produced in the surf zone can contribute >50% of the total SSA population a few meters above the ocean surface even 30-40 km offshore.[19,20] This means that near-shore or coastal marine aerosol measurements need to take into account spatial and temporal variability in human activities or weather events that could lead to elevated concentrations of nonmarine-derived surfactants in coastal seawater,[21] as these changes could have a significant impact on the value of $\delta^{13}C_{sub}$.

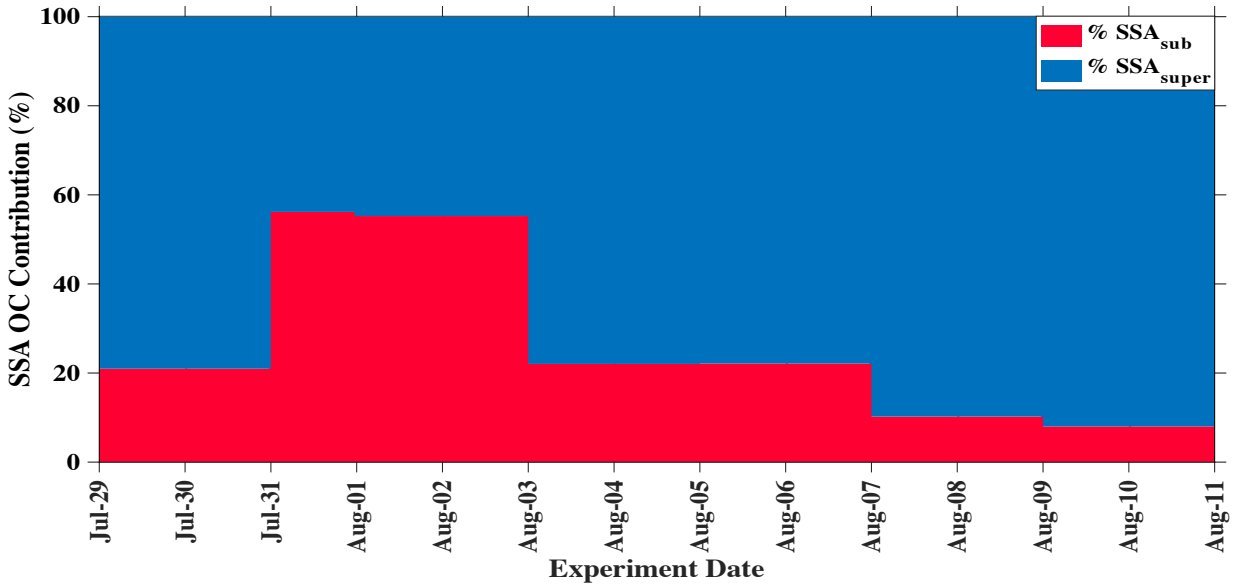

Figure 5.2 The proportional contribution of SSA_{sub} carbon (red) and SSA_{super} carbon (blue) to the total OC amount for each SSA sampling period. SSA_{super} contributed >40% of the OC in each sampling period and contributed >75% of the OC in 5 of the 7 SSA samples.

In addition to considering the organic composition of SSA_{sub}, submicron marine aerosol studies must also account for carbon contributions from secondary marine aerosol (SMA). Our size-segregated OC measurements on pure, nascent SSA indicate the majority of OC usually resides in SSA_{super} (Figure 5.2). Thus, field observations showing larger OC contributions by submicron marine aerosols may be due to formation of secondary marine aerosol,[22,23] most of which is submicron sized (Figure 5.1).[24] The potential contribution of SMA to marine aerosol carbon is generally unaccounted for in isotopic source apportionment studies, primarily because the $\delta^{13}C$ value of isolated SMA has not been measured. Based on SMA's formation from isotopically-light gas phase precursors (e.g. isoprene), it is expected that the $\delta^{13}C$ value of SMA will be more negative than primary SSA.[2,25] Since SMA may constitute a significant portion of submicron marine aerosol carbon, future studies addressing the carbon isotopic composition of SMA would be helpful to build from our work measuring $\delta^{13}C_{sub}$ and constrain the likely $\delta^{13}C$

values for marine-derived submicron aerosols. Furthermore, establishing distinct $\delta^{13}C$ values for SSA_{sub} and SMA may enable future studies to differentiate between secondary and primary aerosols in the pristine marine atmosphere. Because SSA_{sub} and SMA have different cloud formation properties,[24] distinguishing the contributions of primary and secondary marine aerosols will improve modelling estimates of cloud cover and radiative balance in the remote marine environment.

5.4 Acknowledgements

This work was funded by the National Science Foundation Center for Aerosol Impacts on Chemistry of the Environment (NSF-CAICE), a Center for Chemical Innovation (CHE-1801971). The authors thank the entire SeaSCAPE team, and especially Dr. Kathryn Mayer, Dr. Jon Sauer, Prof. Timothy Bertram, and Prof. Christopher Cappa for designing and overseeing the campaign.

Chapter 5, in part, has been submitted for publication of the material as it may appear in Environmental Science and Technology. Crocker, D. R.; Kaluarachchi, C.P.; Cao, R; Dinasquet, J.; Franklin, E. B.; Morris, C.K.; Nguyen, T.; Torres R.R.; Martz, T. D.; Malfatti, F. M.; Goldstein, A.H.; Tivanski, A. V.; Prather, K. A.; Thiemens M. H. The dissertation author was the primary investigator and author of this paper.

5.5 References

(1) Bosch, C.; Andersson, A.; Kirillova, E. N.; Budhavant, K.; Tiwari, S.; Praveen, P. S.; Russell, L. M.; Beres, N. D.; Ramanathan, V.; Gustafsson, Ö. Source-Diagnostic Dual-Isotope Composition and Optical Properties of Water-Soluble Organic Carbon and Elemental Carbon in the South Asian Outflow Intercepted over the Indian Ocean. *J. Geophys. Res.* **2014**, *119* (20), 11,743-11,759. https://doi.org/10.1002/2014JD022127.

(2) Kirillova, E. N.; Andersson, A.; Sheesley, R. J.; Kruså, M.; Praveen, P. S.; Budhavant, K.; Safai, P. D.; Rao, P. S. P.; Gustafsson, Ö. 13C- And 14C-Based Study of Sources and Atmospheric Processing of Water-Soluble Organic Carbon (WSOC) in South Asian Aerosols. *J. Geophys. Res. Atmos.* **2013**, *118* (2), 614–626. https://doi.org/10.1002/jgrd.50130.

(3) Aggarwal, S. G.; Kawamura, K.; Umarji, G. S.; Tachibana, E.; Patil, R. S.; Gupta, P. K. Organic and Inorganic Markers and Stable C-, N-Isotopic Compositions of Tropical Coastal Aerosols from Megacity Mumbai: Sources of Organic Aerosols and Atmospheric Processing. *Atmos. Chem. Phys. Discuss.* **2012**, *12* (8), 20593–20630. https://doi.org/10.5194/acpd-12-20593-2012.

(4) Crocker, D. R.; Hernandez, R. E.; Huang, H. D.; Pendergraft, M. A.; Cao, R.; Dai, J.; Morris, C. K.; Deane, G. B.; Prather, K. A.; Thiemens, M. H. Biological Influence on D13C and Organic Composition of Nascent Sea Spray Aerosol. *ACS Earth Sp. Chem.* **2020**, *4* (9), 1686–1699. https://doi.org/10.1021/acsearthspacechem.0c00072.

(5) DeMott, P. J.; Hill, T. C. J.; McCluskey, C. S.; Prather, K. A.; Collins, D. B.; Sullivan, R. C.; Ruppel, M. J.; Mason, R. H.; Irish, V. E.; Lee, T.; Hwang, C. Y.; Rhee, T. S.; Snider, J. R.; McMeeking, G. R.; Dhaniyala, S.; Lewis, E. R.; Wentzell, J. J. B.; Abbatt, J.; Lee, C.; Sultana, C. M.; Ault, A. P.; Axson, J. L.; Martinez, M. D.; Venero, I.; Santos-Figueroa, G.; Stokes, M. D.; Deane, G. B.; Mayol-Bracero, O. L.; Grassian, V. H.; Bertram, T. H.; Bertram, A. K.; Moffett, B. F.; Franc, G. D. Sea Spray Aerosol as a Unique Source of Ice Nucleating Particles. *PNAS* **2016**, *113* (21), 5797–5803. https://doi.org/10.1073/pnas.1514034112.

(6) Wolf, M. J.; Goodell, M.; Dong, E.; Dove, L. A.; Zhang, C.; Franco, L. J.; Shen, C.; Rutkowski, E. G.; Narducci, D. N.; Mullen, S.; Babbin, A. R.; Cziczo, D. J. A Link between the Ice Nucleation Activity and the Biogeochemistry of Seawater. *Atmos. Chem. Phys.* **2020**, *20* (23), 15341–15356. https://doi.org/10.5194/acp-20-15341-2020.

(7) Creamean, J. M.; Cross, J. N.; Pickart, R.; McRaven, L.; Lin, P.; Pacini, A.; Hanlon, R.; Schmale, D. G.; Ceniceros, J.; Aydell, T.; Colombi, N.; Bolger, E.; DeMott, P. J. Ice Nucleating Particles Carried From Below a Phytoplankton Bloom to the Arctic Atmosphere. *Geophys. Res. Lett.* **2019**, *46* (14), 8572–8581. https://doi.org/10.1029/2019GL083039.

(8) Mitts, B. A.; Wang, X.; Lucero, D. D.; Beall, C. M.; Deane, G. B.; DeMott, P. J.; Prather, K. A. Importance of Supermicron Ice Nucleating Particles in Nascent Sea Spray. *Geophys. Res. Lett.* **2021**, *48* (3). https://doi.org/10.1029/2020GL089633.

(9) McCluskey, C. S.; Hill, E. T. C. J.; Sultana, C. M.; Laskina, O.; Trueblood, J.; Santander,

M. V.; Beall, C. M.; Michaud, J. M.; Kreidenweis, S. M.; Prather, K. A.; Grassian, V.; Demott, P. J. A Mesocosm Double Feature: Insights into the Chemical Makeup of Marine Ice Nucleating Particles. *J. Atmos. Sci.* **2018**, *75* (7), 2405–2423. https://doi.org/10.1175/JAS-D-17-0155.1.

(10) Alpert, P. A.; Aller, J. Y.; Knopf, D. A. Ice Nucleation from Aqueous NaCl Droplets with and without Marine Diatoms. *Atmos. Chem. Phys.* **2011**, *11* (12), 5539–5555. https://doi.org/10.5194/acp-11-5539-2011.

(11) Wilson, T. W.; Ladino, L. A.; Alpert, P. A.; Breckels, M. N.; Brooks, I. M.; Browse, J.; Burrows, S. M.; Carslaw, K. S.; Huffman, J. A.; Judd, C.; Kilthau, W. P.; Mason, R. H.; McFiggans, G.; Miller, L. A.; Najera, J. J.; Polishchuk, E.; Rae, S.; Schiller, C. L.; Si, M.; Temprado, J. V.; Whale, T. F.; Wong, J. P. S.; Wurl, O.; Yakobi-Hancock, J. D.; Abbatt, J. P. D.; Aller, J. Y.; Bertram, A. K.; Knopf, D. A.; Murray, B. J. A Marine Biogenic Source of Atmospheric Ice-Nucleating Particles. *Nature* **2015**, *525* (7568), 234–238. https://doi.org/10.1038/nature14986.

(12) Rastelli, E.; Corinaldesi, C.; Dell'anno, A.; Lo Martire, M.; Greco, S.; Cristina Facchini, M.; Rinaldi, M.; O'Dowd, C.; Ceburnis, D.; Danovaro, R. Transfer of Labile Organic Matter and Microbes from the Ocean Surface to the Marine Aerosol: An Experimental Approach. *Sci. Rep.* **2017**, *7* (1). https://doi.org/10.1038/s41598-017-10563-z.

(13) Cochran, R. E.; Laskina, O.; Jayarathne, T.; Laskin, A.; Laskin, J.; Lin, P.; Sultana, C.; Lee, C.; Moore, K. A.; Cappa, C. D.; Bertram, T. H.; Prather, K. A.; Grassian, V. H.; Stone, E. A. Analysis of Organic Anionic Surfactants in Fine and Coarse Fractions of Freshly Emitted Sea Spray Aerosol. *Environ. Sci. Technol.* **2016**, *50* (5), 2477–2486. https://doi.org/10.1021/acs.est.5b04053.

(14) Loh, A. N.; Bauer, J. E.; Druffel, E. R. M. Variable Ageing and Storage of Dissolved Organic Components in the Open Ocean. *Nature* **2004**, *430* (7002), 877–881. https://doi.org/10.1038/nature02780.

(15) Hwang, J.; Druffel, E. R. M.; Bauer, J. E. Incorporation of Aged Dissolved Organic Carbon (DOC) by Oceanic Particulate Organic Carbon (POC): An Experimental Approach Using Natural Carbon Isotopes. *Mar. Chem.* **2006**, *98* (2–4), 315–322. https://doi.org/10.1016/j.marchem.2005.10.008.

(16) Ceburnis, D.; Garbaras, A.; Szidat, S.; Rinaldi, M.; Fahrni, S.; Perron, N.; Wacker, L.; Leinert, S.; Remeikis, V.; Facchini, M. C.; Prevot, A. S. H.; Jennings, S. G.; Ramonet, M.; O'Dowd, C. D. Quantification of the Carbonaceous Matter Origin in Submicron Marine Aerosol by 13C and 14C Isotope Analysis. *Atmos. Chem. Phys.* **2011**, *11* (16), 8593–8606. https://doi.org/10.5194/acp-11-8593-2011.

(17) Shank, L. M.; Howell, S.; Clarke, A. D.; Freitag, S.; Brekhovskikh, V.; Kapustin, V.; McNaughton, C.; Campos, T.; Wood, R. Organic Matter and Non-Refractory Aerosol over the Remote Southeast Pacific: Oceanic and Combustion Sources. *Atmos. Chem. Phys.* **2012**, *12* (1), 557–576. https://doi.org/10.5194/acp-12-557-2012.

(18) Miyazaki, Y.; Yamashita, Y.; Kawana, K.; Tachibana, E.; Kagami, S.; Mochida, M.;

Suzuki, K.; Nishioka, J. Chemical Transfer of Dissolved Organic Matter from Surface Seawater to Sea Spray Water-Soluble Organic Aerosol in the Marine Atmosphere. *Sci. Rep.* **2018**, *8* (1), 1–10. https://doi.org/10.1038/s41598-018-32864-7.

(19) Tedeschi, G.; van Eijk, A. M. J.; Piazzola, J.; Kusmierczyk-Michulec, J. T. Influence of the Surf Zone on the Marine Aerosol Concentration in a Coastal Area. *Boundary-Layer Meteorol.* **2017**, *163* (2), 327–350. https://doi.org/10.1007/s10546-016-0229-7.

(20) Vignati, E.; de Leeuw, G.; Berkowicz, R. Modeling Coastal Aerosol Transport and Effects of Surf-Produced Aerosols on Processes in the Marine Atmospheric Boundary Layer. *J. Geophys. Res.* **2001**, *106* (2000), 20,225-20,238.

(21) Petras, D.; Minich, J. J.; Cancelada, L. B.; Torres, R. R.; Kunselman, E.; Wang, M.; White, M. E.; Allen, E. E.; Prather, K. A.; Aluwihare, L. I.; Dorrestein, P. C. Non-Targeted Tandem Mass Spectrometry Enables the Visualization of Organic Matter Chemotype Shifts in Coastal Seawater. *Chemosphere* **2021**, *271*, 129450. https://doi.org/10.1016/j.chemosphere.2020.129450.

(22) Turekian, V. C.; Macko, S. A.; Keene, W. C. Concentrations, Isotopic Compositions, and Sources of Size-Resolved, Particulate Organic Carbon and Oxalate in near-Surface Marine Air at Bermuda during Spring. *J. Geophys. Res. Atmos.* **2003**, *108* (5). https://doi.org/10.1029/2002jd002053.

(23) Cavalli, F.; Facchini, M. C.; Decesari, S.; Mircea, M.; Emblico, L.; Fuzzi, S.; Ceburnis, D.; Yoon, Y. J.; O'Dowd, C. D.; Putaud, J. P.; Dell'Acqua, A. Advances in Characterization of Size-Resolved Organic Matter in Marine Aerosol over the North Atlantic. *J. Geophys. Res. D Atmos.* **2004**, *109* (24), 1–14. https://doi.org/10.1029/2004JD005137.

(24) Mayer, K. J.; Wang, X.; Santander, M. V.; Mitts, B. A.; Sauer, J. S.; Sultana, C. M.; Cappa, C. D.; Prather, K. A. Secondary Marine Aerosol Plays a Dominant Role over Primary Sea Spray Aerosol in Cloud Formation. *ACS Cent. Sci.* **2020**, *6* (12), 2259–2266. https://doi.org/10.1021/acscentsci.0c00793.

(25) Rudolph, J.; Anderson, R. S.; Czapiewski, K. V.; Czuba, E.; Ernst, D.; Gillespie, T.; Huang, L.; Rigby, C.; Thompson, A. E. The Stable Carbon Isotope Ratio of Biogenic Emissions of Isoprene and the Potential Use of Stable Isotope Ratio Measurements to Study Photochemical Processing of Isoprene in the Atmosphere. *J. Atmos. Chem.* **2003**, *44* (1), 39–55. https://doi.org/10.1023/A:1022116304550.